LAURENS, JOHANNES BERNARDUS

ANALYSIS OF GAS MIXTURES BY MEANS OF FOURIER TRANSFORM INFRARED SPECTROSCOPY

MSc UP 1992

ANALYSIS OF GAS MIXTURES BY MEANS OF FOURIER TRANSFORM INFRARED SPECTROSCOPY

by

JOHANNES BERNARDUS LAURENS

Submitted in partial fullfilment of the

requirements for the degree

Master of Science

in the

Faculty of Science

University of Pretoria

Mei 1992

CONTENTS

ACKNOWLEDGEMENTS

I wish to express my sincere thanks to the following persons:

1. Prof Anton Heyns for his kind and appreciated support.

2. Prof Egmont Rohwer for his carefully considered suggestions during the design of the gas cells.

3. Annette, Werner and Anneke for their continuous encouragement.

4. Sasol, especially Dr Hans le Roux, for their financial support.

5. Mrs Annatjie Kok for her excellent and professional typing work.

SUMMARY

FT-IR spectroscopy as a rapid and sensitive method for on-line gas analysis was investigated. Background knowledge of the IR spectroscopy of carbon dioxide and methane was obtained by undertaking a study of their high resolution spectra. As a result of the CO_2 molecule conforming to Einstein-Bosè statistics the uneven rotational lines are absent.

An excellent correlation between a theoreticaly calculated spectrum of the methane ν_4 band and an experimental spectrum was found, by taking the first and second order Coriolis coupling into account. Once the theoretical interpretation of the FT-IR spectra was well-understood, quantitative analysis on gas mixtures were done. Results of on-line measurements are reported and discussed.

Two types of gas-cells, originally designed in our laboratories are discussed. These cells can be used to selectively enhance the signal of a low concentration component, in the presence of an overlapping signal, by way of condensation as well as polar adsorbtion.

OPSOMMING

FT-IR spektroskopie is ondersoek as 'n vinnige sensitiewe metode vir oplyn gasanalise. 'n Agtergrondstudie aangaande die IR spektroskopie van koolstofdioksied en metaan is gedoen deur die hoë resolusie spektra te bestudeer. Dit is bevestig dat die onewe rotasielyne van koolstofdioksied afwesig is as gevolg van Einstein-Bosè statistiek.

'n Korrelasie tussen 'n teoreties berekende spektrum van die ν_4 band van metaan en 'n eksperimentele spektrum is verkry deurdat eerste- en tweede orde Coriolis koppeling in ag geneem is. Nadat die teoretiese interpretasie van die FT-IR spektra goed verstaan is, is daar oorgegaan na kwantitatiewe gasanalise. Resultate van oplyn metings word gerapporteer en bespreek.

Twee oorspronklike ontwerpte gasselle word bespreek. Hierdie selle kan gebruik word om die sein van 'n lae konsentrasie komponent selektief te versterk veral wanneer daar oorvleuelende sterk seine teenwoordig is. Die beginsel hiervan berus op kondensasie en polêre adsorbsie.

CHAPTER I

INTRODUCTION

Analysis of raw-gas mixtures, originating from the Sasol-Gasification plant, was investigated in researching the possibility of FT-IR spectroscopy as a rapid and sensitive method for online gas analysis. A typical FT-IR spectrum of the raw gas, in a flow through gas cell is shown in fig. I.1. The main components of the raw-gas are: carbon monoxide (21%), carbon dioxide (27%) and methane (9,5%). (See table I-1 for the vibrational wavenumbers of each component). Hydrogen, the fourth main component, lacking a changing dipole moment can not be measured by infra-red detection methods.

Table I-1. Vibrational wavenumbers and symmetries of the main components.

Component	Wavenumber/cm^{-1}	Symmetry
CO	2143	Σ^+
CO_2	2349	Σ_u^+
	3609	Σ_u^+
	3716	Σ_u^+
CH_4	1306	T_2
	3018	T_2

In order to obtain background knowledge of the IR spectroscopy of the main components of this gas mixture a high resolution FT-IR study of carbon dioxide and methane was undertaken. The theory of the high resolution FT-IR spectroscopy of linear and spherical top rotors is also outlined.

In the case of CO_2 it was confirmed that the alternating uneven rotational lines are absent as

a result of the CO_2 molecule conforming to Einstein-Bosè statistics. The interatomic distances of the ν_2 and ν_3 vibrations were determined.

The effect of first and second order Coriolis coupling were taken into account in generating a theoretical vibrational-rotational spectrum of the ν_4 band of methane. A correlation between the theoretical and experimental spectra was found. Once the theoretical interpretation of the FT-IR spectra was well understood, we proceeded to a quantitative analysis of gas mixtures by means of FT-IR measurements.

Quantitative measurements of the main components were performed from spectra obtained at a resolution of 4 cm^{-1} since low resolution spectrophotometers are more mobile and less costly than their high-resolution counterparts. The K-Matrix method was used for the qualitative processing of the online measured spectra.

Two types of gas cells were originally designed, built and tested in our laboratories, namely:

i. Liebig type -

ii. Liebig-Metal Light Pipe type gas cell.

These cells were used to selectively enhance the signal of the H_2S in the presence of an overlapping CO signal. In both types of cells the H_2S can be captured inside the cell, by way of condensation, whilst the unwanted gases flow through the cell. After the condensate was allowed to evaporate an infra-red spectrum could be recorded. The analytical possibilities of both cells were explored and the results were discussed.

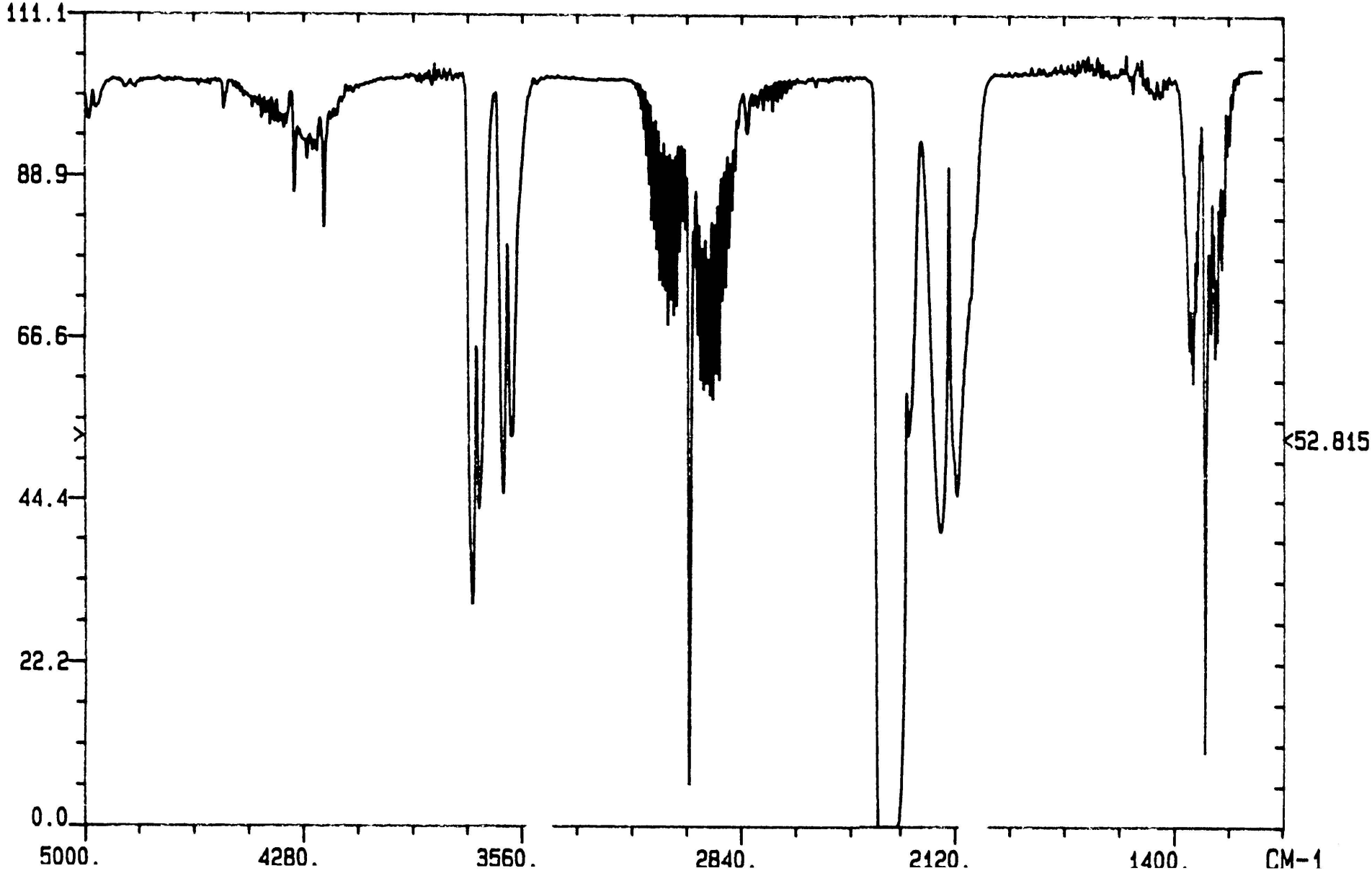

Fig. I.1

CHAPTER II

HIGH RESOLUTION FT-IR SPECTRUM OF CO_2

1. Vibrational spectrum

The CO_2 molecule is linear and belongs to the point group $D_{\infty h}$. The normal modes of vibration of CO_2 transform as Σ_g^+, Σ_u^+ and Π_u. Counting Π_u as two representations, one finds that there are four degrees of freedom. Since there are four normal modes of vibration and two chemical bonds, two of these modes are stretching modes and two are bending modes. The vibrational modes as well as their symmetries are shown in fig. II.1.

The totally symmetric ν_1 vibration is Raman active whilst the ν_3 and the ν_2 vibrations are infrared active.

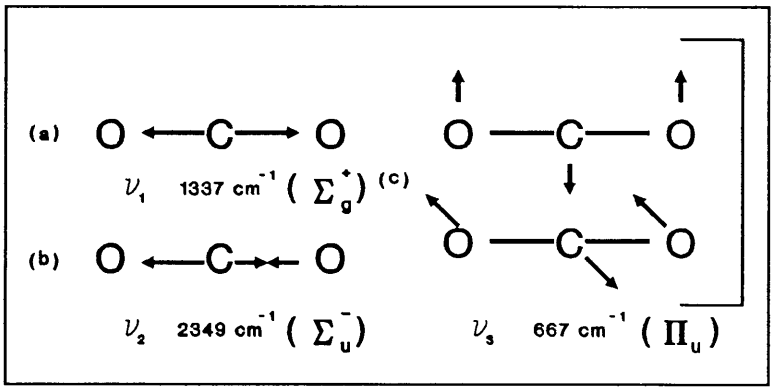

Fig. II.1 Normal modes of vibration of CO_2. The symmetry of each vibration is given in parentheses.

The FT-IR spectrum can be seen in fig. II.2 (low resolution).

2. Rotational motion

Energy levels

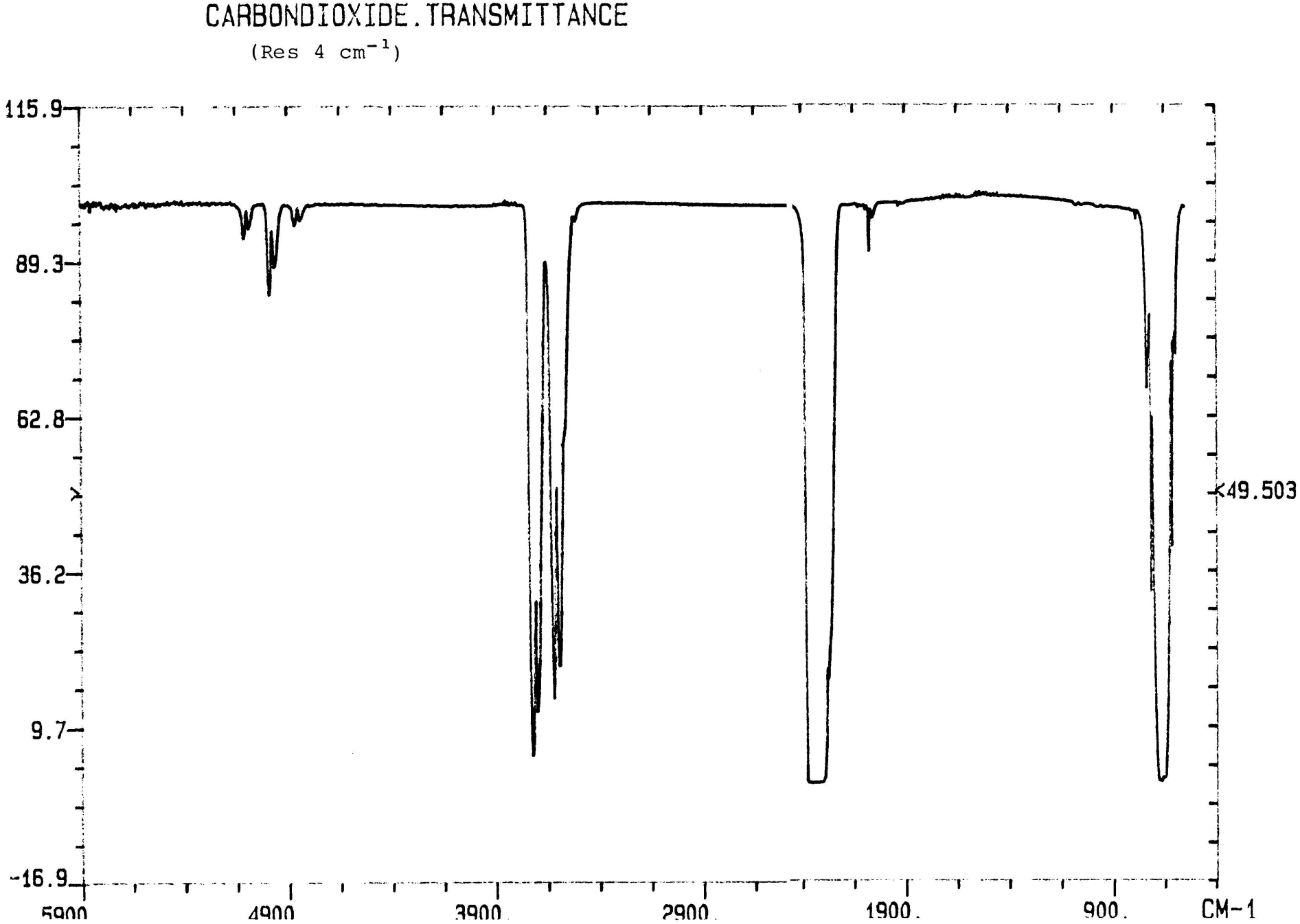

Fig. II.2

The angular momentum of the electrons about the internuclear axis is zero and therefore the moment of inertia I_c about the internuclear axis is exactly equal to zero (See fig. II.3). The energy levels are given by the same formula as for diatomic molecules [1].

$$F(J) = BJ(J+1) - D^2J^2(J+1)^2 + \ldots\ldots \qquad \text{II-1}$$

where $B = \dfrac{h}{8\pi^2 c I_B}$

I_B is the moment of inertia about an axis perpendicular to the internuclear axis going through the center of mass and $I_B = I_C$.

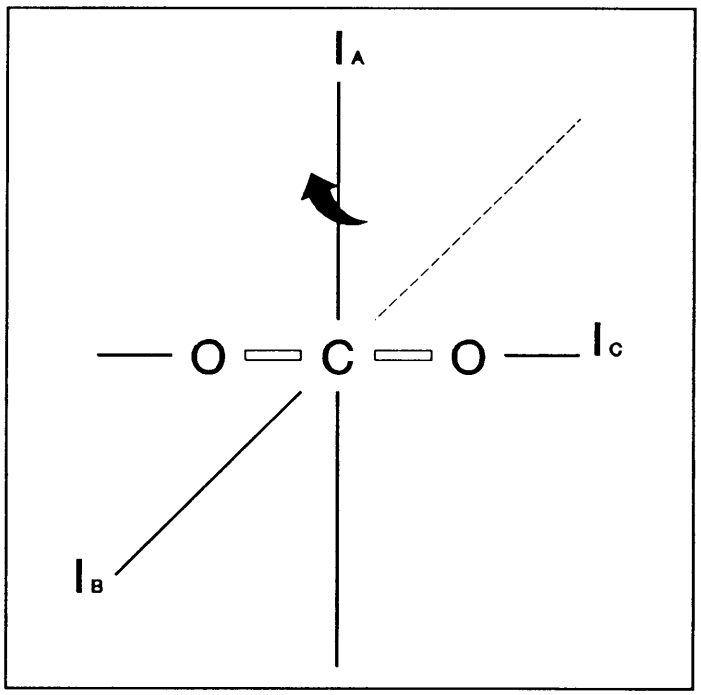

Fig. II.3

The general formula

$$I_B = \sum_i m_i r_i^2 \qquad \text{II-2}$$

must be used to calculate the moment of inertia where r_i is the distance of the i'th nucleus of mass m_i from the centre of mass. If equation II-2 is applied to the CO_2 molecule

$$I_B = 2m_o r_o^2 \qquad \text{II-3}$$

with m_o = mass of oxygen atom

r_o = bond length between oxygen and carbon atoms.

The term $D^2J^2(J+1)^2$ in eq. II-1 comes in because of the non-rigidity of the molecule. This term is exceedingly small compared to the term $BJ(J+1)$. It represents the influence of the centifugal force which results in a very slight increase in the internuclear distances when the molecule is rotating in the various vibrational levels. The constant D is related to B by the formula

$$D = \frac{3B^3}{\omega^2} \qquad \text{II-4}$$

where ω is the frequency of the totally symmetric vibration (see fig. II.1).

3. Interaction of Rotation and Vibration

In a first approximation the energy of a linear molecule, carrying out simultaneous rotation and vibration, is simply the sum of the rotational- and vibrational energy

$$T = G(v_1,v_2,v_3,.....) + F(J) \qquad \text{II-5}$$

where the terms G and F represent the vibrational and rotational energy respectively. The interaction between rotation and vibration manifests itself in that the rotational constant B has a slightly different value for the different vibrational levels. This is because the moment of inertia I changes during a vibration in such a way that the average value of $\frac{1}{I}$ is not the same as its value in the equilibrium position.

The rotational constant $B_{[v]}$ in vibrational state v_i is given by

$$B_{v_1,v_2,v_3} = B_{[v]} = B_e - \sum_i \alpha_i(v_i + \frac{d_i}{2}) \qquad \text{II-6}$$

It is to be expected that $B_{[v]}$ will be somewhat smaller than the constant B_e, which corresponds to the equilibrium separation r_e. With increasing vibration, because of

the anharmonicity, the mean nuclear separation will be greater. Here α_i is small compared to B_e, since the change in internuclear distances by vibration is small compared to the internuclear distance itself. In eq. II-6, d_i is the degree of degeneracy of the vibration ν_i and [v] stands for all the vibrational quantum numbers.

4. Symmetry properties

The total eigenfunction in zero approximation is a product of the electronic, vibrational and rotational eigenfunctions.

$$\psi_T = \psi_e\psi_v\psi_r \qquad \text{II-7.}$$

The rotational level of a linear polyatomic molecule is called positive or negative depending on whether the total eigenfunction ψ_T remains unaltered or changes its sign by reflection of all particles (electrons and nuclei) at the origen (inversion). This operation is illustrated in fig. II.4.

Inversion of the electronic part of the wave function can be accomplished by rotating the entire molecule by 180 deg. about an axis perpendicular to the internuclear axis and then performing a reflection through a plane perpendicular to this rotation axis and passing through the internuclear axis. Since the first step in the process leaves the coordinates of the electrons unchanged with respect to the nuclei, it does not alter ψ_e. The second step reflects the electronic wave function through the designated plane, and the result of this reflection depends on the particular wave function that describes the electronic state of the molecule [2].

For linear molecules, with even numbers of electrons, the electronic ground-state function is positive both above and below any plane passing through the internuclear axis. It can therefore be concluded that an inversion of ψ_e through the origin leaves ψ_e unaltered.

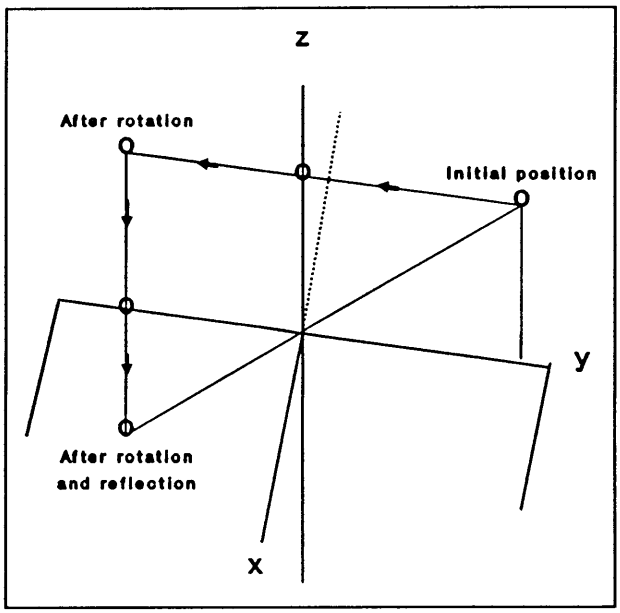

Fig. II.4 Illustration that rotation by 180 deg around an axis and reflection through a plane perpendicular to the axis correspond to inversion through the origin.

The vibrational component ψ_v, of the total wave function, depends on the magnitude of the internuclear distance. It follows that ψ_v will also be unaffected by an inversion through the origen since this operation leaves the magnitude of the internuclear distance unaltered.

If the electronic and vibrational eigenfunctions are unchanged by all symmetry operations of the molecule, the symmetry character positive-negative depends on that of ψ_r only. The polar coordinate equivalent to the inversion implied by xyz → -x,-y,-z is obtained by

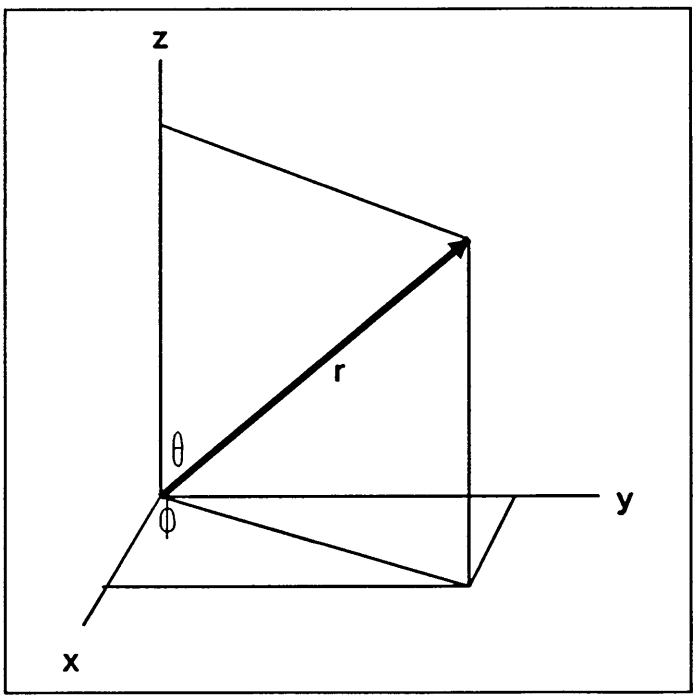

Fig. II.5 Polar coordinates.

replacing r,θ and ϕ by r,π-θ and $\pi+\phi$ (fig. II.5). The effect of this inversion on ψ_r can either be seen analytically by this replacement in the expressions given in table II-1 or diagrammatically from the wave functions depicted in fig. II.6 [2]. On either basis it can be seen that for even values of J the function ψ_r remains unchanged by inversion, while for odd values of J the function ψ_r changes sign. With recognition that ψ_e and ψ_v are unchanged by invertion, it can be deduced that ψ_T behaves in a manner dictated by ψ_r as shown in fig. II.7.

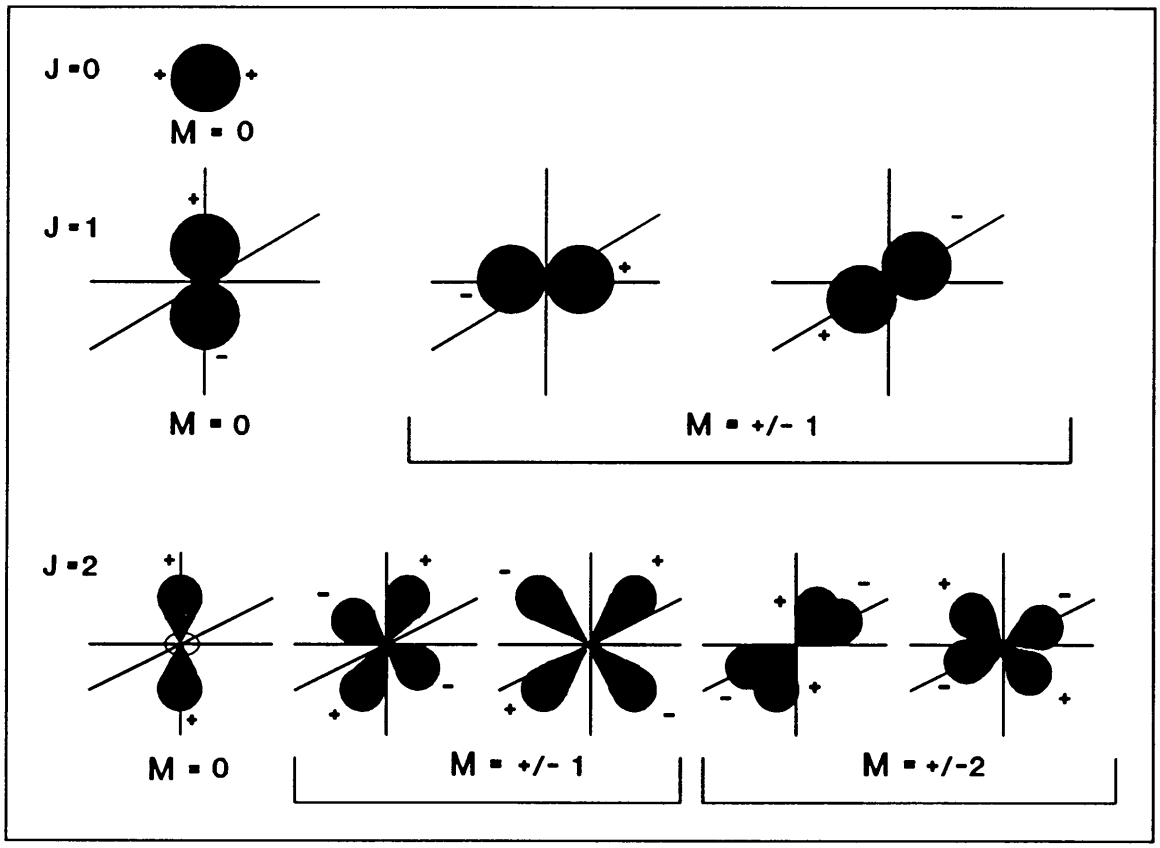

Fig. II.6 Diagrammatic representations of the rotational wave functions for J = 0, 1 and 2.

Table II-1. Some of the Wave Functions for a Rigid Rotating Linear Molecule

J = 0	M = 0	$\psi = \frac{1}{2\sqrt{\pi}}$
J = 1	M = 0	$\psi = \frac{1}{2}\sqrt{\frac{3}{\pi}}\cos\theta$
	M = ±1	$\psi = \frac{1}{2}\sqrt{\frac{3}{2\pi}}\sin\theta e^{\pm i\phi}$ or
		$\psi = \frac{1}{2}\sqrt{\frac{3}{\pi}}\sin\theta\cos\phi$ $\frac{1}{2}\sqrt{\frac{3}{\pi}}\sin\theta\sin\phi$
J = 2	M = 0	$\psi = \frac{1}{4}\sqrt{\frac{5}{\pi}}(3\cos^2\theta - 1)$
	M = ±1	$\psi = \frac{1}{2}\sqrt{\frac{15}{2\pi}}\sin\theta\cos\theta e^{\pm i\phi}$ or
		$\psi = \frac{1}{2}\sqrt{\frac{15}{\pi}}\sin\theta\cos\theta\sin\phi$ $\frac{1}{2}\sqrt{\frac{15}{\pi}}\sin\theta\cos\theta\sin\phi$
	M = ±2	$\psi = \frac{1}{4}\sqrt{\frac{15}{2\pi}}\sin^2\theta e^{\pm 2i\phi}$ or
		$\psi = \frac{1}{4}\sqrt{\frac{15}{\pi}}\sin^2\theta\cos 2\phi$ $\frac{1}{4}\sqrt{\frac{15}{\pi}}\sin^2\theta\sin 2\phi$

5. Nuclear spin statistical weights and their effect on intensities

For CO_2, belonging to the pointgroup $D_{\infty h}$, the property symmetric or antisymmetric with respect to an exchange of identical oxygen nuclei must be added. The spin of the nuclei is the index which determines whether the wave function must be

unchanged, i.e., symmetric, or must be changed in sign, i.e., antisymmetric, with respect to an exchange of identical particles.

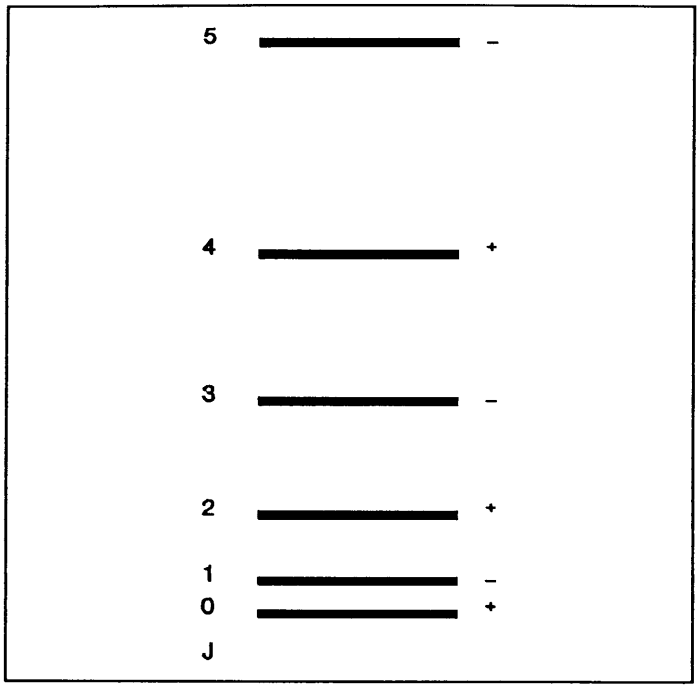

Fig. II.7 The positive-negative character, showing the behavior of ψ_{total} on inversion, of the rotational levels for those molecules with

When the effects of nuclear spin are included the total molecular wave function ψ_T becomes

$$\psi_T = \psi_e\psi_v\psi_r\psi_{ns} \quad \text{II-8.}$$

where ψ_e, ψ_v and ψ_r have the same meanings as in eq. II-7 and ψ_{ns} is the nuclear spin wave function. The concern here is the symmetry properties of ψ_{ns}.

For any molecule containing two or more identical nuclei having $I = n+½$, where n is zero or an integer, exchange of any two of them results in a change of sign of the total wave function ψ_T which is said to be antisymmetric to nuclear exchange. These type of nuclei are said to be Fermi particles (fermions) and obey Fermi-Dirac statistics. For $I = n$, where n is zero or an integer, ψ_T is symmetric to nuclear exchange, and the nuclei are said to be Bosè particles (bosons) and obey Bose-Einstein statistics [3].

Considering the consequences of the above reasoning in the case of CO_2 it can be

assumed that ψ_e and ψ_v are both symmetric to nuclear exchange. This means that it is only necessary to consider the behavior of $\psi_r\psi_{ns}$. Since I = o for ^{16}O, ψ_T and therefore $\psi_r\psi_{ns}$ must be symmetric to nuclear exchange.

$$\psi_T = \underset{s}{\psi_e\psi_v}\ \underset{s}{\psi_r\psi_{ns}}$$

The following two possibilities should be taken into account

	$\psi_r = s$		J even $\Rightarrow$ ψ_r simmetric (s) to exchange
and	$\psi_{ns} = s$		$\uparrow\uparrow$ (ortho)
	or		
	$\psi_r = a$		J uneven $\Rightarrow$ ψ_r anti-symmetric (a) to exchange
and	$\psi_{ns} = a$		$\uparrow\downarrow$ (para)

Since I = o the nuclear spin wave function $\psi_{ns} = 1$ which is symmetric to exchange of nuclei. Therefore as fig. II.8 shows that CO_2 has only levels with the rotational quantum number having even values. (This is in contrast with the O_2 molecule which has only odd J values).

The reasoning above holds for the assumption that the electronic ground state is totally symmetric and that the molecule is also in the totally symmetric (Σ_g^+) vibrational ground state. In $\Pi,\Delta,\ldots$ vibrational levels, for each value of J there is a positive and a negative level of very slightly different energy whose order alternates: +-,-+,+-,.... or -+,+-,-+,....

In the case of CO_2 (point group $D_{\infty h}$) the positive rotational levels are symmetric, the negative antisymmetric with respect to a simultaneous exchange of all pairs of identical nuclei for all vibrational levels that are symmetric with respect to an inversion (species Σ_g^+, Σ_g^-, Π_g, Δ_g), while the reverse is the case for all vibrational levels that are antisymmetric with respect to an inversion (species Σ_u^+, Σ_u^-, Π_u, Δ_u). This is shown in fig. II.9.

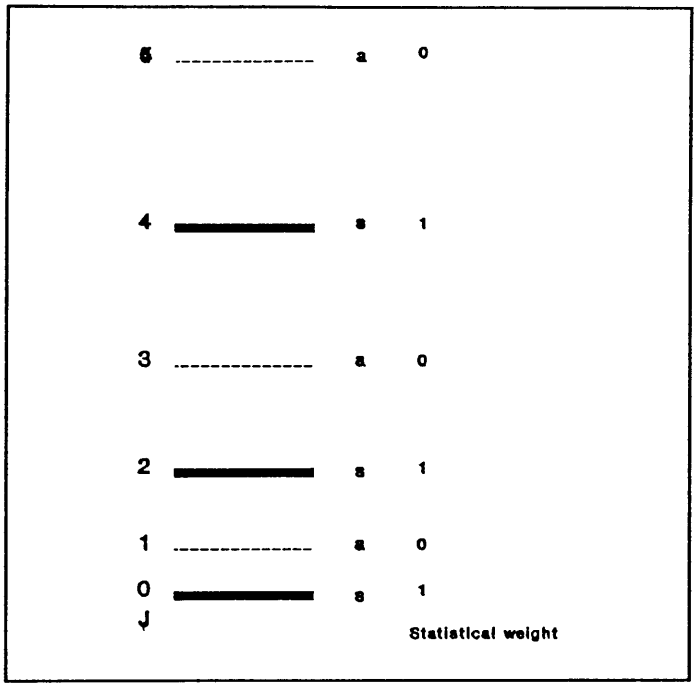

Fig. II.8

6. Coriolis interaction

The reasons why α, of the rotational constant B (see eq. II-6), varies with the vibrational quantum number are

1. The fact that the mean value for $\frac{1}{I}$ is not equal to $\frac{1}{I_e}$ although the mean value of r is r_e.

2. In consequence of the anharmonicity of the vibrations the mean value of r during a vibration is larger than r_e.

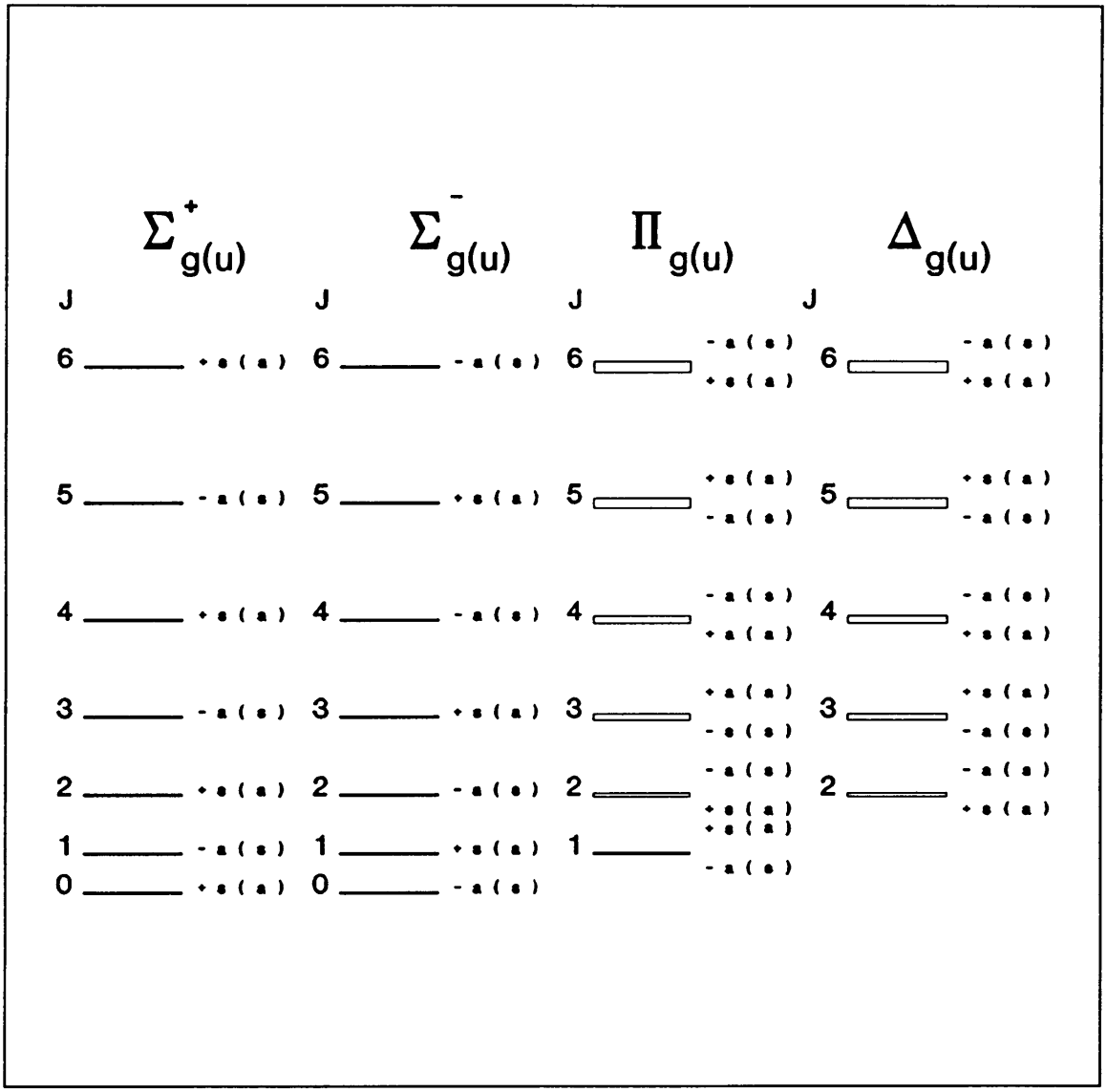

Fig. II.9 Symmetry properties of the rotational levels in various species of vibrational levels of linear molecules of point group $D_{\infty h}$.

3. Coriolis interaction:

For a uniformly rotating coordinate system, apart from the acceleration produced by the acting forces, Coriolis acceleration appears. This acceleration is brought about by the Coriolis force. The magnitude of this force is given by

$$F_{cor} = 2mv_a \omega \sin \eta \qquad \text{II-9}$$

where m is the mass of the particles, v_a its apparent velocity with respect to the moving coordinate system, r its distance from the axis of rotation, ω the angular velocity of the coordinate system with respect to a fixed coordinate system and η the angle between the axis of rotation and the direction of v_a.

It can thus be written that, for the rotational constants α_i, which represent the main influence of the coupling of rotation and vibration

$$\alpha_i = \alpha_i^{harm} + \alpha_i^{anh} + \alpha_i^{Cor} \qquad \text{II-10}$$

In order to visualize the Coriolis force more clearly its effect in CO_2 can be considered. Consider the vibration ν_3 in the rotating molecule. The displacement vectors give at the same time the relative velocities at any instant, for example when the nuclei pass through the equilibrium. The Coriolis force on each nucleus is proportional to this velocity but perpendicular to it and, for a counter-clockwise direction of rotation, always toward the right when looking in the direction of motion. These forces are indicated by the short line arrows in fig. II.10.

It is seen from this figure that during the vibration ν_3 these forces tend to excite the perpendicular vibration ν_2 but with the frequency of ν_3. It can also be seen from fig. II.10 that during the vibration ν_2 these forces tend to excite the parallel vibration ν_3, but with the frequency of ν_2.

If the frequencies of ν_2 and ν_3 were nearly the same, a strong excitation of one of the two vibrations would take place if the other were first excited, in consequence of this

Coriolis coupling. However, this excitation will be very weak when as is usually the case ν_2 and ν_3 have widely different frequencies.

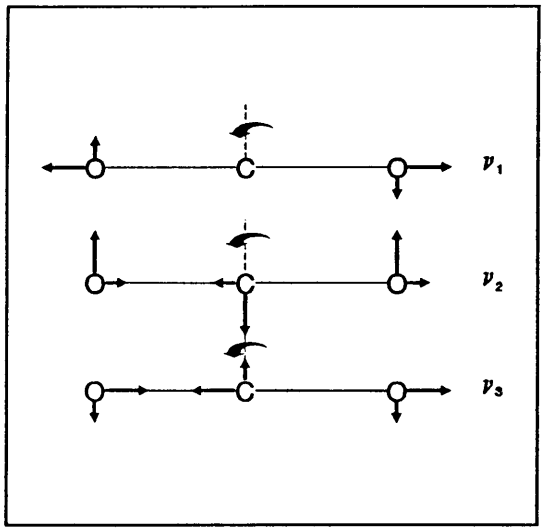

Fig. II.10 Coriolis forces in linear CO_2. - The curved arrow indicates the direction of rotation.

A general rule to determine whether there will be a Coriolis interaction between two vibrations is to obtain the direct product of the two symmetry species. If this product contains either R_x, R_y or R_z, as indicated in the character table (See table II-2), a Coriolis interaction will be present. The above description of a Coriolis interaction is known as a second-order Coriolis interaction.

Table II-2. Character table of the $D_{\infty h}$ point group

$D_{\infty h}$	E	$2C_\infty^\phi$	..	$\infty\sigma^\phi$	i	$2S_\infty^\phi$	..	∞C_2		
Σ_g^+	1	1	..	1	1	1	..	1		$(x^2\text{-}y^2,xy)$
Σ_g^-	1	1	..	-1	1	1	..	-1	R_z	
Π_g	2	2 cos ϕ	..	0	2	-2 cos ϕ	..	0	(R_x,R_y)	(xz,yz)
Δ_g	2	2 cos 2ϕ	..	0	2	2 cos 2ϕ	..	0		$(x^2\text{-}y^2,xy)$
..	..	..	..	..	..	..	..	..		
Σ_u^+	1	1	..	1	1	-1	..	-1	z	
Σ_u^-	1	1	..	-1	-1	-1	..	1		
Π_u	2	2 cos ϕ	..	0	-2	2 cos ϕ	..	0	(x,y)	
Δ_u	2	2 cos 2ϕ	..	0	-2	-2 cos 2ϕ	..	0		
..	..	..	..	..	..	..	..	..		

An example of a first-order Coriolis interaction can be found in the ν_2 bending vibration of CO_2. See fig. II.1(c). A rotation clockwise or anti-clockwise, of the vectors representing the ν_2 vibrational motion of CO_2 converts one of the motions illustrated into the other. Therefore when the molecule is in any excited vibrational state involving ν_2 there is a vibrational angular momentum about the internuclear axis. The magnitude of this momentum is $\ell \frac{k}{2\pi}$ where in general for a vibration ν_i.

$$\ell = v_i, v_i\text{-}2, v_i\text{-}4, \ldots., -v_i$$

in which v_i is the vibrational quantum number for the normal mode ν_i.

In the case of CO_2 spectrum recorded at room temperature $v_2 = 1$ which means that $\ell = \pm 1$. Taking into account this additional angular momentum the term values of equation II-1 are modified to

$$F(J) = B_v[J(J+1)-\ell^2]-D_v^2[J(J+1)-\ell^2]^2 \qquad \text{II-11}$$

where $J = |\ell|, |\ell|+1, |\ell|+2, \ldots.$ which means that the $J = 0$ level is missing for $v_2 = 1$. According to eq. II-11 the term values are independent of the sign of ℓ but this is true only if Coriolis interaction is neglected.

The two components of ν_2 undergo a rather special type of Coriolis interaction. As figure II-1(c) shows, the rotational angular momentum about the z axis due to excitation of ν_2 creates Coriolis forces on the nuclei which convert one co ponent of ν_2 into the other. Since the two interacting vibrations have the same wavenumber the

interaction is large - a so-called first order Coriolis interaction. The effect of this is to modify the term values of eq. II-11 to

$$F_v(J,l^{\pm}) = B_v[J(J+1)-l^2] \pm \frac{q_i}{4}(v_i+1)J(J+1) - D_v^2[J(J+1)-l^2]^2 \qquad \text{II-12}$$

where q_i is a parameter which depends on the coupling between the rotational and vibrational motions for vibration i. (in this case i = 2). The effect of the term involving q_i is to split the term values which differ only in the sign of ℓ by an amount equal to $(\frac{q_i}{2})(v_i+1)(J)(J+1)$. The splitting is known as ℓ-type doubling. It decreases with increasing ℓ. This effect can also be seen in fig. II.9 where it is greatly exagerated.

7. Selection rules and types of infrared bands

(a) The selection rules for the pure vibration spectrum and for the pure rotation spectrum are not changed by the interaction of vibration and rotation. Thus for the rotation-vibration spectrum in the infrared only those vibrational transitions occur for which M_z has the species Σ_u^+ or M_x and M_y have the species π_u.

The vibrational selection rules are

$\Delta\ell = 0, \pm 1$; $\Sigma^+ \leftrightarrow \Sigma^-$, $g \leftrightarrow g$; $u \leftrightarrow u$

and the rotational selection rules are

$\Delta J = 0, \pm 1$ $(J = 0 \leftrightarrow J = 0)$; $+ \longleftrightarrow -$; $s \leftrightarrow a$.

$\Delta J = 0$ is forbidden when $\ell = 0$ for both upper and lower state (Σ - Σ transitions).

(b) The following types of infrared bands of linear molecules can occur

1. Transitions for which $\ell = o$ in both upper and lower state ($\parallel$ bands, Σ - Σ transitions) Only $\Delta J = \pm 1$ can occur which means that only P and R branches occur.
2. Transitions for which $\Delta\ell = \pm 1$ ($\perp$ bands, π - Σ, Δ - Σ, ...). For these bands $\Delta J = o$ as well as $\Delta J = \pm 1$ are possible and therefore a P, Q and R branch will be present.
3. Transitions for which $\Delta\ell = o$ but $\ell \neq o$ ($\parallel$ bands, π - π, Δ - Δ). The P, Q and R branches will also be present. Since $M_z \neq o$ the Q branch is weak, the intensity decreasing from the first line instead of reaching first a maximum like the P and R branches.

Figures II.11; II.12 and II.13 illustrates the above-mentioned types of bands as well as the selection rules.

The formulae for the two branches R and P corresponding to $\Delta J = +1$ and -1 respectively are

$$R(J) = \nu_o + 2B' + (3B' - B'')J + (B' - B'')J^2 \qquad \text{II-13}$$

$$P(J) = \nu_o - (B' + B'')J + (B' - B'')J^2 \qquad \text{II-14}$$

where J is the lower state quantum number, B′ and B″ are the rotational constants for the upper and lower states respectively. The band origin is indicated by ν_o. Higher terms, J^3 and J^4 have to be added if the D is not

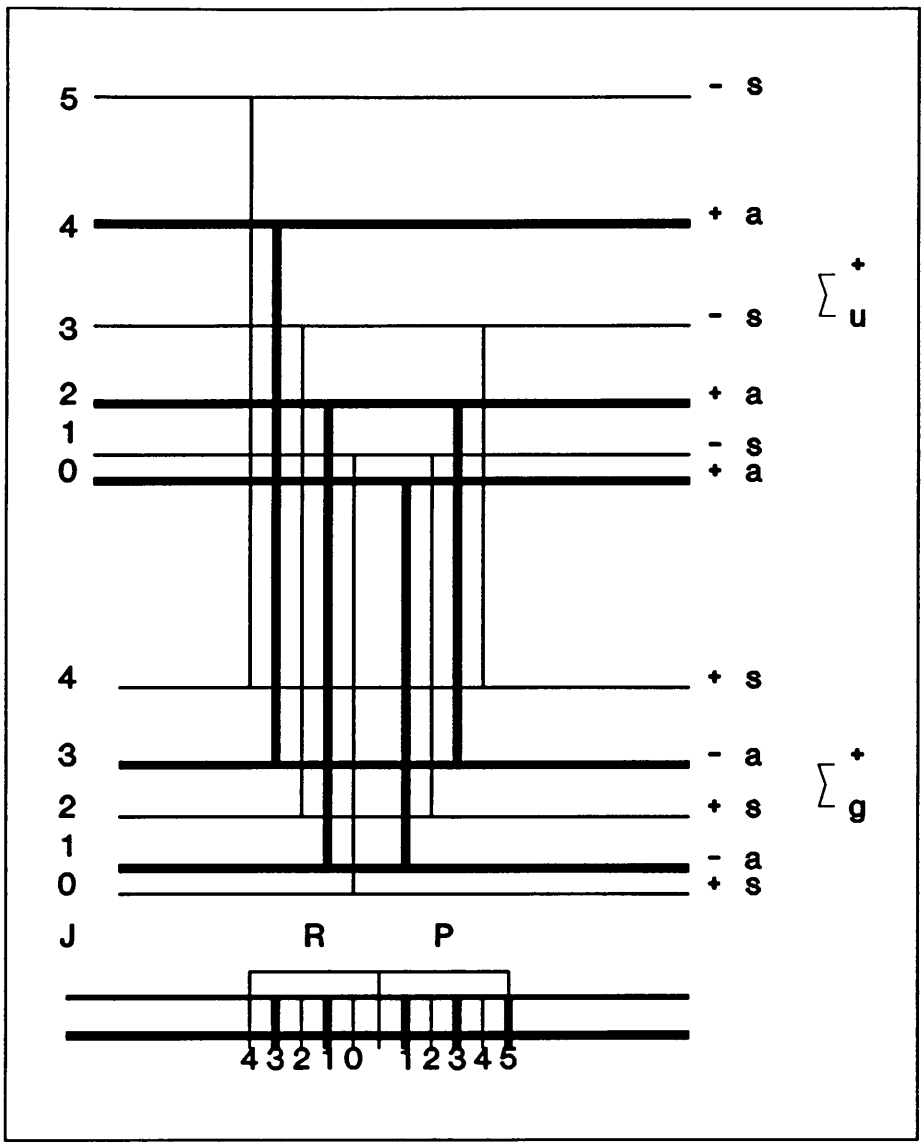

Fig. II.11 $\Sigma_u^+ - \Sigma_g^+$ transition

negligibly small. The two branches can also be represented by a single formula.

$$\nu = \nu_0+(B'+B'')m+(B'-B'')m^2 \qquad \text{II-15}$$

where m = J+1 for the R-branch and m = -J for the P-branch.

The formula for the Q-branch is

$$Q(J) = \nu_0+(B'-B\nu)J+(B'-B'')J^2 \qquad \text{II-16}$$

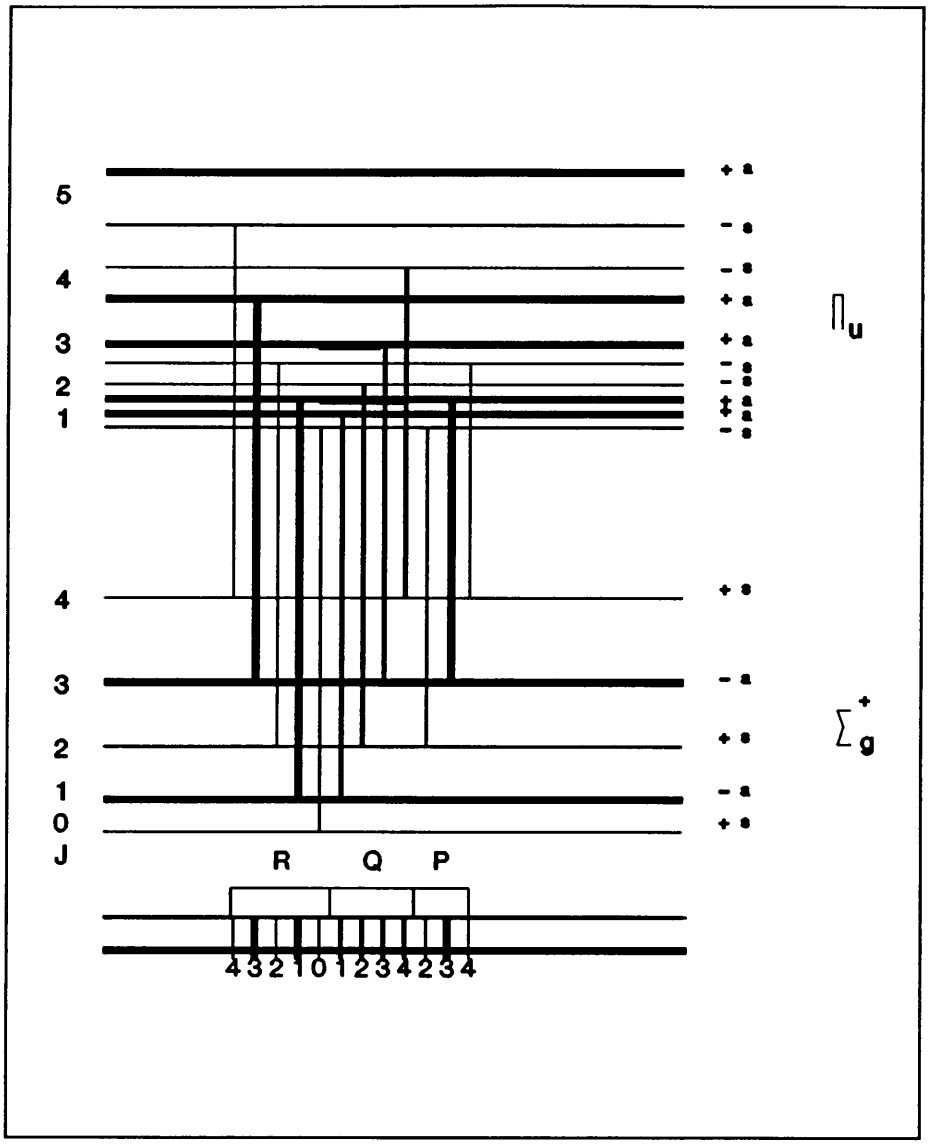

Fig. II.12 The Π_u-Σ_g^+ transition

For the fundamentals and low overtone combination bands B′-B″ is very small and therefore all lines of the Q branch fall practically together unless one makes use of a high-resolution spectrofotometer.

8. Determination of rotational constants -

A reliable method to evaluate rotational constants is called the combination differences method. The principle of this method is as follows:

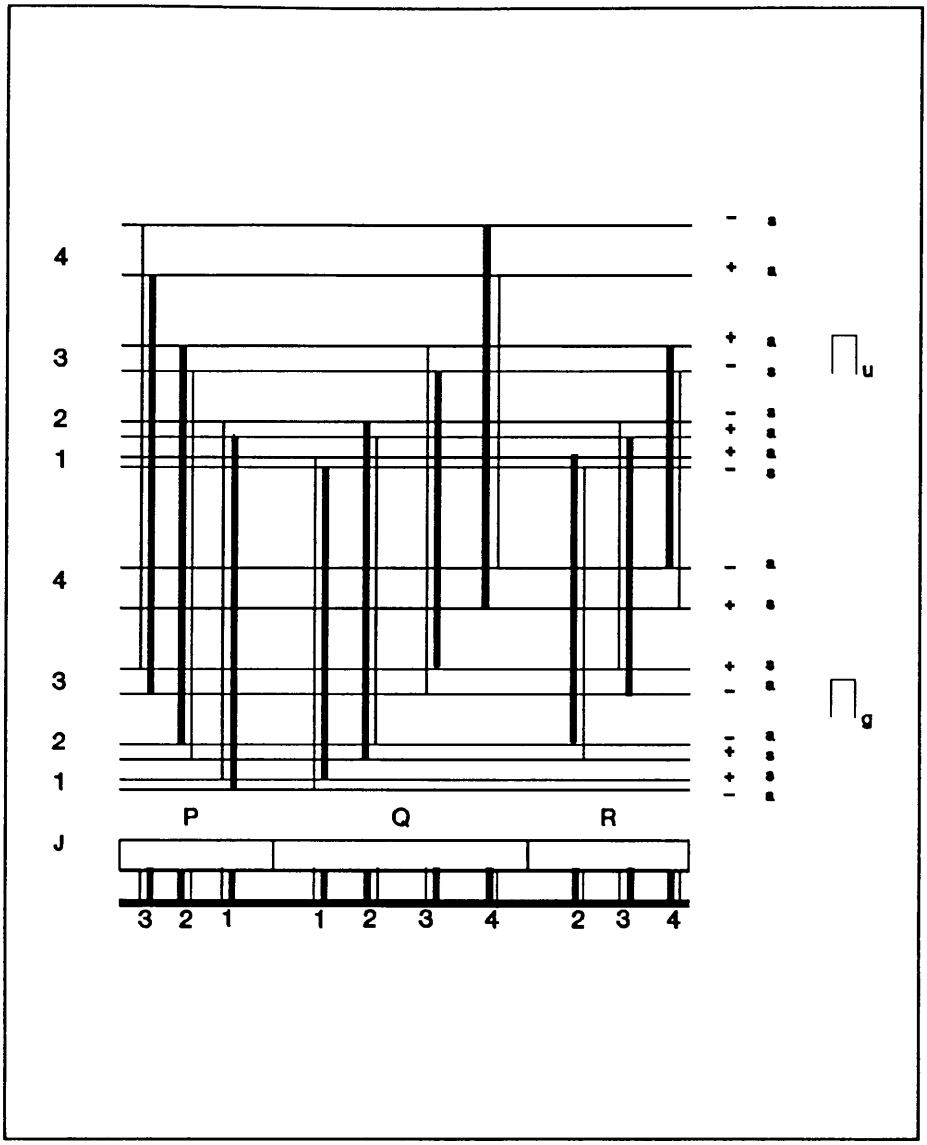

Fig. II.13 Π_u - Π_g transition

Differences in wave number between transitions with a common upper state are dependent on properties of the lower states only. Similarly differences in wavenumber between transitions with a common lower state are dependent on properties of the upper states only.

In the case of a vibration-rotation band it is clear from fig. II.11 that, since R(1) and P(1) have a common lower state with $J'' = 1$ then $\bar{\nu}[R(1)]-\bar{\nu}[P(1)]$ must be a function

of B′ only. The transitions R(1) and P(3) have J′ = 2 in common and, in general, $\bar{\nu}$[R(J-1)]-$\bar{\nu}$[P(J+1)] must be a function of B″ only. It can be seen from this definition that

$$R(J)\text{-}P(J) = F'(J+1)\text{-}F''(J-1) = \Delta_2F'(J) \qquad \text{II-17}$$

and

$$R(J-1)\text{-}P(J+1) = F''(J+1)\text{-}F''(J-1) = \Delta_2F''(J) \qquad \text{II-18}$$

If now eq. II-18 is substituted for F(J) (see eq. II-2) then

$$\begin{aligned}\Delta_2F''(J) &= \bar{\nu}[R(J-1)\text{-}\bar{\nu}[P(J+1)] \\ &= [\bar{\nu}_o+B'J(J+1)\text{-}B''J(J-1)]\text{-}[\bar{\nu}_o+B'J(J+1)\text{-}B''(J+1)(J+2)] \\ &= 4B''(J+½) \qquad \text{II-19}\end{aligned}$$

similarly

$$\begin{aligned}\Delta_2F'(J) &= \bar{\nu}_o+B'(J+1)(J+2)\text{-}B''J(J+1)\text{-}[\bar{\nu}_o+B'(J+1)J\text{-}B''J(J+1)] \\ &= 4B'(J+½) \qquad \text{II-20}\end{aligned}$$

and a graph of $\Delta_2F'(J)$ versus $(J+½)$ is a straight line with slope 4B′.

Any effects of centrifugal distortion will show up as a slight curvature of the $\Delta_2F(J)$ versus $(J+½)$ graphs. If the term - $DJ^2(J+1)^2$ is included in the rotational term value expression then

$$\Delta_2F''(J) = (4B''\text{-}6D'')(J+½)\text{-}8D''(J+½)^3 \qquad \text{II-21}$$

and

$$\Delta_2F'(J) = (4B'\text{-}6D')(J+½)\text{-}8D'(J+½)^3 \qquad \text{II-22}$$

A graph of $\Delta_2''F(J)/J+½$ versus $(J+½)^2$ is a straight line line slope 8D″ and intercept 4B″ or strictly 4B″ - 6D″ but 6D″ may be too small to affect the intercept. Similarly

a graph of $\Delta_2F'(J)/J+½$ versus $(J+½)^2$ is a straight line of slope $8D'$ and intercept $4B'$. The band centre is not quite midway between R(0) and P(1) but its wavenumber can be obtained as follows

$$\bar{\nu}_o = \bar{\nu}[R(0)]-2B' \qquad \text{II-23}$$

or $$\bar{\nu}_o = \bar{\nu}[P(1)]+2B'' \qquad \text{II-24}$$

The formation of the combination differences also gives an extremely valuable and critical check on the correctness of the analyses and of the analysis and the consistency of the data if two or more bands with the same lower or same upper state have been measured, since the $\Delta_2F(J)$ for the common state formed from the two or more bands must agree for every J value within the accuracy of the measurements. The B value of the common state is then, of course, determined from the average of the respective $\Delta_2F(J)$ values.

The difference of the B values $B'-B''$ for a given band can be obtained with still greater accuracy from R(J-1)+P(J) or if a resolved Q branch is present, from Q(J).

$$R(J-1)+P(J) = 2\nu_o-2(B'-B'')J^2 \qquad \text{II-25}$$

in other words, when R(J-1)+(P(J) is plotted against J^2 a straight line is obtained whose slope is $2(B'-B'')$ and whose intercept on the ordinate axis gives an accurate value of ν_o, that is, of the zero line. Similarly according to eq. II-16 when Q(J) is plotted against J(J+1) a straight line of slope $B'-B''$ and intercept ν_o is obtained.

The normal procedure is to determine only one B value from the combination differences, and all the others by finding first the $B'-B''$ value from R(J-1)+P(J) or Q(J). This gives a greater relative than absolute accuracy of the B-values for the

various vibrational states and therefore the rotational constants α, which involve the differences of B values, can be obtained more reliably than if each B were determined independently.

In the case of accurate measurements of Π-Σ bands from R(J)-P(J) or R(J-1)+P(J) only the B value of one ℓ-doubling component of the π state is obtained. If the Q branch is resolved, the other component of the ℓ-doubling can be obtained. The difference of these two B values is the constant q of the ℓ-type doubling.

$$\Delta v = qJ(J+1) \qquad \text{II-26}$$

9. High Resolution FT-IR Spectrum

The FT-IR spectrum of CO_2 has been recorded on a Brucker 113V spectrometer. The resolution was 0,03 cm^{-1}. A 10 cm gas cell was filled with pure CO_2 at atmospheric pressure.

The high resolution spectra of the ν_2 and ν_3 bands are shown in fig. II.14 and Fig. II.15 respectively.

The wavenumbers of the rotation lines of the P and R branches are tabulated in table II-3 and table II-4 respectively (See appendix).

Data on the Q branches could not be obtained since the maximum resolution of the instrument (0,03 cm^{-1}) was not sufficient to resolve the rotation lines of the Q branches.

The quantum mechanics of the vibrations and rotations of a symmetrical linear molecule has been discussed in detail by Dennison [4]. The symmetrical vibration ν_1 of the two extreme atoms along the line connecting them is infrared inactive, since here no change in electric dipole moment results. The symmetrical vibration ν_2 normal to the linear axis necessarily involves changes in the electric dipole moment having components along the axis of rotation and exhibits P, Q and R branches with the Q branch centred at 667,3 cm^{-1}. The third fundamental vibration ν_3 is an unsymmetrical one involving changes in the electric dipole moment normal to the axis of rotation giving rise to an intense absorption band centred at 2349 cm^{-1} with P and R branches. According to Dennison the combination relations are particularly characteristic. While $\Delta\nu_1$ may be an integer, the value of $\Delta\nu_2 + \Delta\nu_3$ must always be odd. Many possibilities are thus excluded, among them the first harmonic bands. Q branches only occur when $\Delta\nu_2$ is odd. The most intense of the combination bands to be expected are $\nu_3 + 2\nu_2$ and $\nu_3 + \nu_1$ both doublets following in the neighbourhood of 3707 cm^{-1}. The data for all the vibration bands are listed in table II-5 [2].

As has been discussed in Sec. 5 of this chapter, a necessary symmetry property of the wave function ψ_T for a linear triatomic molecule with identical extreme atoms excludes either those alternate rotation states for which ψ_R is symmetrical, or those for which ψ_R is antisymmetrical, ψ_R being the factor of ψ_T affected by an interchange of identical atoms. It is to be expected that for those vibration states of CO_2 in which $\ell = 0$ the rotational quantum number J may assume only even or only odd values. Which of these sets is excluded depends upon the symmetry properties of the remaining factors of ψ_T (See Sec. 5). In those bands involving the transitions in

Table II-5

ν_{vacuum}, observed (cm^{-1})	Band type[13]	Upper state [14]		Lower state[14]		ν, calculated[15] (cm^{-1})
		$v_1\ v_2^l\ v_3$	Species	$v_1\ v_2^l\ v_3$	Species	
667.3	I. ⊥ v.s.	$0\ 1^1\ 0$	Π_u	$0\ 0^0\ 0$	Σ_g^+	667.3*
1285.5[16]	R. pol. v.s.	$0\ 2^0\ 0$	Σ_g^+	$0\ 0^0\ 0$	Σ_g^+	1285.8
1388.3[16]	R. pol. v.s.	$1\ 0^0\ 0$	Σ_g^+	$0\ 0^0\ 0$	Σ_g^+	1388.1
1932.5	I. ⊥ m.	$0\ 3^1\ 0$	Π_u	$0\ 0^0\ 0$	Σ_g^+	1931.9*
2076.5	I. ⊥ m.	$1\ 1^1\ 0$	Π_u	$0\ 0^0\ 0$	Σ_g^+	2088.1*
2284.5	I. ∥ $C^{13}O_2^{16}$	$0\ 0^0\ 1$	Σ_u^+	$0\ 0^0\ 0$	Σ_g^+	(see p.230)
2349.3[17]	I. ∥ v.s.	$0\ 0^0\ 1$	Σ_u^+	$0\ 0^0\ 0$	Σ_g^+	2349.4*
3609	I. ∥ s.	$0\ 2^0\ 1$	Σ_u^+	$0\ 0^0\ 0$	Σ_g^+	3613.2
3716	I. ∥ s.	$1\ 0^0\ 1$	Σ_u^+	$0\ 0^0\ 0$	Σ_g^+	3715.6
4860.5	I. ∥ m.	$0\ 4^0\ 1$	Σ_u^+	$0\ 0^0\ 0$	Σ_g^+	4852.8
4983.5	I. ∥ m.	$1\ 2^0\ 1$	Σ_u^+	$0\ 0^0\ 0$	Σ_g^+	4981.4*
5109	I. ∥ m.	$2\ 0^0\ 1$	Σ_u^+	$0\ 0^0\ 0$	Σ_g^+	5104.3
6077	I. ∥ w.	$0\ 6^0\ 1$	Σ_u^+	$0\ 0^0\ 0$	Σ_g^+	6074.5
6231	I. ∥ w.	$1\ 4^0\ 1$	Σ_u^+	$0\ 0^0\ 0$	Σ_g^+	6231.4
6351	I. ∥ w.	$2\ 2^0\ 1$	Σ_u^+	$0\ 0^0\ 0$	Σ_g^+	6354.4
6510	I. ∥ w.	$3\ 0^0\ 1$	Σ_u^+	$0\ 0^0\ 0$	Σ_g^+	6518.9
6976	I. ∥ w.	$0\ 0^0\ 3$	Σ_u^+	$0\ 0^0\ 0$	Σ_g^+	6973.1
8193	P.I. ∥ v.w.	$0\ 2^0\ 3$	Σ_u^+	$0\ 0^0\ 0$	Σ_g^+	8192.9
8293	P.I. ∥ v.w.	$1\ 0^0\ 3$	Σ_u^+	$0\ 0^0\ 0$	Σ_g^+	8295.5
11496.5[18]	P.I. ∥ v.w.	$0\ 0^0\ 5$	Σ_u^+	$0\ 0^0\ 0$	Σ_g^+	11496.5*
12672.4[18]	P.I. ∥ v.w.	$0\ 2^0\ 5$	Σ_u^+	$0\ 0^0\ 0$	Σ_g^+	12672.4*
12774.7[18]	P.I. ∥ v.w.	$1\ 0^0\ 5$	Σ_u^+	$0\ 0^0\ 0$	Σ_g^+	12774.7*
618.1	I. ⊥ m.	$0\ 2^0\ 0$	Σ_g^+	$0\ 1^1\ 0$	Π_u	618.5
668.3	I. ⊥	$0\ 2^2\ 0$	Δ_g	$0\ 1^1\ 0$	Π_u	668.1*
720.5	I. ⊥ m.	$1\ 0^0\ 0$	Σ_g^+	$0\ 1^1\ 0$	Π_u	720.8*
1264.8[16]	R. m.	$0\ 3^1\ 0$	Π_u	$0\ 1^1\ 0$	Π_u	1264.6
1409.0[16]	R. m.	$1\ 1^1\ 0$	Π_u	$0\ 1^1\ 0$	Π_u	1409.8
1886	I. ⊥ w.	$0\ 4^0\ 0$	Σ_g^+	$0\ 1^1\ 0$	Π_u	1880.1
2094	I. ⊥ m.	$1\ 2^2\ 0$	Δ_g	$0\ 1^1\ 0$	Π_u	2094.9
2137	I. ⊥ m.	$2\ 0^0\ 0$	Σ_g^+	$0\ 1^1\ 0$	Π_u	2131.5
596.8	I. ⊥ w.	$0\ 3^1\ 0$	Π_u	$0\ 2^2\ 0$	Δ_g	596.5
647.6	I. ⊥ w.	$0\ 3^1\ 0$	Π_u	$0\ 2^0\ 0$	Σ_g^+	646.1
740.8	I. ⊥ w.	$1\ 1^1\ 0$	Π_u	$0\ 2^2\ 0$	Δ_g	741.7
790.8	I. ⊥ v.w.	$1\ 1^1\ 0$	Π_u	$0\ 2^0\ 0$	Σ_g^+	791.3
960.8	I. ∥ w.	$0\ 0\ 1$	Σ_u^+	$1\ 0^0\ 0$	Σ_g^+	961.3
1063.6	I. ∥ w.	$0\ 0\ 1$	Σ_u^+	$0\ 2^0\ 0$	Σ_g^+	1063.6*
1242.[16]	R. w.	$0\ 4^2\ 0$	Δ_g	$0\ 2^2\ 0$	Δ_g	1248.0
1305.1[19]	R. v.w.	$0\ 4^2\ 0$	Δ_g	$0\ 2^0\ 0$	Σ_g^+	1297.6
1325.0	R. v.w.	?		?		?[20]
1344.1[19]	R. v.w.	$1\ 2^0\ 0$	Σ_g^+	$0\ 2^2\ 0$	Δ_g	1340.4
1369.4[19]	R. v.w.	$1\ 2^2\ 0$	Δ_g	$1\ 0^0\ 0$	Σ_g^+	1374.1
1430.[16]	R. w.	$1\ 2^2\ 0$	Δ_g	$0\ 2^2\ 0$	Δ_g	1426.8
1528	R. w.	$2\ 0^0\ 0$	Σ_g^+	$0\ 2^0\ 0$	Σ_g^+	1513.0

which $\Delta\ell = \pm 1$ alternate lines will be completely suppressed and the proper J transitions may be assigned only after it has been decided which are the missing levels.

This decision has been made on a theoretical basis in Section 5. The presence of a Q branch complicates this decision for a Q-branch can be so broad that it totally obscures several of the neighbouring rotation lines. The band centred at 720 cm^{-1} (ν_1-ν_2) is favourable for this type of observation. The vibration-rotation spectrum of this band is shown in fig. II.16 and the wavenumbers of the rotation lines are tabulated in table II.6

Table II-6

J	R(J)	P(J)
2	722.340946	718.438763
4	723.922913	716.871867
6	725.45968	715.304962
8	727.011514	713.722996
10	728.548281	712.156096
12	730.100115	710.559063
14	731.621816	708.992163
16	733.17365	707.39513
18	734.710417	705.813164
20	736.232118	704.201065
22	737.768886	702.619098
24	739.275521	701.006999
26	740.797222	699.3949
28	742.303856	697.797867
30	743.810491	696.185768
32	745.317126	694.588735
34	746.823761	692.976636
36	748.315329	691.34947
38	749.821964	689.722305
40	751.313532	688.110206
42	752.8051	686.498107
44	754.296669	684.870941
46	755.788237	683.243776
48	757.279805	681.631676
50	758.771374	680.019577
52	760.247876	678.407478
54	761.73944	676.810445

If their positions could be determined precisely a criterion would be provided for assigning odd and even J values as is indicated by the band patterns in the right section of fig. II.17. The rotation lines adjacent to the bands, centred at 2349 cm^{-1} (ν_3) and 720 cm^{-1} (ν_1-ν_2), taken from fig. II.15 and II.16 have been plotted in the right sections of fig. II.17 and fig. II.18. The position of the zero branches show clearly that even numbers must be used for the J values of the upper states (also for the lower states). This conclusion is in agreement with the reasoning in Sec. 5, where it was concluded, on the basis of the symmetry of the wave functions, that only the even J values are allowed.

Fig. II.14 High resolution FT-IR spectrum (0,03 cm^{-1}) of the ν_2 band of CO_2

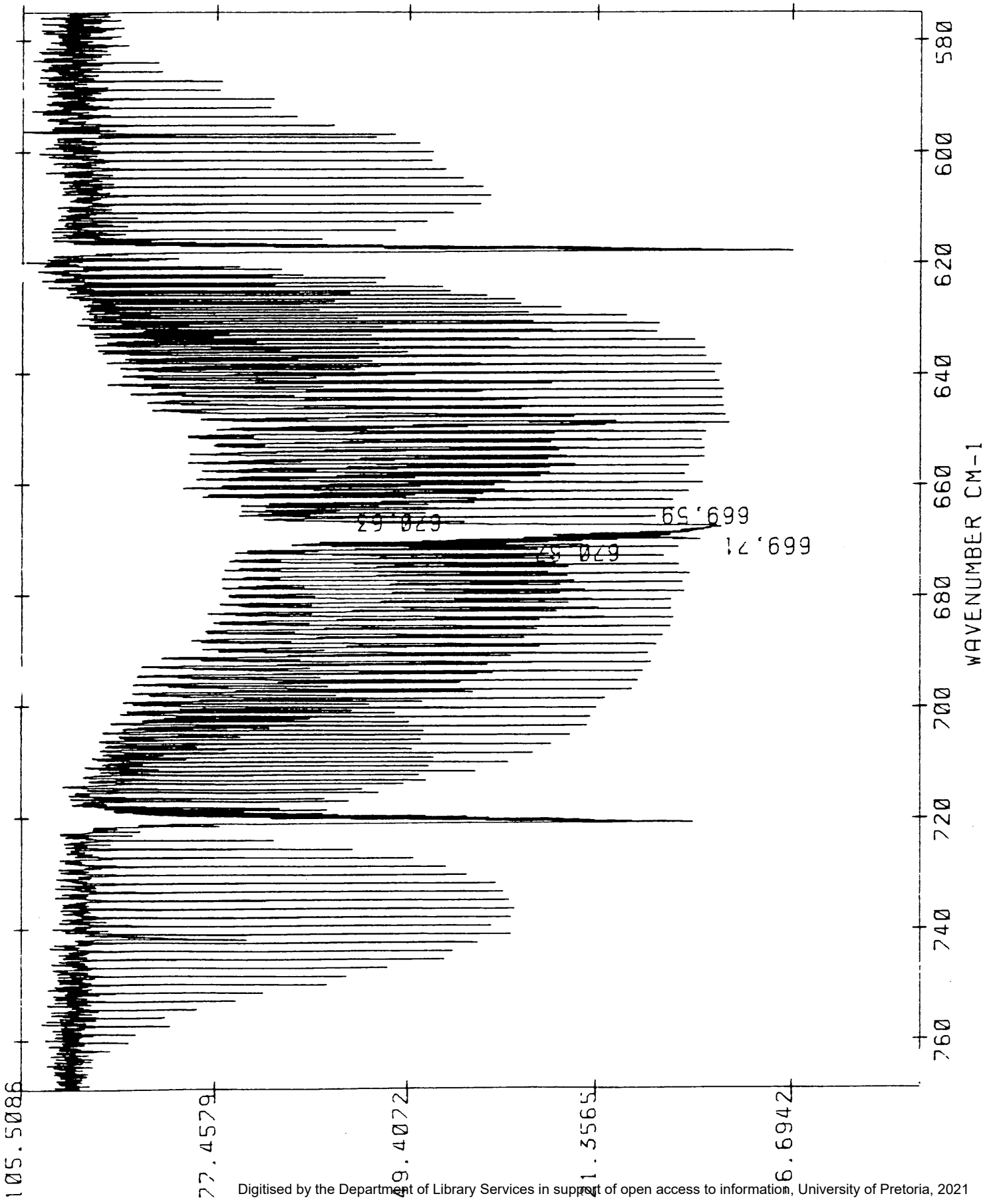

Fig. II.15 High resolution FT-IR spectrum (0,03 cm^{-1}) of the ν_3 band of CO_2

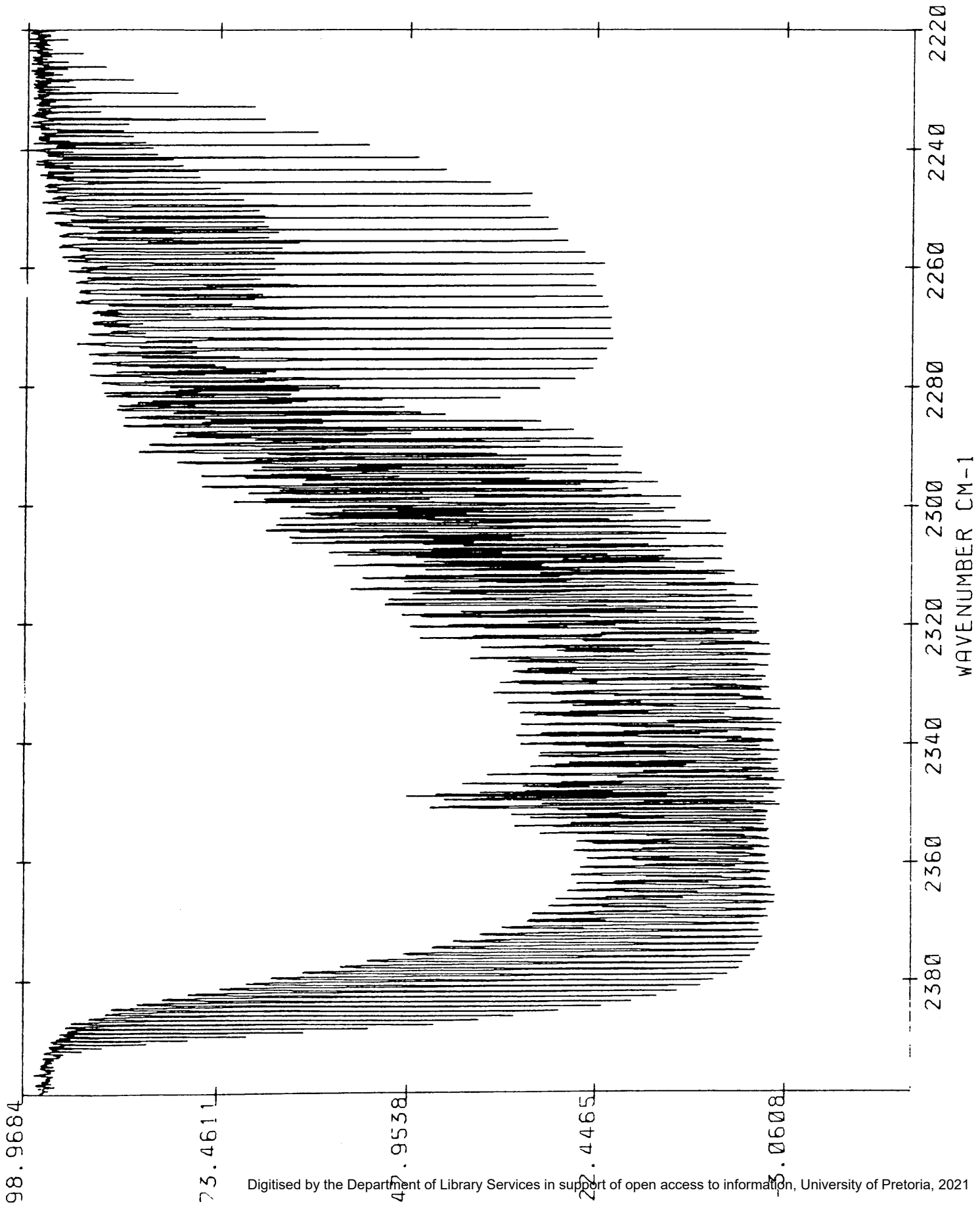

Fig. II.16 High resolution FT-IR spectrum (0,03 cm^{-1}) of the (ν_1-ν_2) band of CO_2

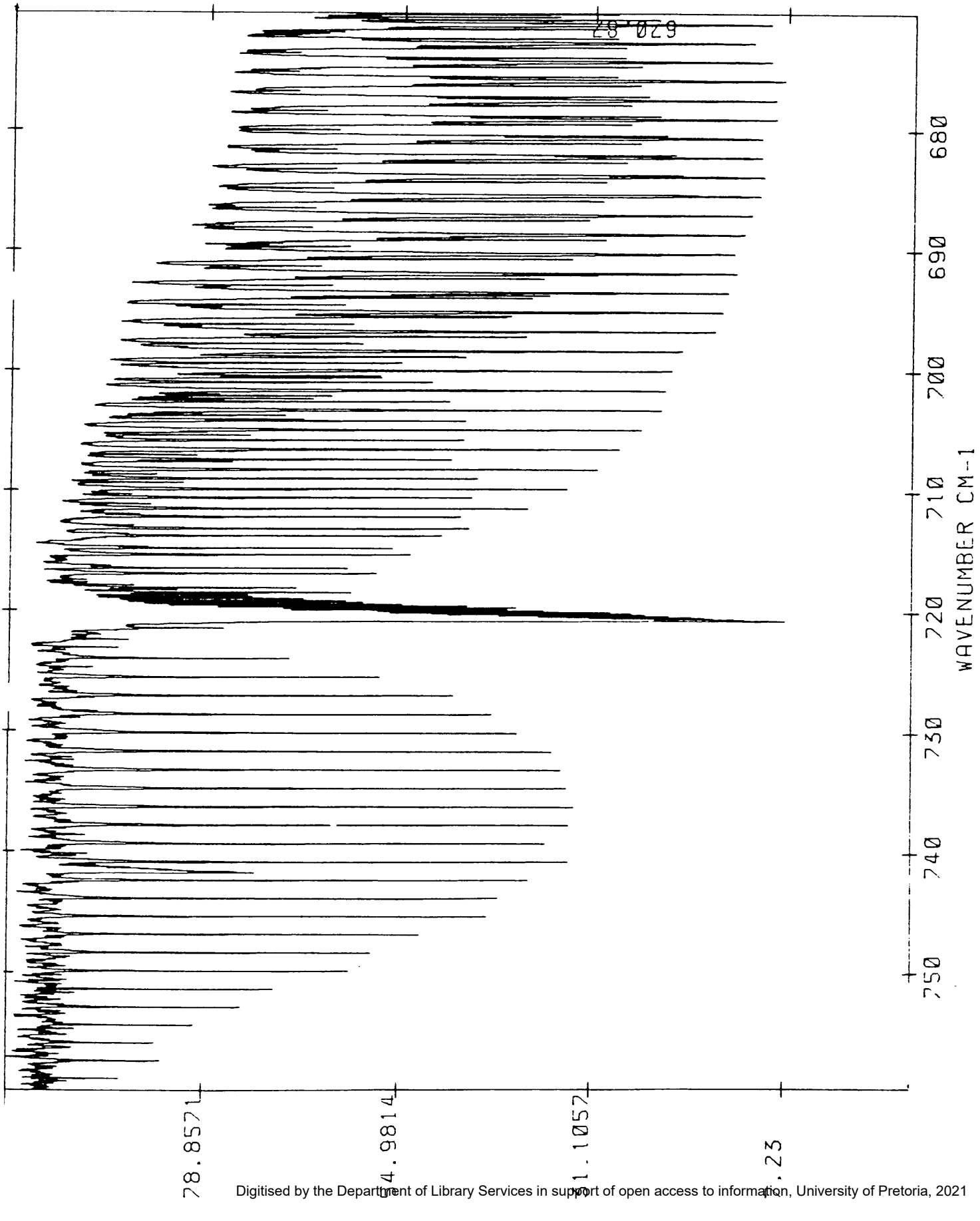

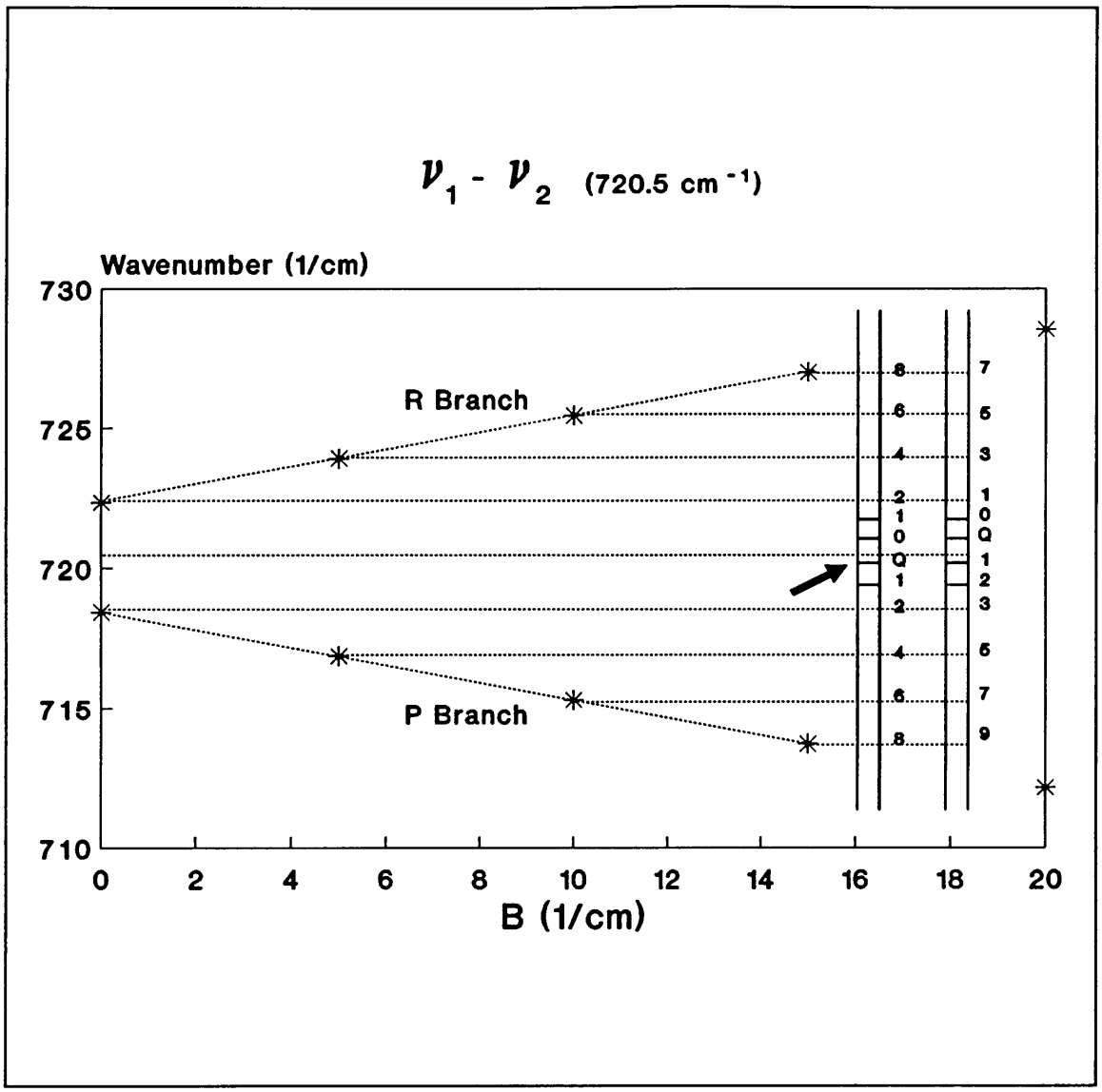

Fig. II.17

The intersection of the two straight lines in figs. II.17 and II.18 falls at 720,3 cm^{-1} and 2349,5 cm^{-1} respectively.

10. Experimental Determination of Rotational Constants

(a) Without distortion

The calculation of the rotational constants B′ and B″ has been done by the method of combination differences described previously (Sec. II-8).

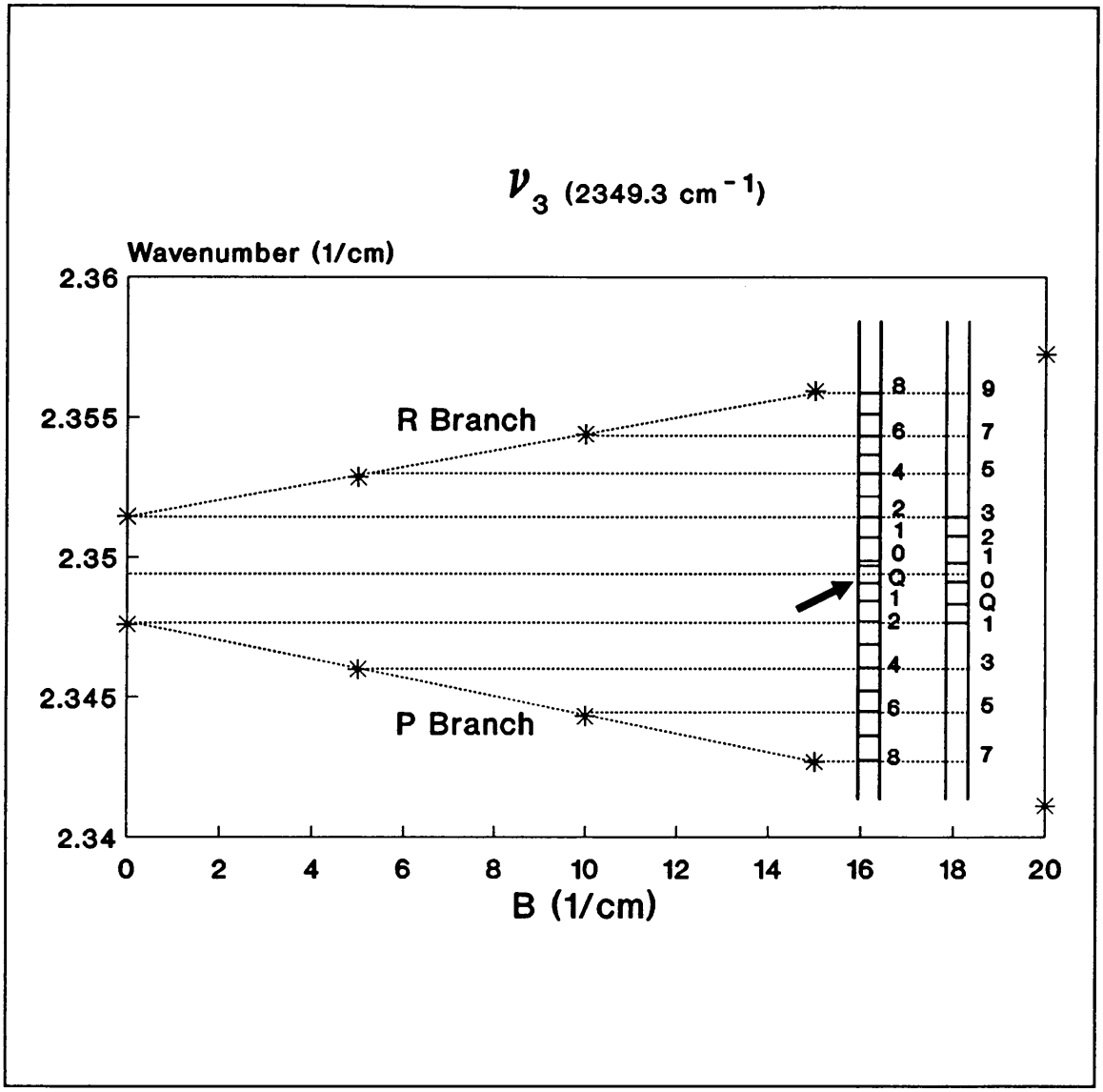

Fig. II.18

$F'(J) = R(J)-P(J)$ as well as $F''(J) = R(J-1)-P(J+1)$ were calculated for ν_2, ν_3 as well as for the difference band $\nu_1-\nu_2$ centred at 720 cm^{-1}. $F'(J)$ as well as $F''(J)$ are shown in tables II-4 to II-6 for these three bands respectively (see appendix).

In the evaluation of the rotational constants the values of $F'(J)$ and $F''(J)$ were plotted against $(J+\frac{1}{2})$ for each band. The plots are shown in figs. II.19 to

II.21. The rotational constants for each vibration is tabulated in table II-7. Eq. II-25 could not be used since every second rotation line is missing. Therefore equations II-19 and II-20 were used.

Table II-7.

Vibration	B″/cm^{-1}	B′/cm^{-1}	r″/Å	r′/Å
ν_2	0,389370723	0,388959284	1,163198085	1,163813134
ν_3	0,384946873	0,382748351	1,169862789	1,173217847
ν_1-ν_3	0,389206065	0,388585126	1,163444111	1,164373301

(b) With distortion

B′,B″ and D′,D″ were calculated by using eq. II-21 and II-22. The plots of F′(J)/J+½ and F″(J)/J+½ against $(J+½)^2$ are shown in fig. II.22 to II.24. The rotational constants are tabulated in table II-11. These plots were generated from the data in tables II-8 to II-10 (See appendix).

The values of B in brackets were ascertained by ignoring some of the data in the lower J values. The reason for ignoring some of the data points is, as can be seen in figs. II.22 to II.24, that there is a great variation in the data at the lower J values. The cause for this is probably due to the inacurate measurements of the wave numbers. The difficulty in obtaining accurate wave numbers for the rotational bands in the ν_3 band is due to the fact that the rotational bands are not sharp. This can be seen in fig. II.25.

By ignoring the lower J values of the ν_3 band the correlation coefficients for

the graphs in fig. II.23 improved from -0,5011 to -0,9848 and from -0,116 to -0,9871 respectively. It can thus be accepted that the values in brackets for the ν_3 band are more reliable.

The effect of the distortion of the bands can be seen from the increase in bond length as the vibration quantum number increases from 0 to 1. (The symbols with the double prime represents the lower state and those with the single prime the upper state.) Note that there is a decrease in bond length for the ν_3 band if all the data is taken into account. This contradiction is corrected when the lower wavenumbers are ignored.

Table II-11

Vibration	B″/cm^{-1}	B′/cm^{-1}	D″/cm^{-1}	D′/cm^{-1}	r″/Å	r′/Å
ν_2	0,3900927952	0,390512291	2,141457435 x 10^{-7}	2,166009773 x 10^{-7}	1,160879021	1,161496676
	(0,390927952)	(0,390341841)	(1,514793993 x 10^{-7})	(1,542405740 x 10^{-7})	(1,160879021)	(1,161750243)
ν_3	0,386336482	0,382831441	3,943263166 x 10^{-8}	1,25203765 x 10^{-8}	1,167756961	1,173090522
	(0,386907562)	(0,383843877)	(1,107640292 x 10^{-7})	(1,116613065 x 10^{-7})	(1,166894831)	(1,171542415)
ν_1-ν_3	0,390695621	0,391114103	1,737587390 x 10^{-7}	1,881728456 x 10^{-7}	1,161224134	1,160602728
	(0,39065134)	(0,391152694)	(1,629906714 x 10^{-7})	(1,988000058 x 10^{-7})	(1,161289946)	(1,160545474)

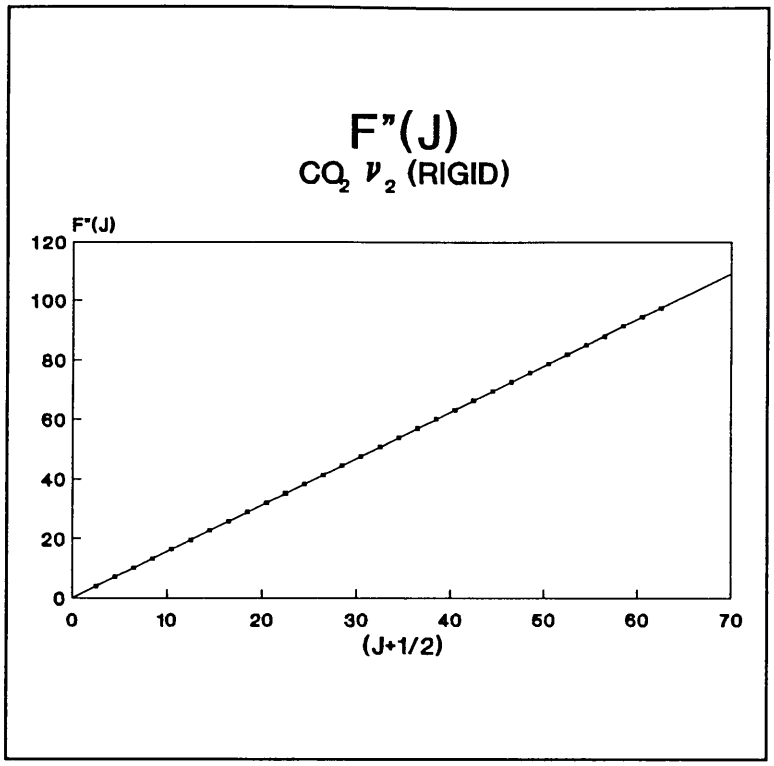

Fig. II.19(a)

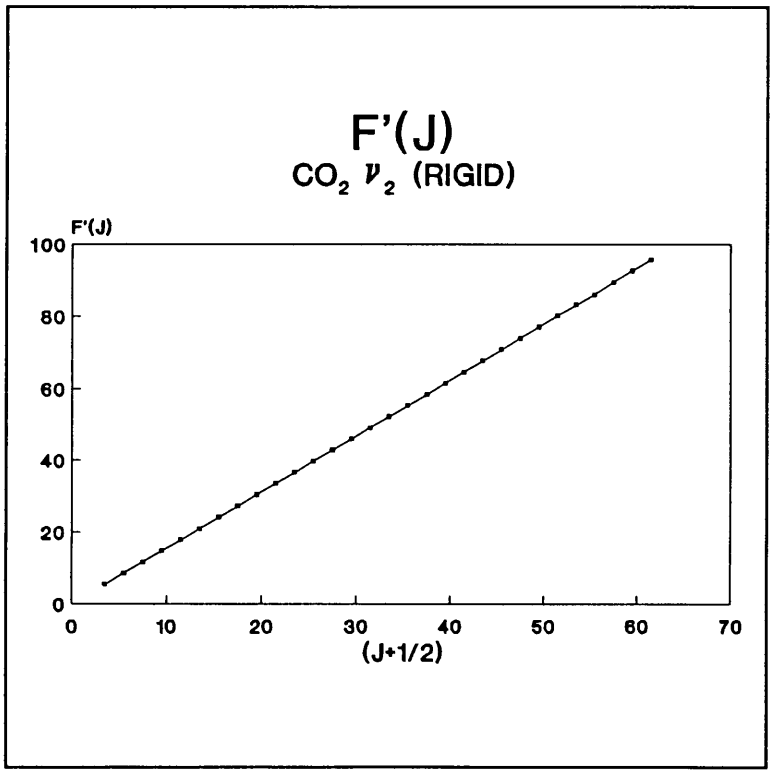

Fig. II.19(b)

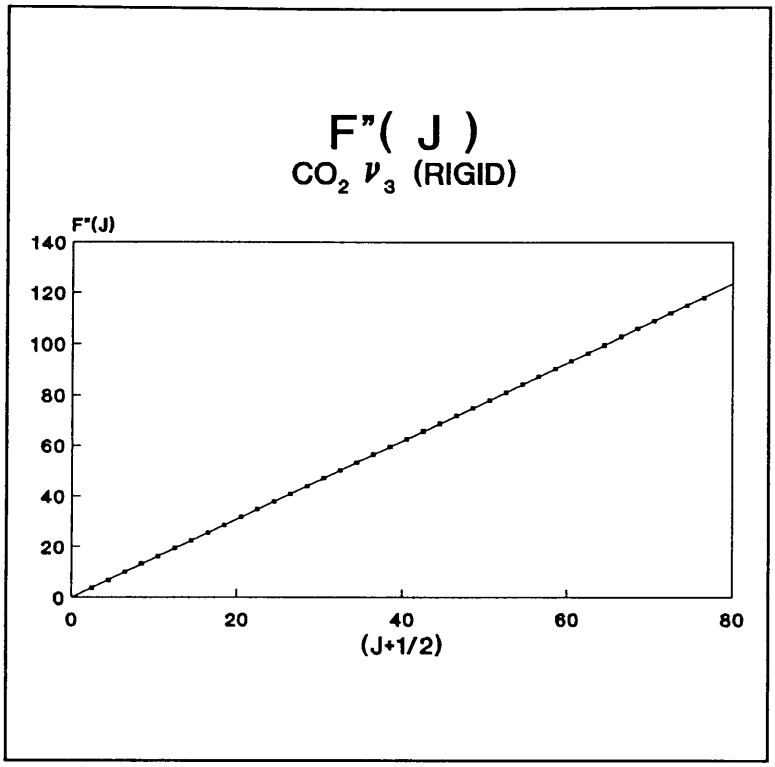

Fig. II.20(a)

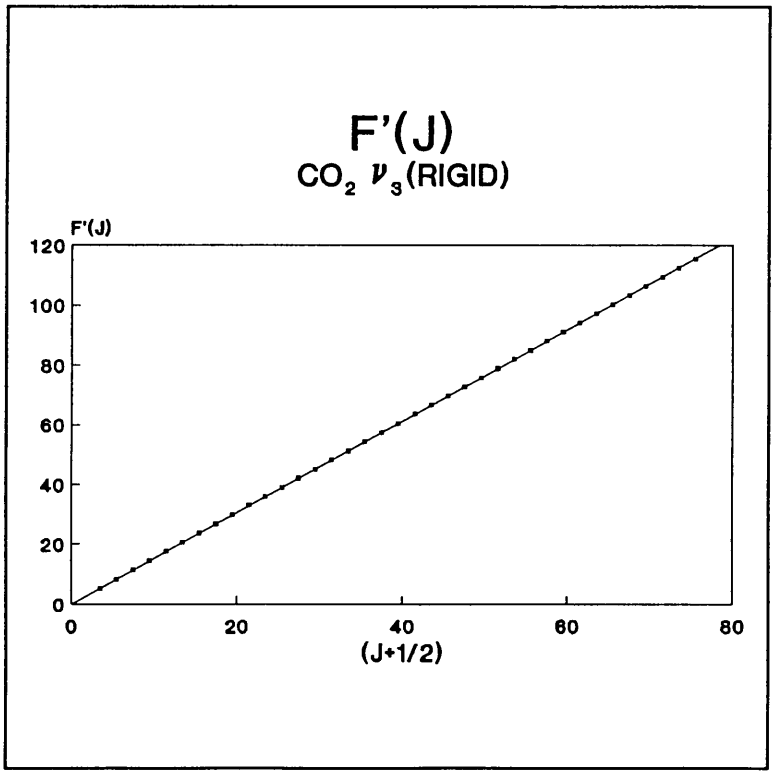

Fig. II.20(b)

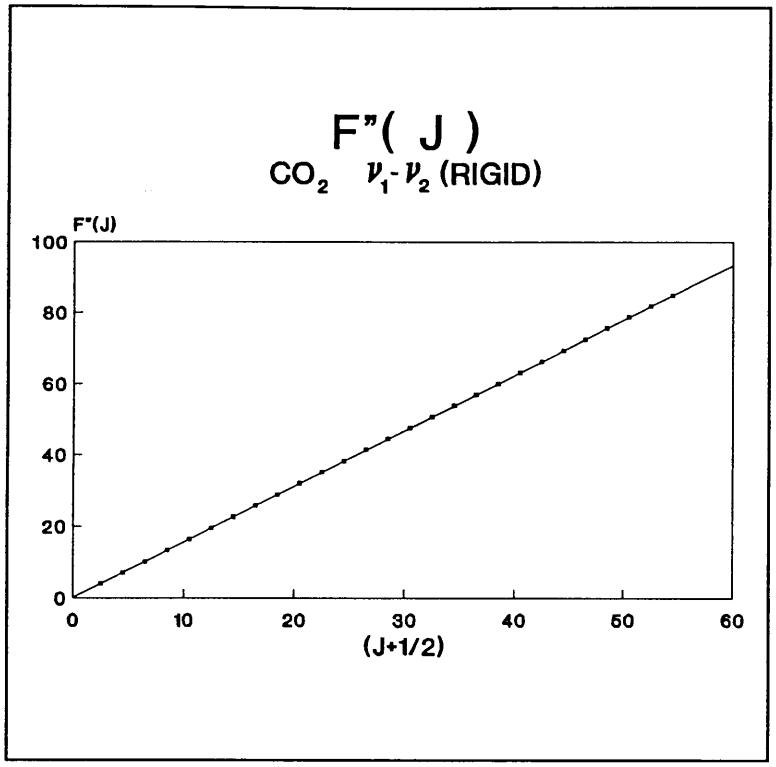

Fig. II.21(a)

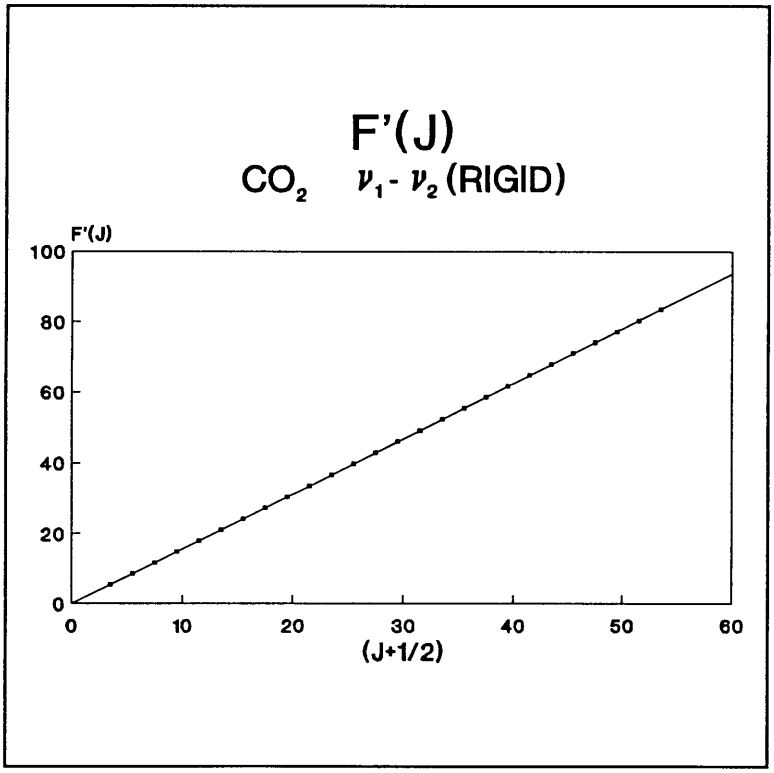

Fig. II.21(b)

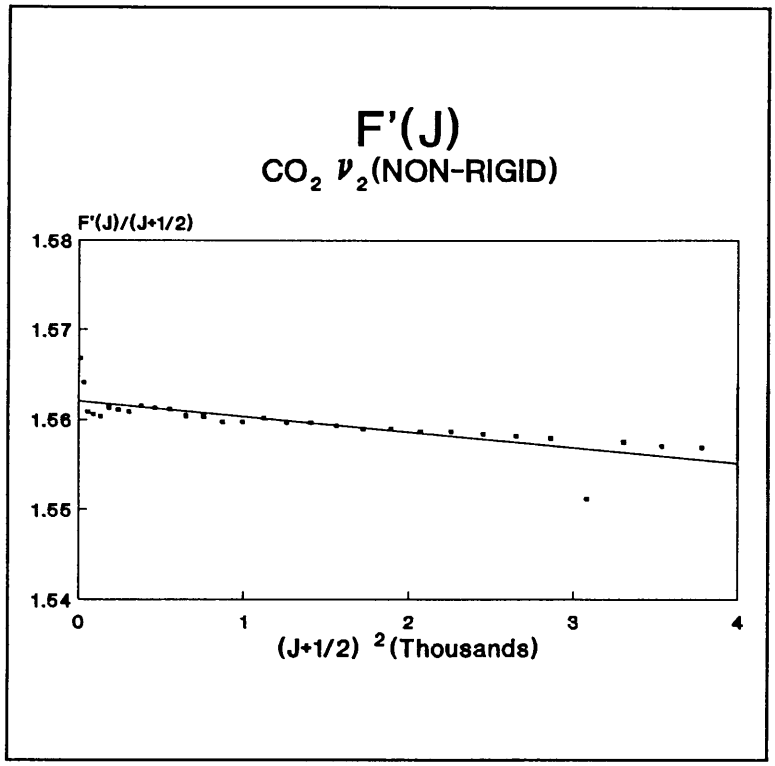

Fig. II.22(a)

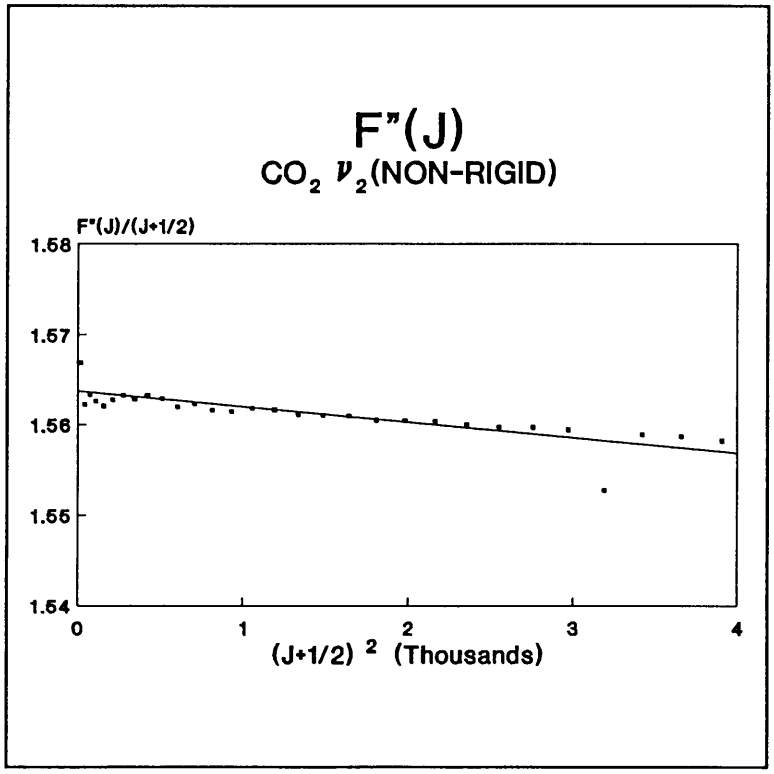

Fig. II.22(b)

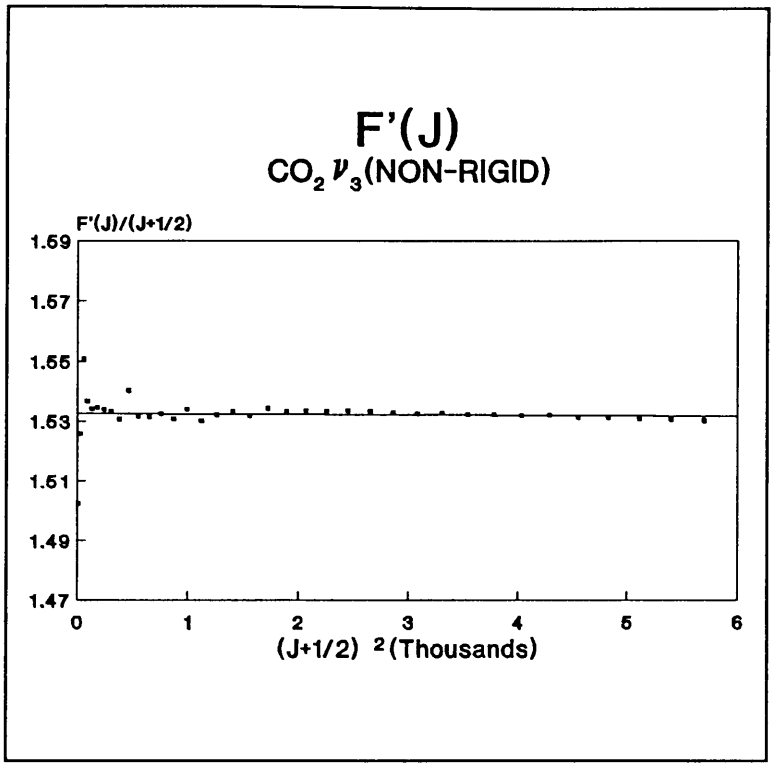

Fig. II.23(a)

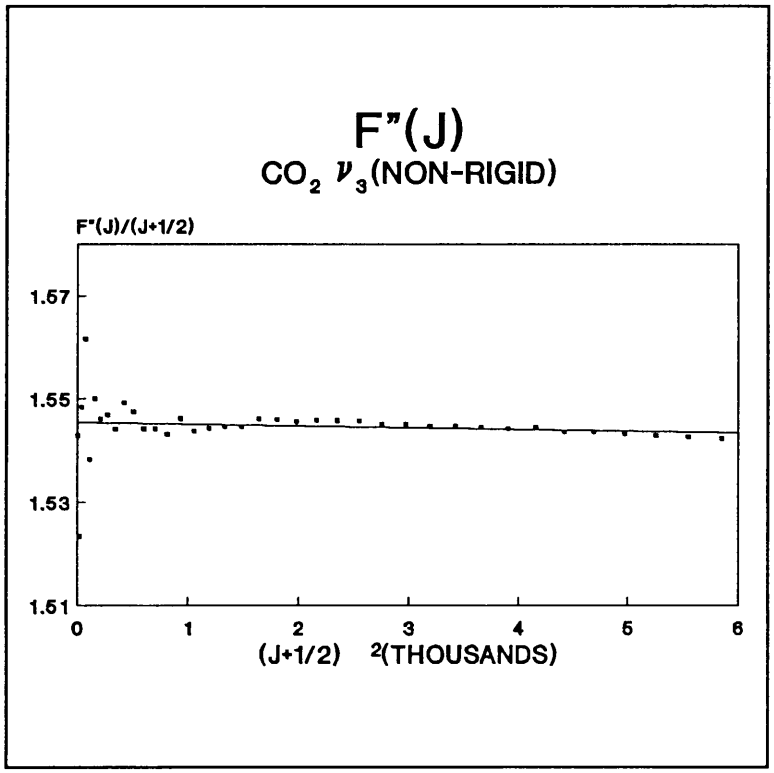

Fig. II.23(b)

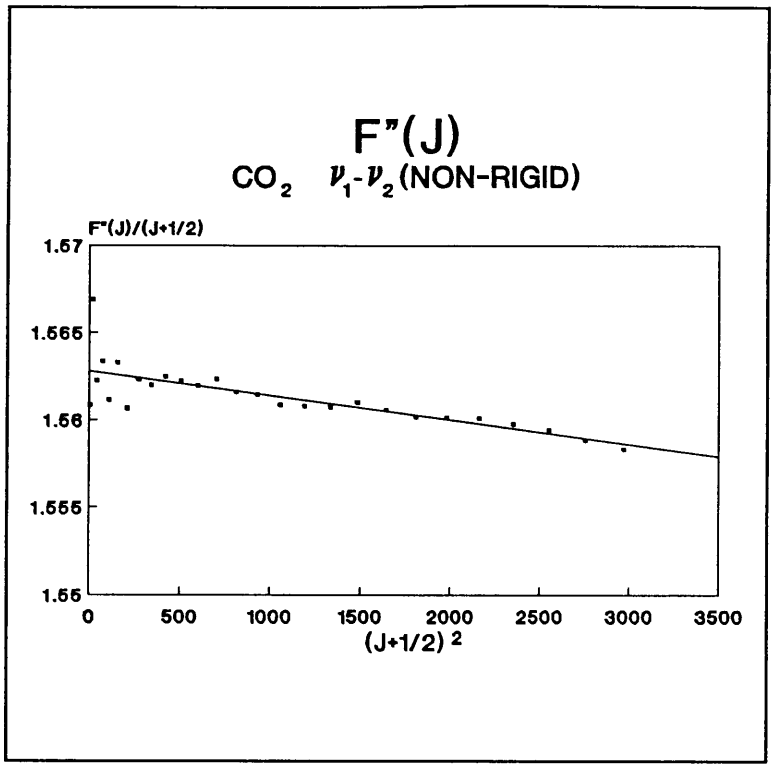

Fig. II.24(a)

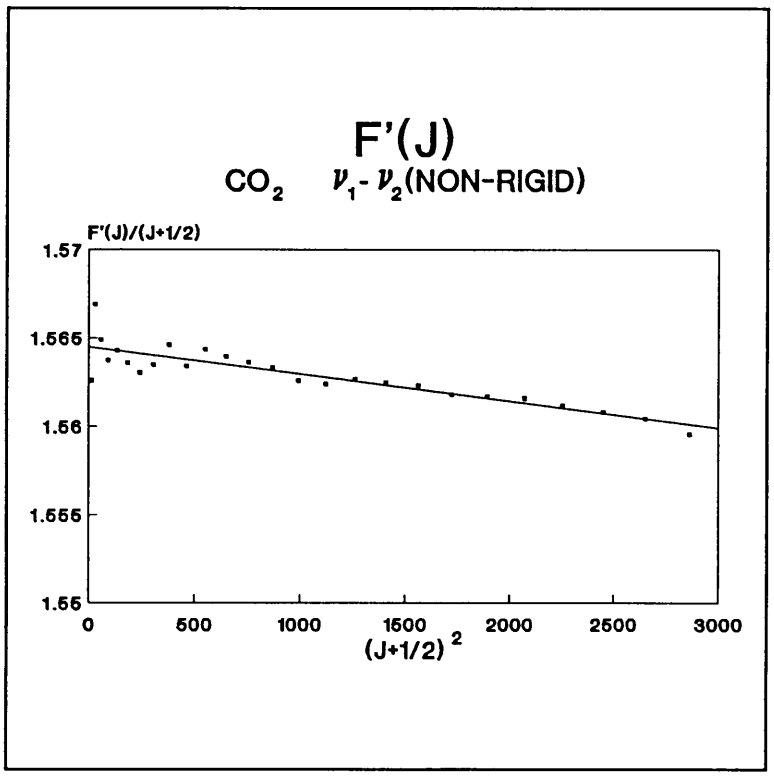

Fig. II.24(b)

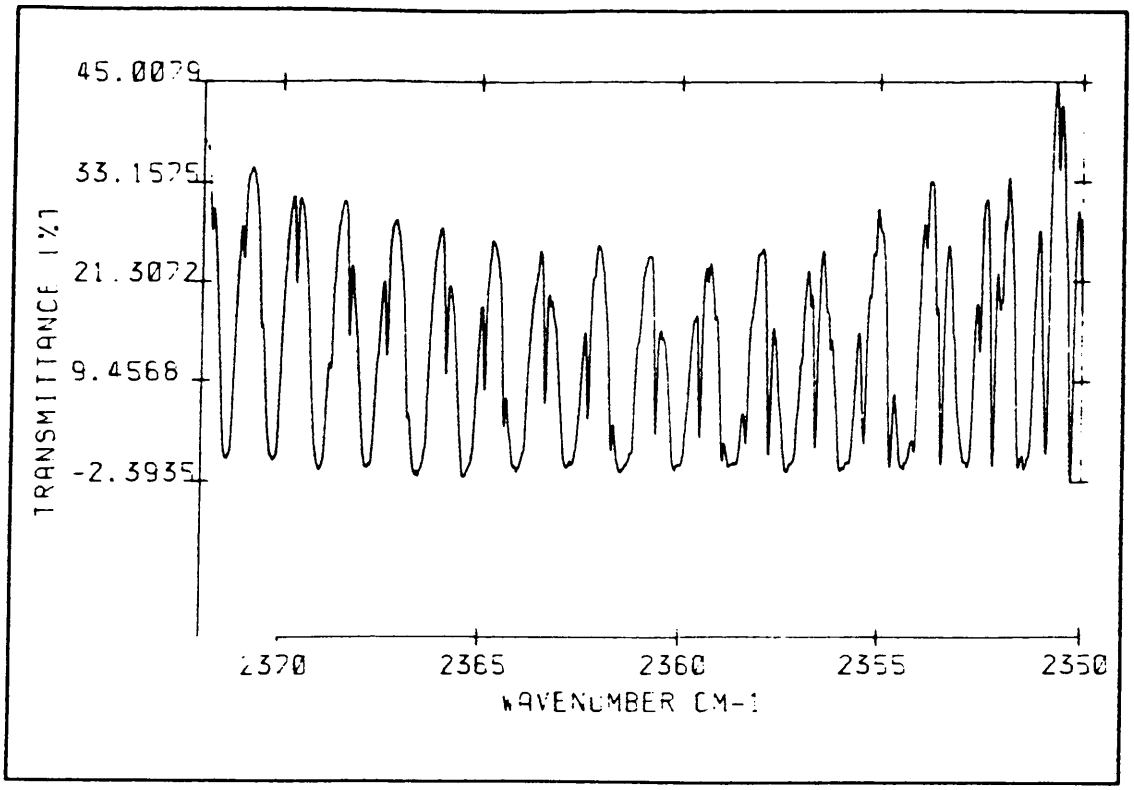

Fig. II.25(a)

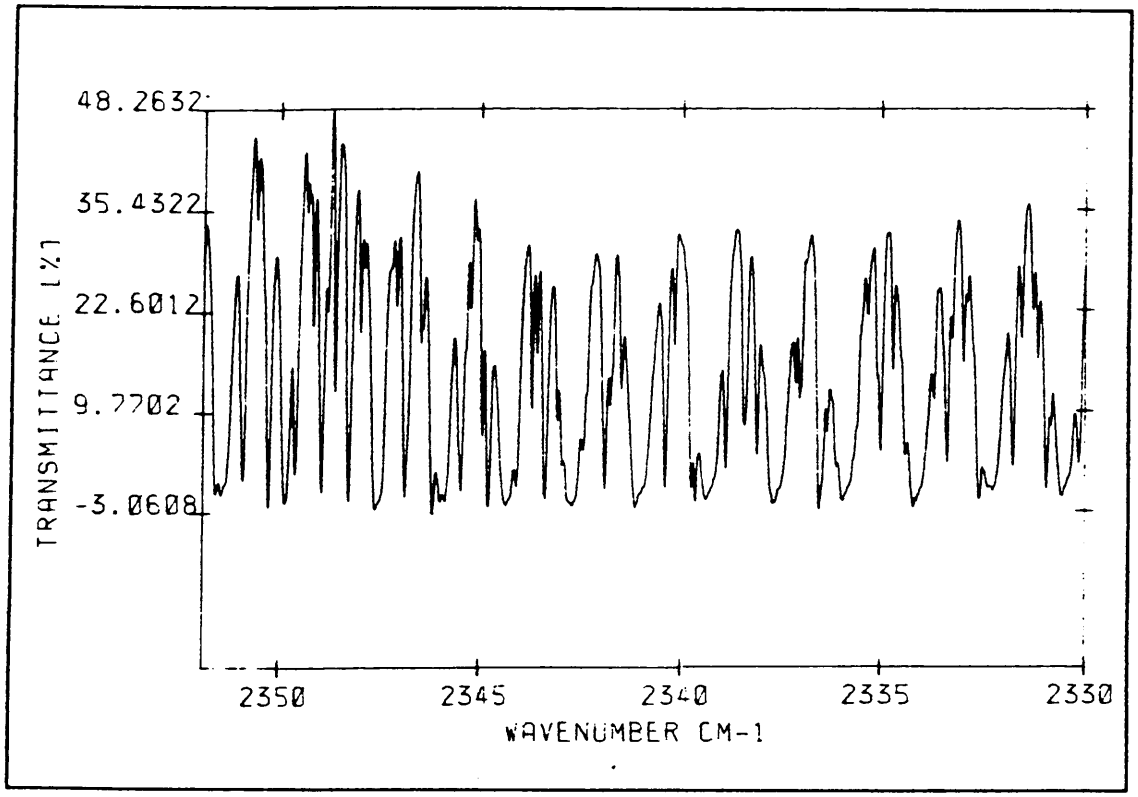

Fig. II.25(b)

CHAPTER III

HIGH RESOLUTION FT-IR SPECTRUM OF METHANE

1. Vibrational spectrum

Methane is a tetrahedral molecule belonging to the point group T_d. The five atom molecule has four fundamentals namely, a totally symmetric (A_1), a doubly degenerate (E), and two triply degenerate (F_2) vibrations. (See fig. III.1). All four are Raman active but only ν_3 and ν_4 are infrared active. (See table III-1).

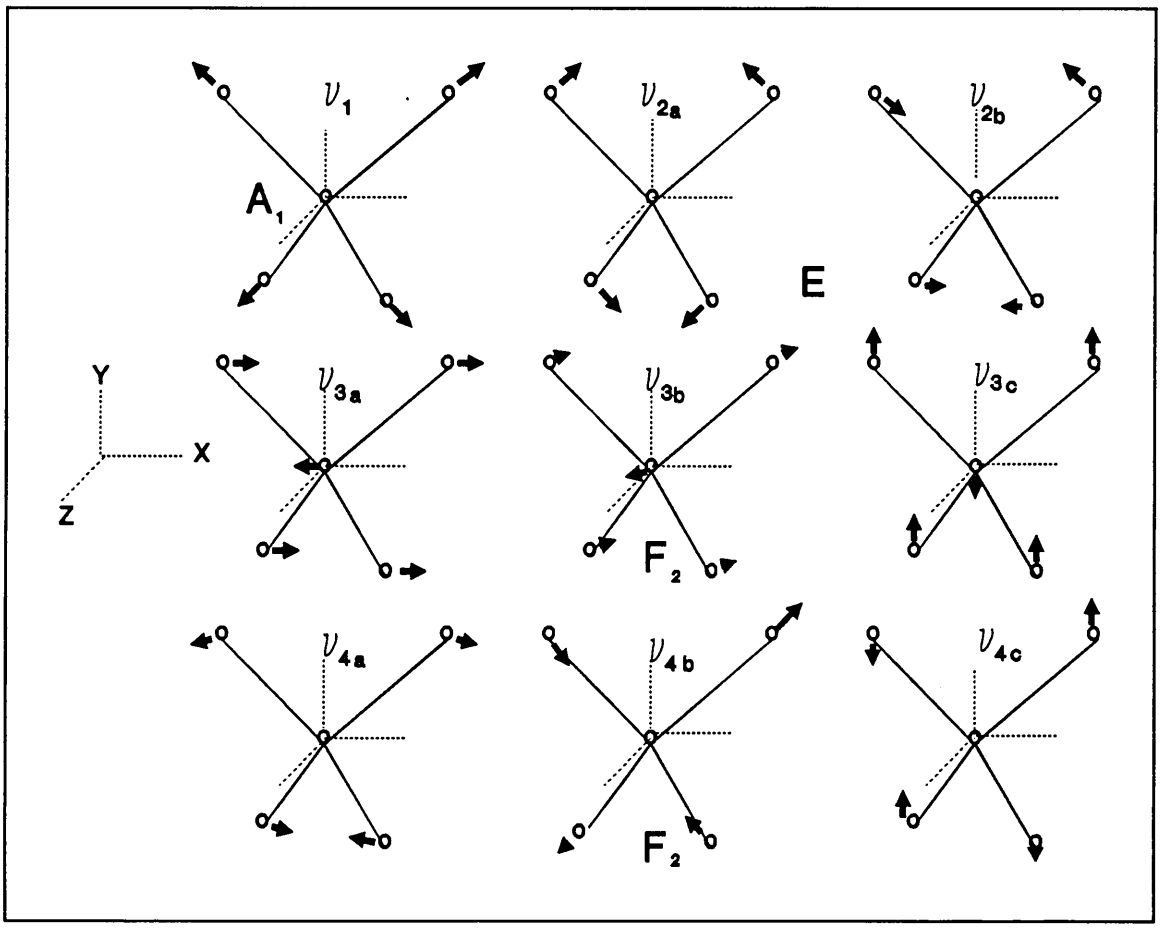

Fig. III.1 Normal vibrations of a tetrahedral XY_4 molecule. - The three two-fold axes (dot-dash lines) are chosen as x, y, and z axes.

Table III-1 Character table of the T_d point group

T_d	E	$8C_3$	$3C_2$	$6S_4$	$6\sigma_2$		
A_1	1	1	1	1	1		$x^2 + y^2 + z^2$
A_2	1	1	1	-1	-1		
E	2	-1	2	0	0		$(2z^2 - x^2 - y^2,$ $x^2 - y^2)$
F_1	3	0	-1	1	-1	(R_x, R_y, R_z)	
F_2	3	0	-1	-1	-1	(x, y, z)	(xy, xz, yz)

The infra-red spectrum of CH_4 shows two extremely intense bands at 1306,4 cm^{-1} and 3018,4 cm^{-1}. All other much weaker infra-red bands can be interpreted on the basis of these two active fundamentals and inactive fundamentals. The FT-IR spectrum in fig. III.2 of methane can be seen in table III-2.

Table III-2 Fundamental frequencies of gaseous CH_4

Fundamental	Wavenumber
ν_1 (A_1)	2914,2 cm^{-1}
ν_2 (E)	1526 cm^{-1}
ν_3 (F_2)	3020,3 cm^{-1}
ν_4 (F_2)	1306,2 cm^{-1}

2. Rotational spectrum

(a) Classical motion

Methane is a spherical top rotor because the moments of inertia about all axis going through the center of mass are exactly equal. For a spherical top, the instantaneous axes of rotation coincides always with the total angular momentum P and any axis fixed in the molecule may be considered as figure axis and describes a simple rotation about P. The component of P along any axis fixed in the molecule is a constant.

Fig. III.2

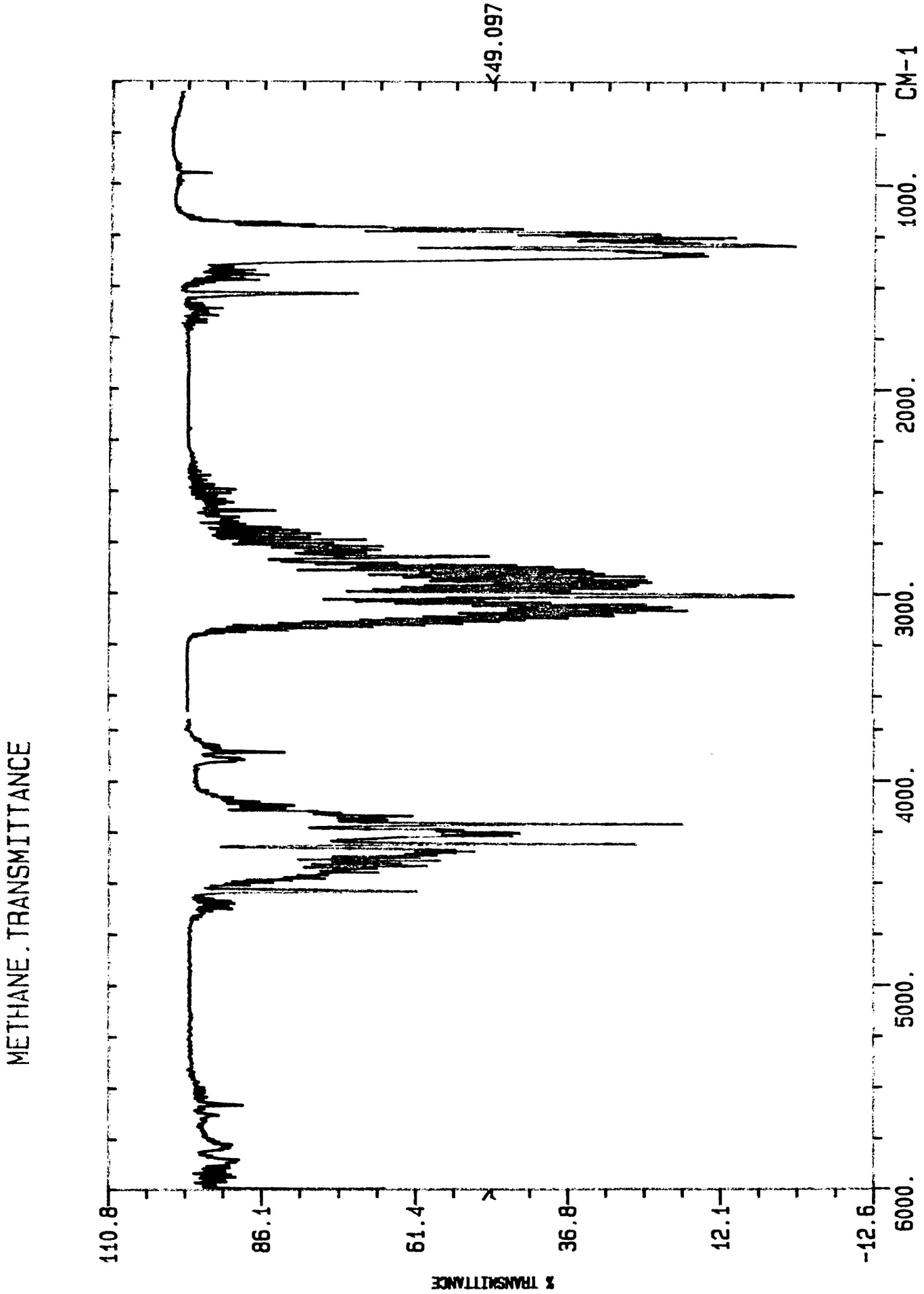

(b) Energy levels

The energy levels of the spherical top are obtained from those of the symmetrical top in eq. III-1 by putting $I_A = I_B$, that is A = B [3]

$$F(J,K) = BJ(J+1) + (A-B)K^2 \qquad \text{III-1}$$

where $A = \frac{h}{8\pi^2 c I_A}$ and $B = \frac{h}{8\pi^2 c I_B}$

The following formula is obtained.

$$F(J) = BJ(J+1) \qquad \text{III-2}$$

All values of J from zero up are possible. The above holds for a rigid spherical top. For a non rigid spherical top, a small term $-DJ^2(J+1)^2$ must be added.

3. Statistical weights and symmetry properties

The spherical top may be considered as a symmetrical top with A = B, that is, one in which all levels with the same J but different K coincide. It is clear that in view of the possible values of K and the double degeneracy for $K \neq 0$, that the spherical top energy level of a given J has a (2J+1)-fold degeneracy in addition to the ordinary (2J+1)-fold space degeneracy. The first degeneracy corresponds to the fact that J may have 2J+1 orientations with respect to a fixed direction in the molecule and the second degeneracy corresponds to the fact that J may have 2J+1 orientations with respect to a direction fixed in space. Thus the statistical weight of an energy level with a given J is $(2J+1)^2$. The factor $(2J+1)^2$ gives apart from a constant factor,

corresponding to the nuclear spin, the complete statistical weight.

In the case of methane the additional factor by which the space degeneracy $(2J+1)$ has to be multiplied in order to obtain the total statistical weight is not simply $2J+1$ times the nuclear spin factor. CH_4 has three types (species) of rotational levels A, E and F. The number of component levels of each type varies in a rather complicated way which can be calculated from group theory.

4. Interaction of Rotation and Vibration

(a) Non-degenerate vibrational states

The same reasoning in calculating the energy levels can be followed as in section II-3.

(b) Degenerate vibrational states

The Coriolis forces that occur in the rotating molecule may produce an interaction between mutually degenerate vibrations which in its turn will lead to an appreciable splitting of degeneracy.

There are three types of degenerate vibrational levels in tetrahedral molecules; E, F_1 and F_2. Taking the vibrations, that can be seen in fig. III.1, into consideration, it can be seen that if one component of the doubly degenerate vibration is excited the Coriolis force does not tend to exite the other component. Therefore no Coriolis splitting arises for the doubly degenerate vibrational states. The rotational energy levels are the same as for the non-

degenerate vibrational states. The absence of Coriolis splitting follows quite generally for any state of species E of point group Td from Jahn's general rule [3]. The product E x E of the species of the two interacting vibrations, according to table III-3 is $A_1 + A_2 + E$, that is, does not contain the species of the rotation, which is F_1 in this case.

Table III-3. Multiplication Table.

	A_1	A_2	E	F_1	F_2
A_1	A_1	A_2	E	F_1	F_2
A_2		A_1	E	F_2	F_1
E			$A_1 + A_2 + E$	$F_1 + F_2$	$F_1 + F_2$
F_1				$A_1 + E + F_1 + F_2$	$A_2 + E + F_1 + F_2$
F_2					$A_1 + E + F_1 + F_2$

However, for the triply degenerate vibrational states the Coriolis interaction does cause a splitting. This is most easily seen by considering the vibration ν_3 of CH_4 in fig. III.1. The rotation about the Z axis, if the component ν_{3a} is excited, the Coriolis force tends to excite ν_{3c}, whereas ν_{3b} is uninfluenced. A splitting occurs in this case into three components, one of which has the original frequency. The other two are not simply ν_{3a} and ν_{3c}, but linear combinations of these vibrations which no longer tend to go over into each other in consequence of the Coriolis force.

The vibrational energy values for the three sublevels are given by the following formulae [ ]

$$F^{+}(J) = B_{[v]}J(J+1) + 2B_{[v]}\xi_i(J+1) \qquad \text{III-3}$$

$$F^{\circ}(J) = B_{[v]}J(J+1) \qquad \text{III-4}$$

$$F^{-}(J) = B_{[v]}J(J+1) - 2B_{[v]}\xi_i J \qquad \text{III-5}$$

where ξ_i is the magnitude of p in units of $\frac{h}{2\pi}$ for the particular vibrational state.

5. Symmetry properties of the rotational levels

The rotational eigenfunctions of the spherical top molecules have certain symmetry properties which correspond to the symmetry types (species) of the rotational subgroup to which the molecule belongs. For methane, which belongs to the pointgroup Td, the rotational subgroup is T. The species of this group are A, E and F. Depending on the behaviour of the total eigenfunction $\psi \approx \psi_e\psi_v\psi_r$ with respect to the symmetry elements of T, there are three over-all species of rotational levels, A, E and F.

If $\psi_e\psi_v$ is totally symmetric (A vibrational state), the species of the rotational levels depend on the symmetry of ψ_r only. The symmetry of the first 15 rotational states can be seen in table III-4.

Table III-4.

J	CHARACTER	J	CHARACTER
0	A_1	8	$A_1 + 2E + 2F_1 + 2F_2$
1	F_2	9	$A_1 + A_2 + E + 2F_1 + 3F_2$
2	$E + F_2$	10	$A_1 + A_2 + 2E + 2F_1 + 3F_2$
3	$A_1 + F_1 + F_2$	11	$A_2 + 2E + 3F_1 + 3F_2$
4	$A_1 + E + F_1 + F_2$	12	$2A_1 + A_2 + 2E + 3F_1 + 3F_2$
5	$E + F_1 + 2F_2$	13	$A_1 + A_2 + 2E + 3F_1 + 4F_2$
6	$A_1 + A_2 + E + F_1 + 2F_2$	14	$A_1 + A_2 + 3E + 3F_1 + 4F_2$
7	$A_1 + E_1 + 2F_1 + 2F_2$	15	$2A_1 + A_2 + 2E + 4F_1 + 4F_2$

If $\psi_e\psi_v$ is not totally symmetric with respect to the rotational subgroup T (E or F vibrational states), the species of $\psi_e\psi_v$ given in table III-4 must be multiplied by E and F to obtain the symmetry of each of these vibrational states. By using table III-3 this multiplication can be done. The over-all species of the levels obtained in such a manner are given in fig. III.3 b and c.

If the influence of the nuclear spin is disregarded, it can be seen from fig. III.3a that the statistical weight of a set of levels with a given J is 2J+1, 2(2J+1) and 3(2J+1) for the vibrational levels of species A, E and F respectively. However, in order to obtain the actual statistical weight the nuclear spin I has to be taken into account.

Coriolis splitting of the rotational levels

If finer interaction of vibration and rotation is taken into account, a splitting of the sublevels occurs. This splitting is largely due to the Coriolis interaction of the

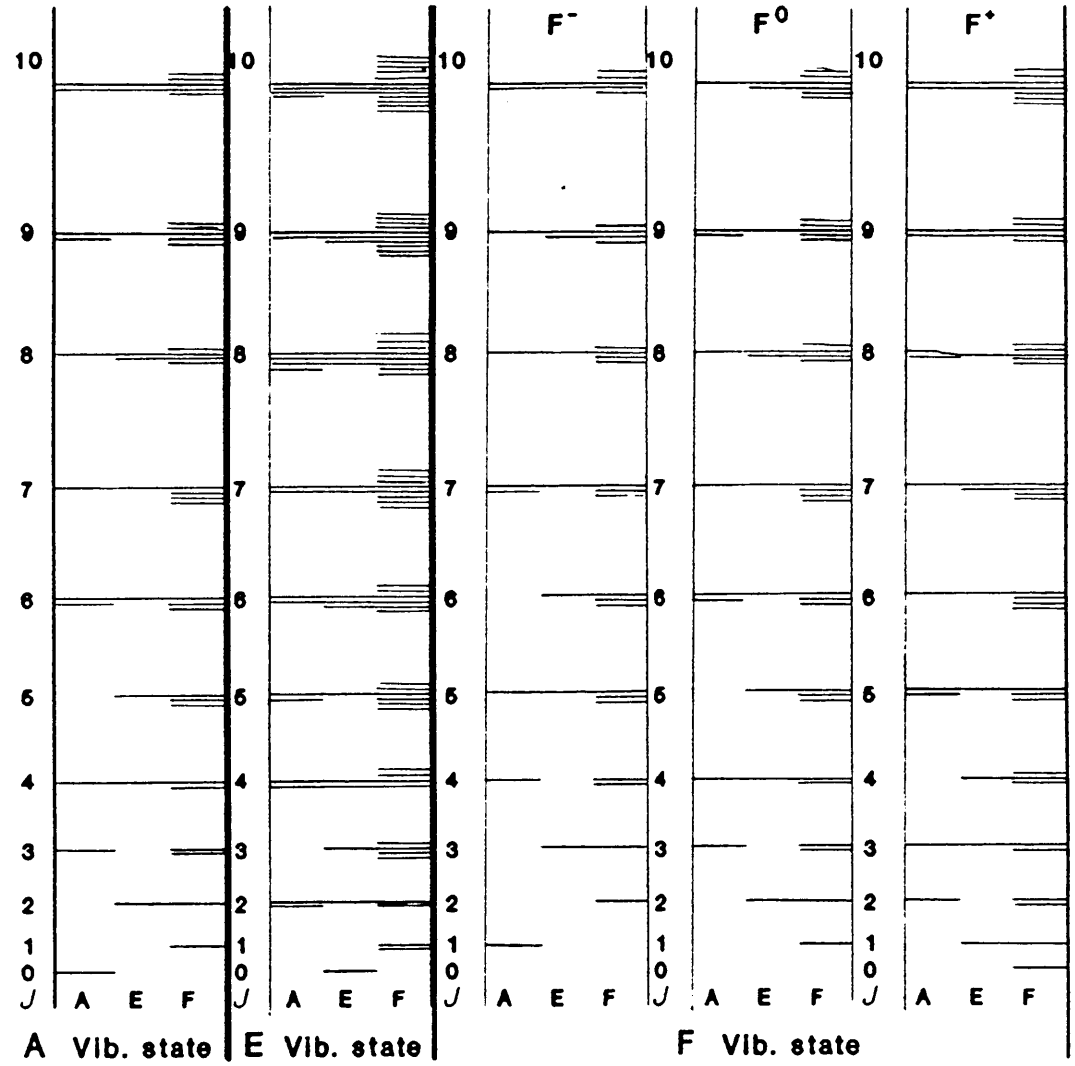

Fig. III.3 Species of the rotational levels of a spherical top molecule of point group T_d (a) in an A, (b) in an E, (c) in an F vibrational state. - A doubly or triply degenerate level is drawn as one line. Thus in (a) for J = 6 there are three F levels, one E and one A level. Levels drawn close together coincide when there is no Coriolis interaction (see text).

different vibrations. The splitting will be larger the closer together are the two interacting vibrational levels and will be proportional to J(J+1). This is in contrast to the Coriolis splitting of a triply degenerate vibrational state which is proportional to J.

The rotational structure of the ν_4 band at approximately 1306 cm^{-1} is considerably

more complex than is expected. The anomalous spacing between rotational bands of this sort results mainly from a Coriolis interaction between this band and the nearby, infra-red inactive, ν_2 vibration. The ν_4 and ν_2 vibrational bands belong to the F and E degenerate representations of T_d respectively. This effect causes both a splitting as well as a shift in the energy levels of the ν_4 band [7]. In order to calculate the energy spectrum, the correct vibrational-rotational wave functions for ν_4 and ν_2 must first be calculated. From this it is possible to calculate the matrix elements of the Coriolis operator as well as the perturbed energy levels. The matrix elements are shown in table III-5 (See appendix).

The wave numbers of the unperturbed lines, but taking into account the Coriolis interaction ξ_4, due to the degeneracy of the vibration, are given by

$$R(J) = \nu_4 + 2B(1-\xi_4)(J+1)$$

$$Q(J) = \nu_4$$

$$P(J) = \nu_4 - 2B(1-\xi_4)J$$

$\xi_4\hbar$; is the internal angular momentum and ν_4 includes the vibrational frequency as well as an additional term in ξ_4 which is independent of J. Changes of the moment of inertia of the molecule as well as any centrifugal distortion can be neglected, since these terms are small.

The unperturbed levels of ν_2 are given by

$$R(J) = \nu_2 + BJ(J+1)$$

$$Q(J) = \nu_2$$

$$P(J) = \nu_2 - B'J(J+1)$$

The calculated wavenumbers of the unperturbed energy levels of ν_2 are given in table III-5. B was taken as 5,27 cm^{-1} and ν_2 as 1536 cm^{-1} [7].

The uncorrected perturbations can be determined in the following way: A′ is the transpose of A and the elements of the latter are the matrix elements a_{ij} of Jahn [6]. The matrix AA′ has in m rows and n columns and any element not given explicitly in table III-5 are zero. The latent roots (eigenvalues) of the Hermitean square AA′, ϵ_i^2 are related to the uncorrected perturbations as follows

$$\bar{E}_{uncorrect} = B^2\xi_{24}^2\epsilon_i^2/\Delta$$

where $\Delta = \nu_2 - \nu_4$; $\xi_{24}^2 = \frac{M}{2m_o + M}$; m_o is the mass of the central atom and M $= m_o + 4m$, the total mass of the molecule. For methane the numerical factor $f = \frac{B^2\xi_{24}}{\Delta}$ is approximately 0,05. The eigenvalues were calculated and are tabulated in table III-7 column 4. The uncorrected perturbations were calculated and are listed in table III-7 column 5.

These perturbations must be further corrected for the R and the P branch since the energy difference between the levels of ν_2 and ν_4 varies with J on account of ξ_4. In order to do this, the calculated perturbations must be multiplied by the factors

$$R_{fact} = \frac{\nu_2 - \nu_4}{(\nu_2 - \nu_4) + 2J\xi_4 B}$$

and

$$P_{fact} = \frac{\nu_2 - \nu_4}{(\nu_2 - \nu_4) - 2(J+1)\xi_4 B}$$

for the R and P branches respectively. The results of the calculation carried out in this manner are shown in table III-7 both for the corrected and uncorrected perturbations. The perturbation is the greatest for the Q branch and some of the sublevels are perturbed by as much as 13 cm^{-1}. In calculating the corrections to the P and R branch levels B = 5,27 and ξ_4 = 0,45 were assumed. The values used for ν_4 and ν_2 were 1306 cm^{-1} and 1536 cm^{-1} respectively.

6. Relative Intensities

The intensities in the ν_4 band depend upon three factors

(a) The transition amplitude or sum of matrix elements squared of the electric moment from one single state.

(b) The statistical weight of the initial energy level.
This weight is determined by the rotational and nuclear spin degeneracy.

(c) The Boltzmann factor of the initial energy level.

An "i" factor, defined as the product of the transition amplitude and the degree of degeneracy the initial level would have in the absence of nuclear spin, can be introduced at this stage. This i-factor must then be multiplied by a correcting nuclear spin factor g and by the Boltzmann factor to give the theoretical line strength.

The total transition amplitudes for a symmetrical top are shown in table III-8.

Table III-8

TRANSITION		AMPLITUDE	TOTAL
$J \rightarrow J-1$	$K \rightarrow K-1$	$\frac{(J+K)(J-1+K)}{2J(2J+1)}$	$\frac{2J-1}{2J+1}$
	$K \rightarrow K$	$\frac{J^2-K^2}{J(2J+1)}$	
	$K \rightarrow K+1$	$\frac{(J-K)(J-1-K)}{2J(2J+1)}$	
$J \rightarrow J$	$K \rightarrow K-1$	$\frac{(J+K)(J+1-K)}{2J(J+1)}$	1
	$K \rightarrow K$	$\frac{K^2}{J(J+1)}$	
	$K \rightarrow K+1$	$\frac{(J-K)(J+1+K)}{2J(J+1)}$	
$J \rightarrow J+1$	$K \rightarrow K-1$	$\frac{(J+1-K)(J+2-K)}{2(J+1)(2J+1)}$	$\frac{2J+3}{2J+1}$
	$K \rightarrow$	$\frac{(J+1)^2-K^2}{(J+1)(2J+1)}$	
	$K \rightarrow K+1$	$\frac{(J+1+K)(J+2+K)}{2(J+1)(2J+1)}$	

From these amplitudes the transition amplitudes of methane can be obtained by

summation over the transitions in the quantum number K as shown in the table. Assuming the initial level degeneracies as $(2J+1)^2$ the intensity factors (i-factors) can be obtained as is shown in table III-9.

Table III-9 Intensity ("i"-factors) for spherical top

J	R(J)	Q(J)	P(J)
	$(2J+1)(2J+3)$	$(2J+1)^2$	$(2J+1)(2J-1)$
0	3	-	-
1	15	9	3
2	35	25	15
3	63	49	35
4	99	81	63
5	143	121	99
6	195	169	143
7	255	225	195
8	323	289	255
9	399	361	323
10	483	441	399
11	575	529	483
12	675	625	575
13	783	729	675
14	899	841	783
15	1023	961	899

The nuclear spin factors can be obtained in the following manner: The initial rotational levels can be classified according to the irreducible representations A, E and F of the group T. Those rotational states which transform according to the representation A, have an extra spin weight of 5. The representations transforming according to E and F have no extra weights [9].

If the reduction of the rotational wave function of the J'th rotational level is given by

$$D_J = aA + bE + cF$$

with $a + 2b + 3c = 2J+1$, then the nuclear spin factor of this level is

$$g_J = \frac{5a + 2b + 3c}{2J+1}$$

The spin factors g_J obtained in this way are shown in table III-10 as well as the Boltzmann factors with kT = 200 cm^{-1}. B was taken as 5,27 cm^{-1}.

From tables III-9 and III-10 the theoretical line strengths can be calculated. The results are shown in table III-11.

Table III-10 Spin factors and Boltzmann factors for CH_4.
($B° = 5,27\ cm^{-1}$, $kT = 200\ cm^{-1}$)

J		Spin factor g	E	$e^{-E/kT}$	$ge^{-E/kT}$
0	A	5	0	1	5
1	F	1	10,54	0,9484	0,9451
2	E+F	1	31,62	0,8538	0,8538
3	A+2F	1,571	63,24	0,7290	1,145
4	A+E+2F	1,444	105,40	0,5904	0,8529
5	E+3F	1	158,10	0,4533	0,453
6	2A+E+3F	1,615	221,34	0,3306	0,5339
7	A+E+4F	1,267	295,12	0,2285	0,2895
8	A+2E+4F	1,235	379,44	0,1500	0,1853
9	2A+E+5F	1,421	474,30	0,09329	0,1326
10	2A+2E+5F	1,381	579,70	0,05508	0,0760
11	A+2E+6F	1,174	695,64	0,03087	0,03620
12	3A+2E+6F	1,480	822,12	0,01638	0,02424
13	2A+2E+7F	1,296	959,14	0,008263	0,0107
14	2A+3E+7F	1,276	1106,70	0,003952	0,00504
15	3A+2E+8F	1,387	1264,80	0,001793	0,00248

The upper state vibrational levels are split by the Coriolis perturbation and the total line strength is distributed over the fine structure lines in a manner determined by the spin weights of the individual initial symmetry sublevels from which they originate. When two or more sublevels of the same symmetry type occur for a given value of J, the corresponding intensity is distributed equally over these. The theoretical intensities calculated are shown in table III-12, where the devision necessitated by the occurrence of lines of the same symmetry type is already carried out.

Table III-11 Theoretical line strengths for CH_4

J	R(J)	Q(J)	P(J)
0	15,00	-	-
1	14,23	8,536	2,845
2	29,88	21,35	12,81
3	72,14	56,11	40,08
4	84,40	69,05	53,71
5	64,82	54,85	44,88
6	104,1	90,23	76,35
7	73,82	65,14	56,45
8	59,85	53,55	47,25
9	52,91	47,87	42,83
10	36,74	33,55	30,35
11	20,54	19,17	17,50
12	16,36	15,15	13,94
13	8,386	7,808	7,229
14	4,534	4,241	3,949
15	2,544	2,390	2,236

Table III-12 Theoretical line strength for the fine structure lines

J	R(J)			Q(J)			P(J)		
	A_1 or A_2	E	F_1 or F_2	A_1 or A_2	E	F_1 or F_2	A_1 or A_2	E	F_1 or F_2
0	15	-	-	-	-	-	-	-	-
1	-	-	14,23	-	-	8,54	-	-	2,85
2	-	11,95	17,93	-	8,54	12,81	-	5,12	7,69
3	32,82	-	19,69	25,52	-	15,31	18,23	-	10,94
4	32,47	12,99	19,48	26,57	10,63	15,94	20,67	8,27	12,40
5	-	11,79	17,68	-	9,97	14,96	-	8,16	12,24
6	24,80	9,92	14,88	21,49	8,60	12,89	18,19	7,27	10,91
7	19,42	7,77	11,65	17,14	6,86	10,28	14,86	5,94	8,91
8	14,25	5,70	8,55	12,75	5,10	7,65	11,25	4,50	6,75
9	9,80	3,92	5,88	8,87	3,55	5,32	7,93	3,17	4,76
10	6,34	2,53	3,80	5,79	2,31	3,47	5,24	2,09	3,14

7. Theoretical spectrum

To calculate the optical spectrum, the energies calculated previously is used taking $B = 5{,}27\ cm^{-1}$, $\xi_4 = 0{,}45$ and $\nu_4 = 1306\ cm^{-1}$. A bar-graph of the theoretical spectrum of the P and Q branches generated by using the data in table III-13 is shown in fig. III.3. A bar-graph of the theoretical spectrum of the R branch is shown in

fig. III.4.

8. Experimental spectrum

A 10 cm gas cell with ZnSe windows was filled with pure methane gas (5 kPa). An FT-IR spectrum was recorded with a Bruker 113V spectrophotometer. The resolution obtained was approximately 0,03 cm^{-1}. A bar-graph of the experimental spectrum (fig. III.6) of the ν_4 band is shown in fig. III.5a and III.5b.

It is interesting to note that the bands of the Q branch at high J levels or so much perturbed their wavenumbers are mixed with those of the P branch.

The agreement between the theoretical and experimental spectrum is good, particularly in the P-branch. Exact agreement can only be expected when vibrational and centrifugal changes in the equilibrium configuration as well as the perturbations of other vibrations are also taken into account.

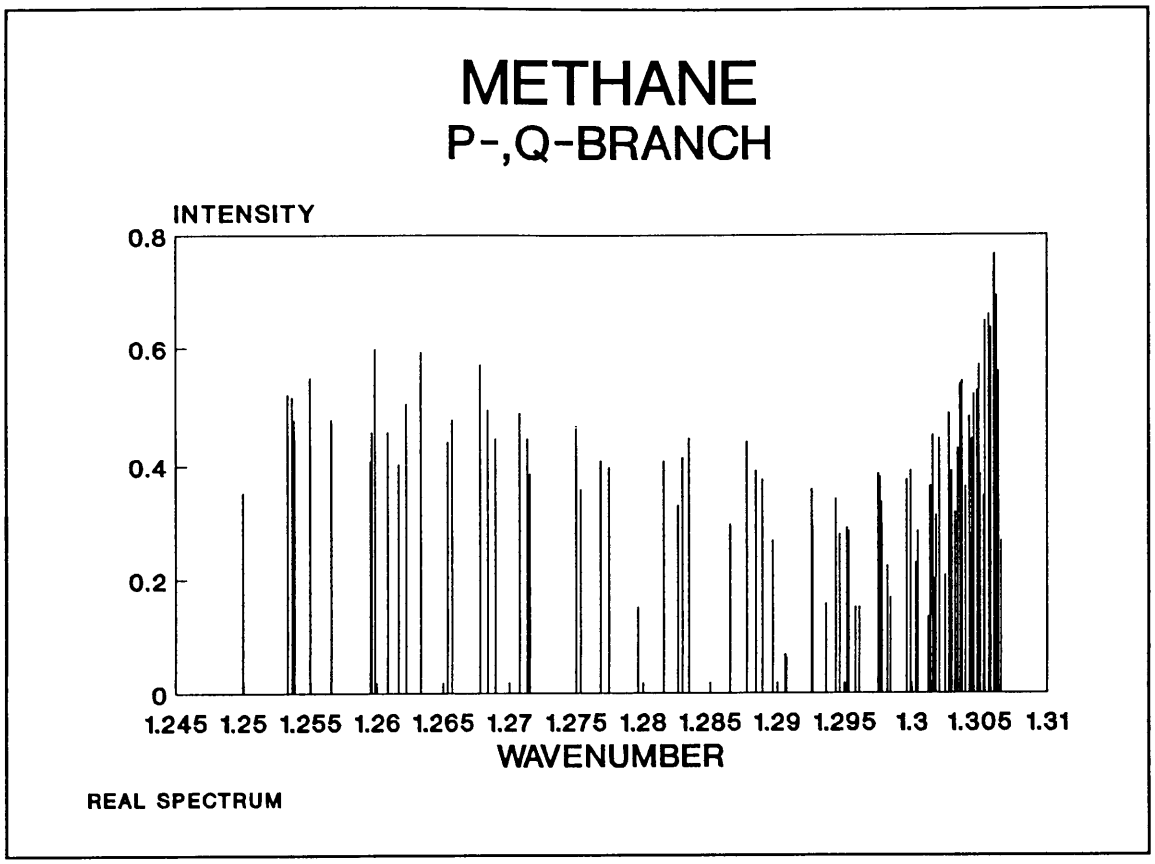

Fig. III.4(a)

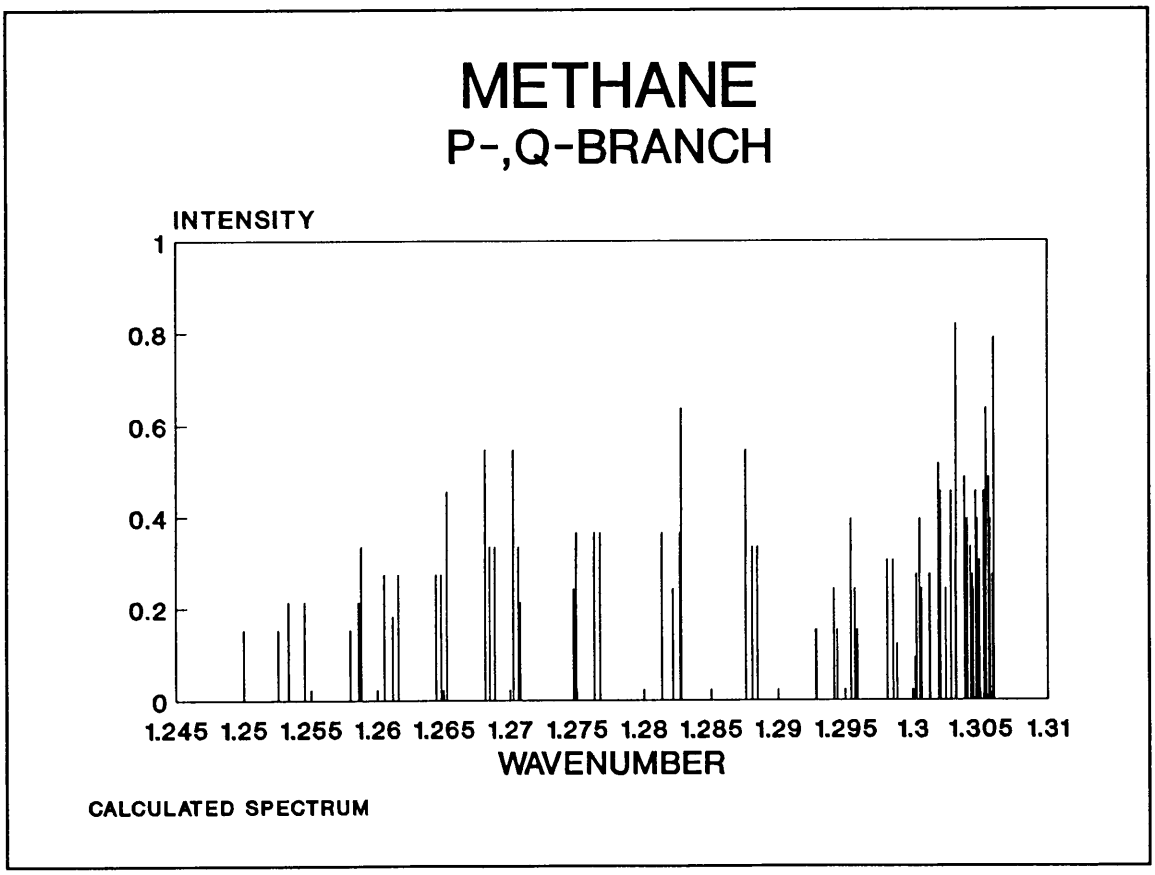

Fig. III.4(b)

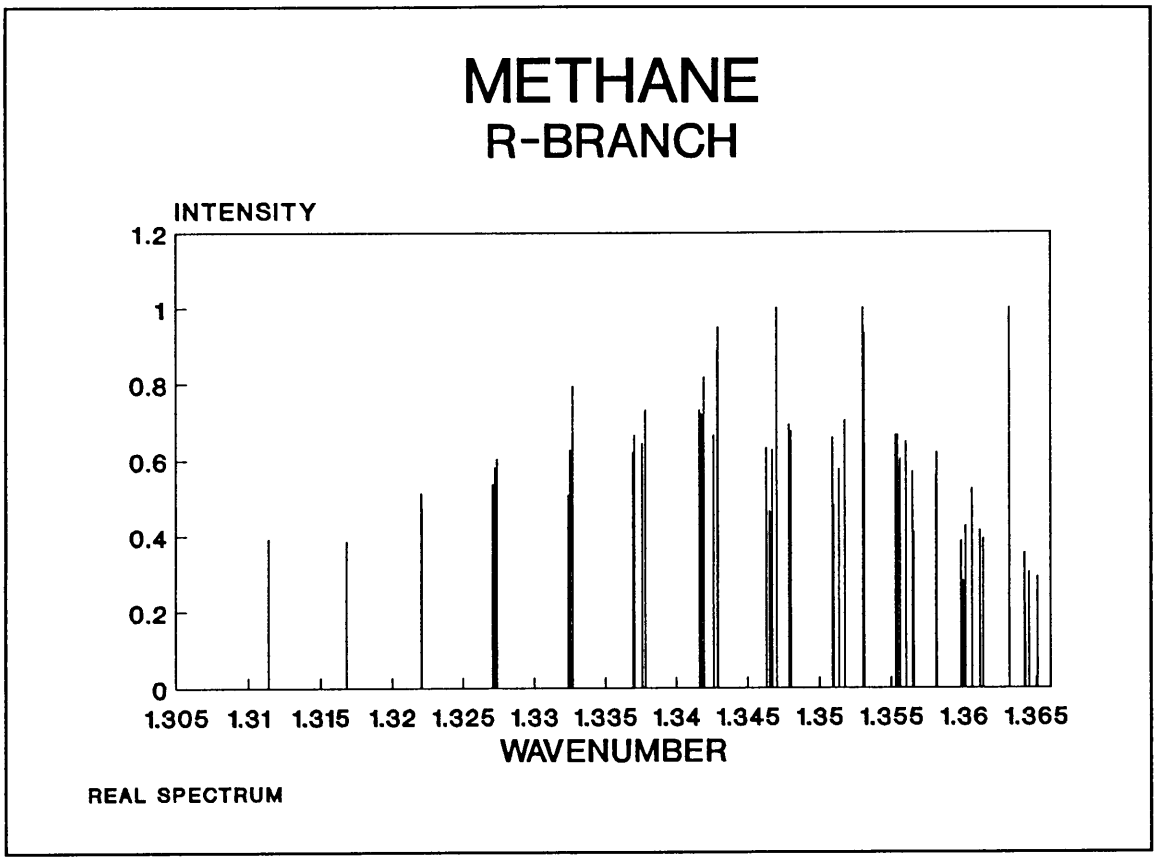

Fig. III.5(a)

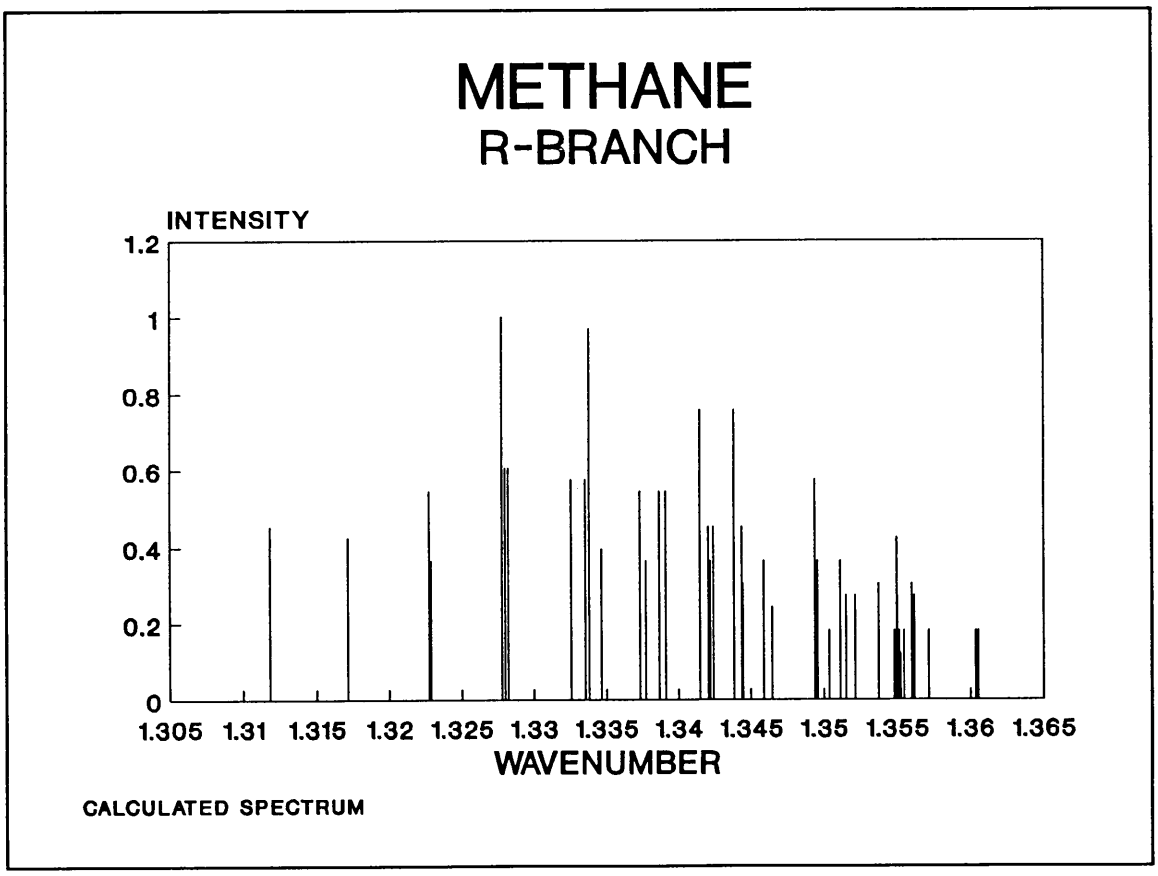

Fig. III.5(b)

HIGH RESOLUTION SPECTRUM

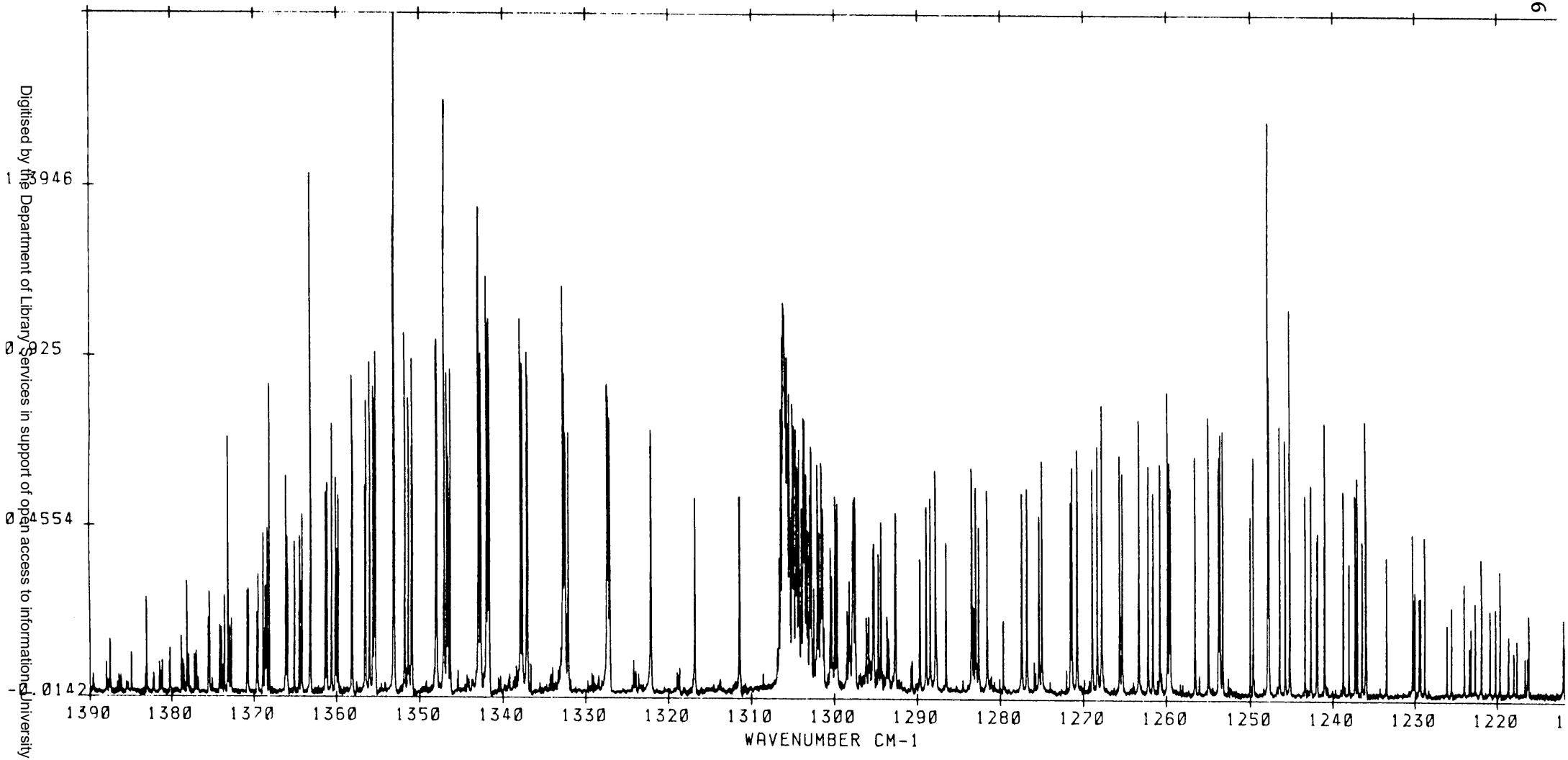

Fig. III.6

Table III-5 Matrix elements of the Coriolis operator A.

R-Branch				Q-Branch				P-Branch			
Lower Level	**Matrix element**			**Lower Level**	**Matrix element**			**Lower Level**	**Matrix element**		
0	A_1		0	1	F_1	a	1,4142	1	F_2	-	0
1	F_2	a	-7,2000	2	E	a	-3,4641	2	E	-	0
2	E	a	8,5714		F_1	a	-2,4495		F_2	a	2,4495
	F_2	a_1	2,9277	3	A_2	-	0	3	A_1	a	-4,8989
		a_2	1,3093		F_1	a_1	-3,8729		F_1	a	-3,4641
3	A_1	a	-4,8989			a_2	3,4641		F_2	a	-1,5492
	F_1	a_1	-2,6458		F_2	a_2	-3,8729	4	A_1	-	0
		a_2	3,4641	4	A_2	a	-7,4833		E	a	3,9279
	F_2	a_2	-3,8729		E	a_1	-5,2915		F_1	a_1	3
4	A_1	a	4,4313			a_2	-2,5298		F_2	a_1	-3,9279
	E	a	5,2432		F_1	a_1	-2,0494			a_2	4,3916
	F_1	a_1	0,8090			a_2	1,7889	5	E	a_1	-3,4641
		a_3	4,8542		F_2	a_1	-6,2609			a_2	-5,7966
	F_2	a_1	3,7075			a_2	-2,0494		F_1	a_1	-0,8944
		a_2	3,1334	5	E	a	-4,6476			a_2	-4,0988
		a_3	-3,7075		$2F_1$	a_{11}	-6,4807		$2F_2$	a_{12}	-3,4641
5	E	a_1	-5,6839			a_{12}	5,4772			a_{21}	-5,3666
		a_2	3,1865			a_{21}	-3,2863			a_{22}	4,0988
		a_3	-3,0382			a_{23}	-3,2863	6	A_1	a	8,7386

Table III-5 (Continued)

R-Branch				Q-Branch				P-Branch			
Lower Level	**Matrix element**			**Lower Level**	**Matrix element**			**Lower Level**	**Matrix element**		
	F_1	a_1	-4,5573		F_2	a_1	3,2863		A_2	a	4,8989
		a_2	3,8431			a_2	-6,4807		E	a	3,3029
	$2F_2$	a_{12}	-5,6839			a_3	-3,2863		F_1	a_1	4,9543
		a_{21}	6,0764	6	A_1	a	9,7101			a_2	.0
		a_{22}	1,4412		A_2	a	-3,4641			a_3	6,6058
		a_{23}	-7,1253		E	a_1	-2,4495		$2F_2$	a_{11}	-4,1779
6	A_1	a	8,8994			a_2	6,8661			a_{12}	6,1791
	A_2	a	-6,8034			a_3	7,8558			a_{13}	-1,5667
	E	a_1	5,1713		$2F_1$	a_{11}	-4,3916			a_{23}	3,8729
		a_2	3,3637			a_{12}	4,6291				0
	F_1	a_1	2,0702			a_{21}	-2,1712	7	A_1	a	-7,8558
		a_2	-2,6075			a_{23}	-10,1840		E	a_1	-6,7596
		a_3	2,7273		F_2	a_1	-0,9258			a_2	-5,1675
	$2F_2$	a_{11}	3,9279			a_2	-4,3916			a_3	-3,6131
		a_{13}	4,8989			a_3	-2,1712		$2F_1$	a_{11}	-2,2237
		a_{14}	-5,3184	7	A_2	a	-9,0396			a_{12}	-4,2193
		a_{22}	6,3336		E	a_1	-6,3919			a_{21}	5,3184
		a_{24}	0,7171			a_2	-1,5119			a_{23}	-6,8034
7	A_1	a_1	-8,6369		$2F_1$	a_{11}	-9,0000		$2F_2$	a_{12}	-5,2623

Table III-5 (Continued)

R-Branch				Q-Branch				P-Branch			
Lower Level	Matrix element			Lower Level	Matrix element			Lower Level	Matrix element		
		a_2	1,9393			a_{13}	7,4833			a_{21}	-7,2263
	E	a_1	-2,7225			a_{21}	-5,4281			a_{22}	5,7129
		a_2	-3,9724			a_{22}	-3,5406			a_{23}	-0,7703
		a_3	8,4284			a_{24}	1,0690	8	A_1	a	4,0988
	$2F_1$	a_{11}	-6,0329		$2F_2$	a_{11}	5,8797		2E	a_{11}	6,5016
		a_{13}	3,9852			a_{13}	-9,0000			a_{12}	4,2289
		a_{21}	1,3117			a_{14}	-5,4281			a_{21}	-1,4591
		a_{22}	-4,3046			a_{22}	-6,9488			a_{22}	-8,9731
		a_{24}	5,4449			a_{24}	-3,5406		$2F_1$	a_{11}	6,4226
	$2F_2$	a_{13}	-7,4558	8	A_2	a_1	-12,3810			a_{12}	-1,3964
		a_{21}	7,1291			a_2	-7,6622			a_{14}	-7,5895
		a_{23}	2,6980		2E	a_{11}	-8,7547			a_{22}	4,5826
		a_{24}	6,0110			a_{12}	-0,7742		$2F_2$	a_{11}	-4,2406
8	A_1	a	7,3984			a_{13}	-7,9055			a_{13}	7,9373
	2E	a_{11}	5,1858			a_{21}	-5,4180			a_{14}	-2,8723
		a_{13}	7,6334			a_{22}	-7,9055			a_{22}	-8,6948
		a_{21}	-6,7396			a_{23}	-3,2258			a_{24}	6,3992
		a_{22}	7,4481		$2F_1$	a_{11}	-6,4226	9	$2F_1$	a_{11}	-3,5147
		a_{23}	0,2180			a_{13}	7,0711			a_{13}	-4,2565

Table III-5 (Continued)

R-Branch				Q-Branch				P-Branch			
Lower Level	Matrix element			Lower Level	Matrix element			Lower Level	Matrix element		
	$2F_1$	a_{11}	3,3425			a_{21}	-4,7697			a_{21}	7,3164
		a_{12}	-6,9206			a_{22}	-2,2361			a_{22}	-0,6859
		a_{14}	7,3984			a_{24}	-4,2426			a_{24}	-9,7619
		a_{22}	0,6489		$2F_2$	a_{11}	2,8284		$3F_2$	a_{13}	-7,0294
		a_{25}	7,5672			a_{13}	-6,4226			a_{21}	-7,8215
	$2F_2$	a_{11}	4,0262			a_{14}	-4,7697			a_{23}	7,1043
		a_{13}	6,6491			a_{22}	-14,1421			a_{24}	-2,0292
		a_{14}	-6,7199			a_{24}	-2,2361			a_{32}	-8,0000
		a_{22}	9,2338		A_1	a	9,7570			a_{34}	6,3246
		a_{24}	1,919		A_2	a	-5,5857				
		a_{25}	-5,9824		E	a_1	-3,9497				
9	A_1	a_1	-5,0534			a_2	6,8993				
		a_2	7,6221			a_3	8,9443				
	A_2	a_2	-11,7983		$3F_1$	a_{11}	-11,4891				
	E	a_1	-8,2393			a_{13}	9,4868				
		a_2	5,9161			a_{21}	-7,3892				
		a_3	-5,2598			a_{22}	-5,9161				
		a_4	3,1701			a_{24}	4,4272				
	$2F_1$	a_{11}	-7,3892			a_{32}	-3,6878				

Table III-5 (Continued)

R-Branch				Q-Branch				P-Branch			
Lower Level	**Matrix element**			**Lower Level**	**Matrix element**			**Lower Level**	**Matrix element**		
		a_{13}	4,0567			a_{35}	-10,7517				
		a_{21}	2,5355		$2F_2$	a_{11}	8,2219				
		a_{22}	7,2427			a_{13}	-11,4891				
		a_{24}	9,9369			a_{14}	-7,3892				
	$3F_2$	a_{13}	-9,2118			a_{22}	-1,8974				
		a_{21}	7,5895			a_{24}	-5,9161				
		a_{23}	3,9497			a_{25}	-3,6878				
		a_{24}	-7,7459								
		a_{32}	9,9369								
		a_{34}	1,2071								
		a_{35}	-4,9425								

Table III-6

J	P BRANCH UNPERTURBED (V2)	Q BRANCH UNPERTURBED (V2)	R BRANCH UNPERTURBED (V2)
0		1536	1546.54
1	1525.46	1536	1557.08
1	1525.46	1536	1557.08
2	1514.92	1536	1567.62
2	1514.92	1536	1567.62
2	1514.92	1536	1567.62
3	1504.38	1536	1578.16
3	1504.38	1536	1578.16
3	1504.38	1536	1578.16
3	1504.38	1536	1578.16
4	1493.84	1536	1588.7
4	1493.84	1536	1588.7
4	1493.84	1536	1588.7
4	1493.84	1536	1588.7
5	1483.3	1536	1599.24
5	1483.3	1536	1599.24
5	1483.3	1536	1599.24
5	1483.3	1536	1599.24
5	1483.3	1536	1599.24
5	1483.3	1536	1599.24
6	1472.76	1536	1609.78
6	1472.76	1536	1609.78
6	1472.76	1536	1609.78
6	1472.76	1536	1609.78
6	1472.76	1536	1609.78
6	1472.76	1536	1609.78
7	1462.22	1536	1620.32
7	1462.22	1536	1620.32
7	1462.22	1536	1620.32
7	1462.22	1536	1620.32
7	1462.22	1536	1620.32
7	1462.22	1536	1620.32
7	1462.22	1536	1620.32
8	1451.68	1536	1630.86
8	1451.68	1536	1630.86
8	1451.68	1536	1630.86
8	1451.68	1536	1630.86
8	1451.68	1536	1630.86
8	1451.68	1536	1630.86
8	1451.68	1536	1630.86

Table III-6 (Continued)

J	P BRANCH UNPERTURBED (V2)	Q BRANCH UNPERTURBED (V2)	R BRANCH UNPERTURBED (V2)
9	1441.14	1536	1641.4
9	1441.14	1536	1641.4
9	1441.14	1536	1641.4
9	1441.14	1536	1641.4
9	1441.14	1536	1641.4
9	1441.14	1536	1641.4
9	1441.14	1536	1641.4
9	1441.14	1536	1641.4
10	1430.6	1536	1651.94
10	1430.6	1536	1651.94
10	1430.6	1536	1651.94
10	1430.6	1536	1651.94
10	1430.6	1536	1651.94
10	1430.6	1536	1651.94
10	1430.6	1536	1651.94
10	1430.6	1536	1651.94
10	1430.6	1536	1651.94
11	1420.06	1536	1662.48
11	1420.06	1536	1662.48
11	1420.06	1536	1662.48
11	1420.06	1536	1662.48
11	1420.06	1536	1662.48
11	1420.06	1536	1662.48
11	1420.06	1536	1662.48
11	1420.06	1536	1662.48
11	1420.06	1536	1662.48

Table III-7(a)

J	SIM P-BR	P BRANCH UNPERTURBED (V4)	P BRANCH EIGENVALUES	P BRANCH UNCORRECTED PERTURBATIONS	P BRANCH CORRECTED PERTURBATIONS	P BRANCH PERTURBED (V4)
1	F_2	1300.203	0	0	0	1300.203
2	E	1294.406	0	0	0	1294.406
2	F_2	1294.406	6	-0.3	-0.3	1294.106
3	F_2	1288.609	2.4	-0.12	-0.1152468203	1288.4937532
3	F_1	1288.609	12	-0.6	-0.5762341014	1288.0327659
3	A_1	1288.609	24	-1.2	-1.2	1287.409
4	A_1	1282.812	0	0	0	1282.812
4	F_1	1282.812	3	-0.15	-0.1412608658	1282.6707391
4	E	1282.812	15.4285	-0.771425	-0.7264810895	1282.0855189
4	F_2	1282.812	34.7142	-1.73571	-1.73571	1281.07629
5	F_2	1277.015	6.8	-0.34	-0.3140915444	1276.7009085
5	F_1	1277.015	17.6	-0.88	-0.8129428209	1276.2020572
5	E	1277.015	45.6	-2.28	-2.106260945	1274.9087391
5	F_2	1277.015	50.8	-2.54	-2.346485966	1274.6685514
6	E	1271.218	10.9091	-0.545455	-0.545455	1270.672545
6	F_2	1271.218	14.1618	-0.70809	-0.641904105	1270.5760959
6	A_2	1271.218	24	-1.2	-1.0878347752	1270.1301652
6	F_2	1271.218	58.929	-2.94645	-2.6710423113	1268.5469577
6	F_1	1271.218	68.1818	-3.40909	-3.0904388783	1268.1275611
6	A_1	1271.219	76.3636	-3.81818	-3.81818	1267.39982
7	A_1	1265.421	5.14285	-0.2571425	-0.2571425	1265.1638575
7	F_2	1265.421	14.8844	-0.74422	-0.6622762693	1264.7587237
7	F_1	1265.421	20.1758	-1.00979	-0.8977152961	1264.5232847
7	F_1	1265.421	77.1428	-3.85714	-3.4324424084	1261.9885576
7	E	1265.421	85.4505	-4.272525	-3.8020906685	1261.6189093
7	F_2	1265.421	98.2584	-4.91292	-4.371973783	1261.0490262
8	A_1	1259.624	16.8	-0.84	-0.7475102338	1258.8764898
8	F_1	1259.624	20.49	-1.0245	-1.0245	1258.5995

Table III-7(a) (Continued)

J	SIM P-BR	P BRANCH UNPERTURBED (V4)	P BRANCH EIGENVALUES	P BRANCH UNCORRECTED PERTURBATIONS	P BRANCH CORRECTED PERTURBATIONS	P BRANCH PERTURBED (V4)
8	E	1259.624	33.7402	-1.68701	-1.4742052652	1258.1497947
8	F_1	1259.624	101.309	-5.06545	-4.4264782429	1255.1975218
8	F_2	1259.624	125.794	-6.2897	-5.4962975065	1254.1277025
9	F_2	1253.827	-	-	-	1253.827
9	F_2	1253.827	-	-	-	1253.827
9	F_2	1253.827	-	-	-	1253.827
9	F_1	1253.827	25.1443	-1.257215	-1.257215	1252.569785
8	E	1259.624	192.351	-9.61755	-8.2555925865	1251.3684074
9	F_1	1253.827	154.62	-7.731	-6.6362001015	1247.1907999
10	F_2	1248.03	22.18	-1.109	-0.9194030927	1247.1105969
10	F_1	1248.03	30.44	-1.522	-1.2617957683	1246.7682042
10	E	1248.03	95.76	-4.788	-3.969433731	1244.0605663
10	F_2	1248.03	101.36	-5.068	-4.2015643586	1243.8284356
10	A_2	1248.03	124	-6.2	-5.1400353242	1242.8899647
10	F_2	1248.03	145.64	-7.282	-6.0370543921	1241.9929456
10	F_1	1248.03	149.33	-7.4665	-6.1900118949	1241.8399881
10	A_1	1248.03	161.65	-8.0825	-6.7006992755	1241.3293007
11	E	1242.233	25.71	-1.2855	-1.0478146385	1241.1851854
11	F_2	1242.233	26.69	-1.3345	-1.0877546753	1241.1452453
11	A_2	1242.233	28.8	-1.44	-1.1737480198	1241.059252
11	F_2	1242.233	111.83	-5.5915	-4.557647259	1237.6753527
11	F_1	1242.233	121.99	-6.0995	-4.9717194771	1237.2612805
11	A_1	1242.233	150.06	-7.503	-6.115716245	1236.1172838
11	F_1	1242.233	176.24	-8.812	-7.1826857991	1235.0503142
11	E	1242.233	184.98	-9.249	-7.538885719	1234.6941143
11	F_2	1242.233	194.77	-9.7385	-7.9378785355	1234.2951215
8	F_2	1259.624	800.0054	-40.00027	-33.161742061	1226.4622579

Table III-7(b)

J	SIM Q-BR	Q BRANCH UNPERTURBED (V4)	Q BRANCH EIGENVALUES	Q BRANCH UNCORRECTED PERTURBATIONS	Q BRANCH PERTURBED (V4)
3	A_2	1306	0	0	1306
1	F_1	1306	2	-0.1	1305.9
2	F_1	1306	6	-0.3	1305.7
4	F_1	1306	7.39999	-0.3699995	1305.6300005
2	E	1306	12	-0.6	1305.4
6	A_2	1306	12	-0.6	1305.4
5	F_1	1306	13.8054	-0.69027	1305.30973
3	F_2	1306	15	-0.75	1305.25
5	E	1306	21.6	-1.08	1304.92
7	F_1	1306	22.33	-1.1165	1304.8835
6	F_2	1306	24.8571	-1.242855	1304.757145
3	F_1	1306	27	-1.35	1304.65
8	F_1	1306	30.3424	-1.51712	1304.48288
9	A_2	1306	31.2	-1.56	1304.44
4	E	1306	34.3999	-1.719995	1304.280005
6	F_1	1306	39.3972	-1.96986	1304.03014
8	E	1306	39.7534	-1.98767	1304.01233
10	F_1	1306	41.12	-2.056	1303.944
7	E	1306	43.1428	-2.15714	1303.84286
9	F_2	1306	43.1454	-2.15727	1303.84273
9	F_1	1306	43.2	-2.16	1303.84
4	F_2	1306	43.3999	-2.169995	1303.830005
4	A_2	1306	56	-2.8	1303.2
7	F_2	1306	56.6428	-2.83214	1303.16786
10	E	1306	60.48	-3.024	1302.976
5	F_2	1306	63.5999	-3.179995	1302.820005
8	F_2	1306	71.1501	-3.557505	1302.442495
10	F_2	1306	75.58	-3.779	1302.221
5	F_1	1306	79.3945	-3.969725	1302.030275

Table III-7(b) (Continued)

J	SIM Q-BR	Q BRANCH UNPERTURBED (V4)	Q BRANCH EIGENVALUES	Q BRANCH UNCORRECTED PERTURBATIONS	Q BRANCH PERTURBED (V4)
7	A_2	1306	81.71429	-4.0857145	1301.9142855
6	A_1	1306	94.2857	-4.714285	1301.285715
9	A_1	1306	95.2	-4.76	1301.24
8	F_1	1306	106.657	-5.33285	1300.66715
6	F_1	1306	109.745	-5.48725	1300.51275
6	E	1306	114.857	-5.74285	1300.25715
10	A_2	1306	120.8	-6.04	1299.96
9	E	1306	143.2	-7.16	1298.84
7	F_2	1306	149.214	-7.4607	1298.5393
7	F_1	1306	157.812	-7.8906	1298.1094
10	F_2	1306	169.3	-8.465	1297.535
10	F_1	1306	185.76	-9.288	1296.712
8	E	1306	202.246	-10.1123	1295.8877
8	F_2	1306	205.849	-10.29245	1295.70755
8	A_2	1306	211.999	-10.59995	1295.40005
9	F_1	1306	263.2	-13.16	1292.84
9	F_2	1306	263.254	-13.1627	1292.8373
10	A_1	1306	330.25	-16.5125	1289.4875
10	E	1306	335.59	-16.7795	1289.2205
10	F_1	1306	378.85	-18.9425	1287.0575

Table III-7(c)

J	SIM R-BR	R BRANCH UNPERTURBED (V4)	R BRANCH EIGENVALUES	R BRANCH UNCORRECTED PERTURBATIONS	R BRANCH CORRECTED PERTURBATIONS	R BRANCH PERTURBED (V4)
9	F_2	1363.97	65.2	-3.26	-3.4749804191	1360.4950196
9	F_1	1363.97	67.1766	-3.35883	-3.5803277549	1360.3896722
9	F_2	1363.97	122	-6.1	-6.6484068465	1357.3215932
8	F_2	1358.173	37.3001	-1.865005	-2.0326741001	1356.1403259
8	A_1	1358.173	54.7368	-2.73684	-2.9828894744	1355.1901105
9	A_2	1363.97	139.2	-6.96	-7.7601376736	1356.2098623
8	F_1	1358.173	57.3263	-2.866315	-3.1958331919	1354.9771668
8	E	1358.173	58.8435	-2.942175	-3.2804142327	1354.8925858
9	E	1363.97	145.782	-7.2891	-8.1270717696	1355.8429282
9	F_2	1363.97	156	-7.8	-8.901370434	1355.0686296
9	F_1	1363.97	161.509	-8.07545	-9.2157143424	1354.7542857
9	A_1	1363.97	166.628	-8.3314	-9.5078048248	1354.4621952
8	F_2	1358.173	108.0151	-5.400755	-6.3118900503	1351.8611099
7	F_1	1352.376	22.33	-1.1165	-1.3048592727	1351.0711407
8	F_1	1358.173	114.042	-5.7021	-6.6640734963	1351.5089265
8	E	1358.173	127.261	-6.36305	-7.436529149	1350.7364709
7	A_1	1352.376	46.3833	-2.319165	-2.7104200225	1349.66558
7	F_2	1352.376	47.0182	-2.35091	-2.7475205667	1349.6284794
7	E	1352.376	94.2352	-4.71176	-5.5066580623	1346.8693419
7	F_2	1352.376	102.805	-5.14025	-6.1557957054	1346.2202043
6	E	1346.579	38.0571	-1.902855	-2.2787970696	1344.3002029
6	F_2	1346.579	40.1017	-2.005085	-2.4012243825	1344.1777756
6	A_2	1346.579	46.2857	-2.314285	-2.7715122152	1343.8074878
7	F_1	1352.376	157.812	-7.8906	-9.4495251385	1342.9264749
6	F_2	1346.579	68.2411	-3.412055	-4.1896325936	1342.3893674
6	F_1	1346.579	74.0571	-3.702855	-4.5467033788	1342.0322966
6	A_1	1346.579	79.2	-3.96	-4.862449483	1341.7165505
5	F_2	1340.782	29.3097	-1.465485	-1.7994562577	1338.9825437

Table III-7(c) (Continued)

J	SIM R-BR	R BRANCH UNPERTURBED (V4)	R BRANCH EIGENVALUES	R BRANCH UNCORRECTED PERTURBATIONS	R BRANCH CORRECTED PERTURBATIONS	R BRANCH PERTURBED (V4)
5	F_1	1340.782	35.5385	-1.776925	-2.1818707191	1338.6001293
5	E	1340.782	51.6923	-2.584615	-3.1736262299	1337.6083738
5	F_2	1340.782	54.6902	-2.73451	-3.4449104453	1337.3370896
4	E	1334.985	5.24318	-0.262159	-0.3302654872	1334.6547345
4	A_1	1334.985	19.6364	-0.98182	-1.2368877691	1333.7481122
4	F_1	1334.985	24.2182	-1.21091	-1.5254932355	1333.4595068
4	F_2	1334.985	37.3091	-1.865455	-2.3500829819	1332.634917
3	F_2	1329.188	15	-0.75	-0.9448430739	1328.2431569
3	F_1	1329.188	19	-0.95	-1.2287222975	1327.9592777
3	A_1	1329.188	24	-1.2	-1.5520702705	1327.6359297
2	E	1323.391	8.57142	-0.428571	-0.5543102566	1322.8366897
2	F_2	1323.391	10.2857	-0.514285	-0.6651720492	1322.725828
1	F_2	1317.594	7.2	-0.36	-0.4656210812	1317.1283789
0	A_1	1311.797	0		0	1311.797

Table III-13(a)

J	SIM P-BR	P BRANCH PERTURBED (V4)	P BRANCH INTENSITY (V4)	P BRANCH INTENSITY NORMALISED
1	F_2	1300.203	3	0.0909090909
2	E	1294.406	5	0.1515151515
2	F_2	1294.106	8	0.2424242424
3	F_2	1288.4937532	11	0.3333333333
3	F_1	1288.0327659	11	0.3333333333
3	A_1	1287.409	18	0.5454545455
4	A_1	1282.812	21	0.6363636364
4	F_1	1282.6707391	12	0.3636363636
4	E	1282.0855189	8	0.2424242424
4	F_2	1281.07629	12	0.3636363636
5	F_2	1276.7009085	12	0.3636363636
5	F_1	1276.2020572	12	0.3636363636
5	E	1274.9087391	8	0.2424242424
5	F_2	1274.6685514	12	0.3636363636
6	E	1270.672545	7	0.2121212121
6	F_2	1270.5760959	11	0.3333333333
6	A_2	1270.1301652	18	0.5454545455
6	F_2	1268.5469577	11	0.3333333333
6	F_1	1268.1275611	11	0.3333333333
6	A_1	1267.39982	18	0.5454545455
7	A_1	1265.1638575	15	0.4545454545
7	F_2	1264.7587237	9	0.2727272727
7	F_1	1264.5232847	9	0.2727272727
7	F_1	1261.9885576	9	0.2727272727
7	E	1261.6189093	6	0.1818181818
7	F_2	1261.0490262	9	0.2727272727
8	A_1	1258.8764898	11	0.3333333333
8	F_1	1258.5995	7	0.2121212121
8	E	1258.1497947	5	0.1515151515
8	F_1	1255.1975218	7	0.2121212121
8	F_2	1254.1277025	7	0.2121212121
9	F_2	1253.827	-	0
9	F_2	1253.827	-	0
9	F_2	1253.827	-	0
9	F_1	1252.569785	5	0.1515151515

Table III-13(a) (Continued)

J	SIM P-BR	P BRANCH PERTURBED (V4)	P BRANCH INTENSITY (V4)	P BRANCH INTENSITY NORMALISED
8	E	1251.3684074	5	0.1515151515
9	F_1	1247.1907999	-	0
10	F_2	1247.1105969	-	0
10	F_1	1246.7682042	-	0
10	E	1244.0605663	-	0
10	F_2	1243.8284356	-	0
10	A_2	1242.8899647	-	0
10	F_2	1241.9929456	-	0
10	F_1	1241.8399881	-	0
10	A_1	1241.3293007	-	0
11	E	1241.1851854	-	0
11	F_2	1241.1452453	-	0
11	A_2	1241.059252	-	0
11	F_2	1237.6753527	-	0
11	F_1	1237.2612805	-	0
11	A_1	1236.1172838	-	0
11	F_1	1235.0503142	-	0
11	E	1234.6941143	-	0
11	F_2	1234.2951215	-	0
8	F_2	1226.4622579	7	0.2121212121

Table III-13(b)

J	SIM Q-BR	Q BRANCH PERTURBED (V4)	Q BRANCH INTENSITY (V4)	Q BRANCH INTENSITY NORMALISED
3	A_2	1306	26	0.7878787879
1	F_1	1305.9	9	0.2727272727
2	F_1	1305.7	13	0.3939393939
4	F_1	1305.6300005	16	0.4848484848
2	E	1305.4	9	0.2727272727
6	A_2	1305.4	21	0.6363636364
5	F_1	1305.30973	15	0.4545454545
3	F_2	1305.25	15	0.4545454545
5	E	1304.92	10	0.303030303
7	F_1	1304.8835	10	0.303030303
6	F_2	1304.757145	13	0.3939393939
3	F_1	1304.65	15	0.4545454545
8	F_1	1304.48288	8	0.2424242424
9	A_2	1304.44	9	0.2727272727
4	E	1304.280005	11	0.3333333333
6	F_1	1304.03014	13	0.3939393939
8	E	1304.01233	5	0.1515151515
10	F_1	1303.944	-	0
7	E	1303.84286	7	0.2121212121
9	F_2	1303.84273	5	0.1515151515
9	F_1	1303.84	5	0.1515151515
4	F_2	1303.830005	16	0.4848484848
4	A_2	1303.2	27	0.8181818182
7	F_2	1303.16786	10	0.303030303
10	E	1302.976	-	0
5	F_2	1302.820005	15	0.4545454545
8	F_2	1302.442495	8	0.2424242424
10	F_2	1302.221	-	0
5	F_1	1302.030275	15	0.4545454545
7	A_2	1301.9142855	17	0.5151515152
6	A_1	1301.285715	9	0.2727272727
9	A_1	1301.24	9	0.2727272727
8	F_1	1300.66715	8	0.2424242424
6	F_1	1300.51275	13	0.3939393939
6	E	1300.25715	9	0.2727272727
10	A_2	1299.96	-	0

Table III-13(b) (Continued)

J	SIM Q-BR	Q BRANCH PERTURBED (V4)	Q BRANCH INTENSITY (V4)	Q BRANCH INTENSITY NORMALISED
9	E	1298.84	4	0.1212121212
7	F_2	1298.5393	10	0.303030303
7	F_1	1298.1094	10	0.303030303
10	F_2	1297.535	-	0
10	F_1	1296.712	-	0
8	E	1295.8877	5	0.1515151515
8	F_2	1295.70755	8	0.2424242424
8	A_2	1295.40005	13	0.3939393939
9	F_1	1292.84	5	0.1515151515
9	F_2	1292.8373	5	0.1515151515
10	A_1	1289.4875	-	0
10	E	1289.2205	-	0
10	F_1	1287.0575	-	0

Table III-13(c)

J	SIM R-BR	R BRANCH PERTURBED (V4)	R BRANCH INTENSITY (V4)	R BRANCH INTENSITY NORMALISED
9	F_2	1360.4950196	6	0.1818181818
9	F_1	1360.3896722	6	0.1818181818
9	F_2	1357.3215932	6	0.1818181818
8	F_2	1356.1403259	9	0.2727272727
8	A_1	1355.1901105	14	0.4242424242
9	A_2	1356.2098623	10	0.303030303
8	F_1	1354.9771668	9	0.2727272727
8	E	1354.8925858	6	0.1818181818
9	E	1355.8429282	4	0.1212121212
9	F_2	1355.0686296	6	0.1818181818
9	F_1	1354.7542857	6	0.1818181818
9	A_1	1354.4621952	10	0.303030303
8	F_2	1351.8611099	9	0.2727272727
7	F_1	1351.0711407	12	0.3636363636
8	F_1	1351.5089265	9	0.2727272727
8	E	1350.7364709	6	0.1818181818
7	A_1	1349.66558	19	0.5757575758
7	F_2	1349.6284794	12	0.3636363636
7	E	1346.8693419	8	0.2424242424
7	F_2	1346.2202043	12	0.3636363636
6	E	1344.3002029	10	0.303030303
6	F_2	1344.1777756	15	0.4545454545
6	A_2	1343.8974878	25	0.7575757576
7	F_1	1342.9264749	12	0.3636363636
6	F_2	1342.3893674	15	0.4545454545
6	F_1	1342.0322966	15	0.4545454545
6	A_1	1341.7165505	25	0.7575757576
5	F_2	1338.9825437	18	0.5454545455
5	F_1	1338.6001293	18	0.5454545455
5	E	1337.6083738	12	0.3636363636
5	F_2	1337.3370896	18	0.5454545455
4	E	1334.6547345	13	0.3939393939
4	A_1	1333.7481122	32	0.9696969697
4	F_1	1333.4595068	19	0.5757575758
4	F_2	1332.634917	19	0.5757575758
3	F_2	1328.2431569	20	0.6060606061
3	F_1	1327.9592777	20	0.6060606061
3	A_1	1327.6359297	33	1
2	E	1322.8366897	12	0.3636363636
2	F_2	1322.725828	18	0.5454545455
1	F_2	1317.1283789	14	0.4242424242
0	A_1	1311.797	15	0.4545454545

CHAPTER IV

QUANTITATIVE ANALYSIS

1. Introduction

The marked increase in the use of infrared spectroscopy for quantitative analysis has stemmed partly from technical improvements in the commercially available infrared spectrophotometers. The coupling of microprocessor-based infrared instruments to small microcomputers has fundamentally shifted the balance of favour among various instrumental techniques toward infrared. Computer-coupled infrared systems have become readily available and quite affordable. A number of software packages for quantitative infrared applications is commercially available. The result is that the tedious parts of quantitative analysis, the evaluation of spectra and the arithmetic involved in calibration and determination steps, can be delegated to the very reproducible action of a computer. In the following discussion the theory and an application of quantitative analysis on the infrared spectrum of a gas mixture will be represented.

2. Basic Theory

(1) Beer-Lambert Law

Quantitative analysis in the infrared region is governed by the same principles that affect the interaction of light and matter in other regions of the electromagnetic spectrum. If a homogeneous sample is viewed as a series of

successive slices of uniform thickness, dx, the fraction of light removed by each slice, $\frac{dI}{I}$, is a constant, k. The mathematical statement of this relationship is shown in eq. IV-1. Integration of eq. IV-1 leads to equation IV-2, which states that the transmitted light intensity I decreases exponentially from the incident value I_o with increasing thickness x of the sample.

$$\frac{dI}{I} = k\,dx \qquad \text{IV-1}$$

$$\frac{I}{I_o} = e^{-kx} \qquad \text{IV-2}$$

Equation IV-2 is referred to as Lambert's Law [10]. Beer proposed that eq. IV-2 could be developed into a relationship between chemical concentration (c) of an absorbing material and the logarithm of the relative transmitted intensity, or absorbance (A), pathlength (b) and an absorbtion coefficient (a)

$$A = \log\frac{I_o}{I} = abc \qquad \text{IV-3}$$

Equation IV-3 represents the fundamental relationship of quantitative absorption spectroscopy and is referred to as Beer's Law [11]. In the derivation of Beer's Law the following limiting requirements are assumed.

1. parallel rays (collimated beam)
2. no stray light
3. monochromatic light
4. homogeneously distributed sample
5. no scattering (infinitesimal particle size)

6. parallel entrance and exit planes (non wedged samples)

7. no molecular interaction

If liberties were taken with the above listed requirements, measurement errors will appear to some degree in the resulting spectral data. Errors due to deviations from Beer's Law can be tolerated to an extent dictated by the requirements for analytical precision in a particular application.

Many systematic errors in the measurement of absorbance can be accounted for to a large extent by the process of calibration. In practise the process of quantitative analysis by infrared spectroscopy is fundamentally a two phase operation which consists of

1. Calibration with standard samples

2. Determination of concentrations of unknown samples

The calibration process may help to compensate for liberties taken with the requirements of Beer's Law and it is desirable that the standard samples are formulated to simulate the expected composition of the unknown samples. The techniques used to prepare standard samples should be as similar as possible to those used to prepare the unknown samples. The quality of results obtained from any analysis is limited by the quality of care taken in the preparation of the standards used to develop the calibration parameters.

For each of the above-mentioned steps in the analytical process, a slight rearrangement of the Beer's Law equation is required. For the calibration step eq. IV-3 must be solved for an absorption coefficient (a), assuming that

the concentration is known, as in eq. IV-4

$$a = \frac{A}{bc} \qquad \text{IV-4}$$

Similarly, for the determination step, eq. IV-3 must be rearranged as in equation IV-5, to solve concentration D, using the value of K obtained in equation IV-4

$$D = \frac{U}{ab} \qquad \text{IV-5}$$

where D is the determined concentration in an unknown sample and U the measured absorbance in an unknown sample. The empirically calculated absorption coefficient, a, is used in both equations IV-4 and IV-5.

Although the rearranged equations appear very simple and straight-forward in this form, the fact that the independent variable (i.e. "c" in eq. IV-4) and the absorption coefficient, a, in eq. IV-5 appears in the denominator of the expression has far reaching implications. This statement will be further elaborated (explained) in section 2 of this chapter.

Beer's equations considered so far have been of the form $y = mx$, which suggests that a plot of absorbance versus concentration will be a linear function which passes through the origin. Experimentally this is not always the case. Deviations from linearity are observed when one or more of the limiting hypothesis of Beer's Law are not satisfied. Even if the absorbance vs. concentration curve is not linear, it may not necessarily pass through the origin.

If the relationship between absorbance and concentration is not linear, i.e. there is a deviation from the Beer-Lambert Law, the resulting curve can be approximated as linear over a limited region of interest by adding a nonzero intercept to the Beer-Lambert-equation as is shown in eq. IV-6. This assumption holds only if the curvature is not to severe [12]

$$A = k_1 c + k_o \qquad \text{IV-6}$$

where $k_1 = ab$ assuming that the same optical cell is used for standards and unknowns.

(2) Multicomponent Analysis

(a) K-Matrix

For multicomponent system the Beer-Lambert expression can be expanded to include absorbances of each of the components at each of the analytical wavelengths such as

$$A = k_1C_1 + k_2C_2 + k_3C_3 + \ldots + k_nC_n \qquad \text{IV-7}$$

If the number of components in the analysis is identified by n and a set of w spectral measurement positions has been selected with $w \geq n$, then a total of w equations can be written to describe the contributions to the absorbance at each of the w measurement locations by each of the n components as in equation IV-8 [4].

$$\begin{aligned} A_1 &= k_{11}C_1 + k_{12}C_2 + k_{13}C_3 + \ldots + k_{1n}C_n \\ A_2 &= k_{21}C_1 + k_{22}C_2 + k_{23}C_3 + \ldots + k_{2n}C_n \\ &\vdots \quad\quad \vdots \quad\quad \vdots \quad\quad \vdots \quad\quad \vdots \\ &\vdots \quad\quad \vdots \quad\quad \vdots \quad\quad \vdots \quad\quad \vdots \\ A_w &= k_{w1}C_1 + k_{w2}C_2 + k_{w3}C_3 + \ldots + k_{wn}C_n \end{aligned} \qquad \text{IV-8}$$

All of the equations in the above set apply to the measurement of only one sample. It is convenient to write the above equation in matrix formulism i.e.

$$\begin{bmatrix} A_1 \\ A_2 \\ \vdots \\ \vdots \\ A_w \end{bmatrix} = \begin{bmatrix} k_{11} & k_{12} & \text{----} & k_{1n} \\ k_{21} & k_{22} & \text{----} & k_{2n} \\ \vdots & \vdots & & \vdots \\ \vdots & \vdots & & \vdots \\ k_{w1} & k_{w2} & \text{----} & k_{wn} \end{bmatrix} \begin{bmatrix} C_1 \\ C_2 \\ \vdots \\ \vdots \\ C_n \end{bmatrix} \qquad \text{IV-9}$$

Equation IV-9 can be expressed even more simply by representing each matrix with a single letter

$$A = KC \qquad \text{IV-10}$$

Once the K-matrix is calculated from the calibration procedure, its inverse can be used to determine the concentrations of unknowns from measured absorbances as

$$C = K^{-1} A \qquad \text{IV-11}$$

The elements of the K-matrix can be determined by measuring spectra of individual components, however this does not take into consideration the interactions between molecules of the different components. A better approach is to make similar measurements on at least m standards with $m \geq n$. The calibration problem can then be formulated as

$$\begin{bmatrix} A_{11} & A_{12} & \text{---} & A_{1m} \\ A_{21} & A_{22} & \text{---} & A_{2m} \\ \vdots & \vdots & & \vdots \\ \vdots & \vdots & & \vdots \\ A_{w1} & A_{w2} & \text{---} & A_{wm} \end{bmatrix} = \begin{bmatrix} k_{11} & k_{12} & \text{---} & k_{1n} \\ k_{21} & k_{22} & \text{---} & k_{2n} \\ \vdots & \vdots & & \vdots \\ \vdots & \vdots & & \vdots \\ k_{w1} & k_{w2} & \text{---} & k_{wn} \end{bmatrix} \begin{bmatrix} C_{11} & C_{12} & \text{---} & C_{1m} \\ C_{21} & C_{22} & \text{---} & C_{2m} \\ \vdots & \vdots & & \vdots \\ \vdots & \vdots & & \vdots \\ C_{n1} & C_{n2} & \text{---} & C_{nm} \end{bmatrix} \qquad \text{IV-12}$$

where the A and C matrices have been extended to include a column of a's and a column of c's, respectively for each standard mixture. The K-matrix is identical with that in eq. IV-9. In this case $m \geq n$, i.e. the number of standard mixtures must be equal to or greater than the number of components. The matrix multiplications in eq. IV-12 can be symbolized as

$$\bar{A} = K\bar{C} \qquad \text{IV-13}$$

where $\bar{A}$ and $\bar{C}$ are the extended matrices A and C matrices respectively. Matrices $\bar{A}$ and $\bar{C}$ are not square since in the over-determined case, more standard mixtures (m) are used than components (n). Taking this account the equation for K can be solved by right multiplying both sides of eq. IV-13 by the transpose of $\bar{C}$

$$\bar{A}\bar{C}^t = K\bar{C}\bar{C}^t \qquad \text{IV-14}$$

and both sides by the inverse of the square matrix $(\bar{C}\bar{C}^t)$ which gives

$$K = \bar{A}\bar{C}^t(\bar{C}\bar{C}^t)^{-1} \qquad \text{IV-15.}$$

This equation represents the least-square fit of K and minimizes the sum of the squares of the differences between the observed and calculated absorbances. The inverse of K can be calculated and used in eq. IV-16 to determine concentrations of unknowns from measured absorbances.

$$\bar{C} = K^{-1}\bar{A} \qquad \text{IV-16.}$$

(b) Numerical stability of matrix inversion

The above method requires two matrix inversions namely,

1. the inverse of $(\bar{C}\bar{C}^t)$ must be determined to obtain K
2. the inverse of K must be determined to solve for concentrations

in unknown samples from measured absorbances using eq. IV-16.

Both inversions are time consuming and likely sources of round-off error on a computer.

Non-singularity of the concentration- and absorbtion coefficient matrices is a problem that should be avoided for successful multicomponent analysis since the inverse of a singular matrix is undefined and cannot be calculated. The singular condition occurs when any-one of the following conditions is met

1. a row or column is all zeros.
2. a row or column is a multiple of another row or column.
3. a row or column amounts to a linear combination of two or more other rows or columns respectively.

In the analysis step singularity of the absorption coefficient matrix can be avoided by the correct choice of the analytical wavelengths. If there were no overlap of the analytical bands the absorption coefficient matrix will look like as is shown in eq. IV-17 (i.e. a diagonal matrix)

$$K = \begin{bmatrix} k_{11} & O & O & --- & O \\ O & k_{22} & O & --- & O \\ O & O & k_{33} & & \vdots \\ \vdots & \vdots & & & \vdots \\ O & O & O & --- & k_{wn} \end{bmatrix} \qquad \text{IV-17}$$

The other extreme namely, that the spectra of two or more components overlap to such an extent that they appear to be superimposable, will lead to

a singular absorption coefficient matrix. This means that the inversion of the K-matrix in eq. IV-16 will lead to unreliable results.

In practise the less extreme case is usually experienced. The analytical bands may overlap but are not totally superimposable. In this case the absorption coefficient are not singular, but it approaches singularity and the results of the analysis may be less reliable. When the absorption coefficients are only slightly different in two rows or two columns, the noise has a relative large degree of control in terms of shifting the calibration matrix situation toward or away from singularity. In multicomponent analysis the signal-to-noise ratio in the collected analytical data is a more critical than in single component analysis [13].

Additional difficulties appear when deviations from Beer's Law appears. These deviations can be approximated for by adding a nonzero intercept to the expressions in eq. IV-8. By augmenting eq. IV-12 the matrix equation becomes

$$\begin{bmatrix} A_{11} & A_{12} & \cdots & A_{1m} \\ A_{21} & A_{22} & \cdots & A_{2m} \\ \vdots & \vdots & & \vdots \\ \vdots & \vdots & & \vdots \\ A_{w1} & A_{w2} & \cdots & A_{wm} \end{bmatrix} = \begin{bmatrix} k_{11} & k_{12} & \cdots & k_{1n} & k_{10} \\ k_{21} & k_{22} & \cdots & k_{2n} & k_{20} \\ \vdots & \vdots & & \vdots & \vdots \\ \vdots & \vdots & \cdots & \vdots & \vdots \\ k_{w1} & k_{w2} & & k_{wn} & k_{wo} \end{bmatrix} \begin{bmatrix} C_{11} & C_{12} & \cdots & C_{1m} \\ C_{21} & C_{22} & \cdots & C_{2m} \\ \vdots & \vdots & & \vdots \\ \vdots & \vdots & & \vdots \\ C_{n1} & C_{n2} & \cdots & C_{nm} \\ 1 & 1 & \cdots & 1 \end{bmatrix} \qquad \text{IV-18}$$

The K-matrix is now (w x n + 1) with a column added at the analytical frequencies. These (w x n + 1) k_{wn} values can be determined by a least

squares regression analysis on at least m + 1 standard mixtures.

If the concentrations for the components in the m mixtures are expressed in convenient terms such as percentage or mole fraction, the last row of the $\bar{C}$ matrix is equal to the sum (or 0,01 times the sum in the case of percentages) of the other rows. Therefor if $\bar{C}$ is square the $\bar{C}$ matrix is singular or if $\bar{C}$ is not square ($\bar{C}\bar{C}^t$) is singular and the inverse is indeterminant [14]. The matrix relationship like that in eq. IV-10 is still valid but in this case the relationship of eq. IV-11 must be written as

$$C = (K^tK)^{-1} K^tA \qquad \text{IV-19}$$

Since the K-matrix is not square the inverse cannot be calculated since it contains more columns than rows. This limitation can be overcome by including additional analytical frequencies, i.e. by having more rows than columns (a new row is added to $\bar{K}$ for each analytical frequency) [15].

(c) P-Matrix

The above-mentioned problems can be eliminated by reversing the Beer-Lambert Law and expressing the concentration as a function of absorbance. In matrix notation this becomes

$$\bar{C} = P\bar{A} \qquad \text{IV-20}$$

$$\begin{bmatrix} C_{11} & C_{12} & --- & C_{1m} \\ C_{21} & C_{22} & --- & C_{2m} \\ \vdots & \vdots & & \vdots \\ \vdots & \vdots & & \vdots \\ C_{n1} & C_{n2} & --- & C_{nm} \end{bmatrix} = \begin{bmatrix} p_{11} & p_{12} & --- & p_{1n} & p_{10} \\ p_{21} & p_{22} & --- & p_{2n} & p_{20} \\ \vdots & \vdots & & \vdots & \vdots \\ \vdots & \vdots & & \vdots & \vdots \\ p & p & --- & p_{wn} & p_{wo} \end{bmatrix} \begin{bmatrix} A_{11} & A_{12} & --- & A_{1m} \\ A_{21} & A_{22} & --- & A_{2m} \\ \vdots & \vdots & & \vdots \\ \vdots & \vdots & & \vdots \\ A_{w1} & A_{w2} & --- & A_{wm} \\ 1 & 1 & --- & 1 \end{bmatrix} \qquad \text{IV-21}$$

where the P-matrix replaces the K-matrix as the proportionality matrix. The P-matrix can be easily determined from extended C- and A-matrices using least squares as

$$P = \bar{C}\bar{A}^t(\bar{A}\bar{A}^t)^{-1} \qquad \text{IV-22}$$

The resulting matrix can be used directly in eq. IV-20 as the calibration matrix without going through the inversion process [16]. The P-matrix eliminates the restriction imposed on the K-matrix by addition of the non-zero intercept and it also eliminates one matrix inversion (the determination of K^{-1}).

In some cases, deviations from Beer's Law may be so severe that in order to perform an analysis it may be necessary to fit the standard data with higher order equations, such as quadratic, cubic or logs. For a two-component mixture, the quadratic expression would take the form [17]

$$\begin{aligned} C_1 &= p_{11} A_1 + p_{12} A_2 + p_{13} A_1^2 + p_{14} A_2^2 + p_{15} A_1 A_2 \\ C_2 &= p_{21} A_1 + p_{22} A_2 + p_{23} A_1^2 + p_{24} A_2^2 + p_{25} A_1 A_2 \end{aligned} \qquad \text{IV-23}$$

A power series for the same mixture would be

$$\begin{aligned} C_1 &= p_{11} A_1 + p_{12} A_2 + p_{13} A_1^2 + p_{14} A_2^2 \\ C_2 &= p_{21} A_1 + p_{22} A_2 + p_{23} A_1^2 + p_{24} A_2^2 \end{aligned} \qquad \text{IV-24}$$

3. Practical Considerations

(1) Analytical wavelengths

(a) Sensitivity optimization

The first criterion for the selection of measurement locations for the analysis is that at least one point should be selected for each component which corresponds to the largest absorbance change in the spectrum for a specific change in the concentration of that component in the sample [18]. The usual choice is a peak maximum of a strong band of the component. The apparent maximum of a peak in a mixture does not always correspond to the true maximum of the absorbance coefficient. The apparent maximum of a peak in a mixture does not always correspond to the true maximum of the absorbance coefficient. The apparent maximum depends on the sum of absorbances contributed by adjacent peaks, it is shifted in the direction of the strongest peak.

(b) Selectivity optimization

The overlap of the analytical bands should be minimized [19]. It is preferable that the measurement locations are selected that the K-matrix are close to a diagonal matrix. (See eq. IV-17.)

In practise there will have to be a compromise between the two criteria since the overlap of the two peaks will result in sizeable off diagonal elements in the calibration matrix. Changing the wavenumbers selected to reduce overlap

may lead to a selection of weaker bands, which means that the magnitude of the diagonal element will be diminished. Normally the peak maximum is selected, since the absorbance at that frequency is less sensitive to the lack of frequency reproducibility. In some cases, results can be improved using analytical frequencies on sides of bands [20].

(2) Diverse considerations

(a) In the case of solutions the solvent contributes a certain amount to the sample spectrum at each spectral measurement location.

(b) Atmospheric absorptions may also contribute to the spectrum. This effect can be minimized by purging the sample compartment with a dry inert gas like nitrogen.

(c) The ambient temperature should be fairly constant since a variation in temperature will ultimately influence the repeatability of the results.

(d) The electronic noise of the spectrometer also plays an important role. It is interesting to note that the percentage error of the digital computer can be as much as 0,1% [14].

These effects, added together, will amount to relatively constant contributions to all of the sample spectra in the analysis. It is important that the equations used in the analysis must correspond to the actual contributions to the measured absorbance. If spectral variations are present that can not be accounted for by recognition of the appropriate set of components, it is probable that the matrix mathematics will force the effects of this variations into the absorbance coefficient values in the calibration matrix. These errors

will be translated into concentration errors in the determined results.

4. Advantages of Multicomponent Analysis

(a) Fewer mixtures are required. In the normal approach, three or more mixtures of known concentration of each component may be required for each coefficient of each component. For n components, this can be as many as $3n^2$ mixtures. In multicomponent analysis only n mixtures for n components are needed.

(b) Analyses are developed much faster. A multicomponent analysis for n components can be done in only $\frac{1}{n^2}$ as much time as normal.

(c) Analysis is far more precise since a number of sources of random error are essentially eliminated such as mixture preparation and sample handling.

(d) Analysis is far more accurate since the method of calculation eliminates systematic errors.

5. An application of the multicomponent K-matrix method to a gas mixture

(1) Experimental Section

Raw-gas originating from the Sasol-Gassification plant were analysed on a continuous basis with a Mitchelson 100, FT-IR spectrophotometer manufactured by the BOMEM Company. A 50 mℓ flow-through gas cell, equipped with zinc selenide windows, was used to analyse the sample at a flow rate of 50 mℓ/min. The instrument purging gas flow rate was $1\ell \cdot h^{-1}$.

A reference spectrum was recorded on the same nitrogen used to purge the instrument.

Gas mixtures were taken from the gasification line at intervals of 4 hours, and characterized by Gas Chromatography. These mixtures were used as calibration standards. The concentrations of the three main components in these standard mixtures are tabulated in table IV-1.

Table IV-1

Mixture	CO	CO_2	CH_4
1	21,15	27,74	9,96
2	21,21	28,11	9,63
3	22,67	27,43	9,88
4	23,47	26,98	9,13
5	21,77	27,10	9,58
6	21,92	27,10	10,32

A typical FT-IR spectrum of these gas mixtures are shown in fig. IV.1. The analytical wavelength ranges used to measure the absorbances of the components is given in table IV-2.

Table IV-2

Component	Start/cm^{-1}	End/cm^{-1}	Standard deviation percentage
CO	2156,0	2185,0	0,2163
CO_2	3721,9	3735,4	0,3305
CH_4	3008,4	3018,1	0,0417

The unknown spectra were recorded with time intervals of approximately 5 minutes. Thirty scans were taken at a resolution of 4 cm^{-1} for each unknown.

(2) Results and Discussion

The K-matrix method was used to calculate the unknown concentrations. The standard deviations for each component, in the calibration step, are given in table IV-2.

A plot of typical calculated concentrations, over a period of time, of the three main components is shown in fig. IV.2.

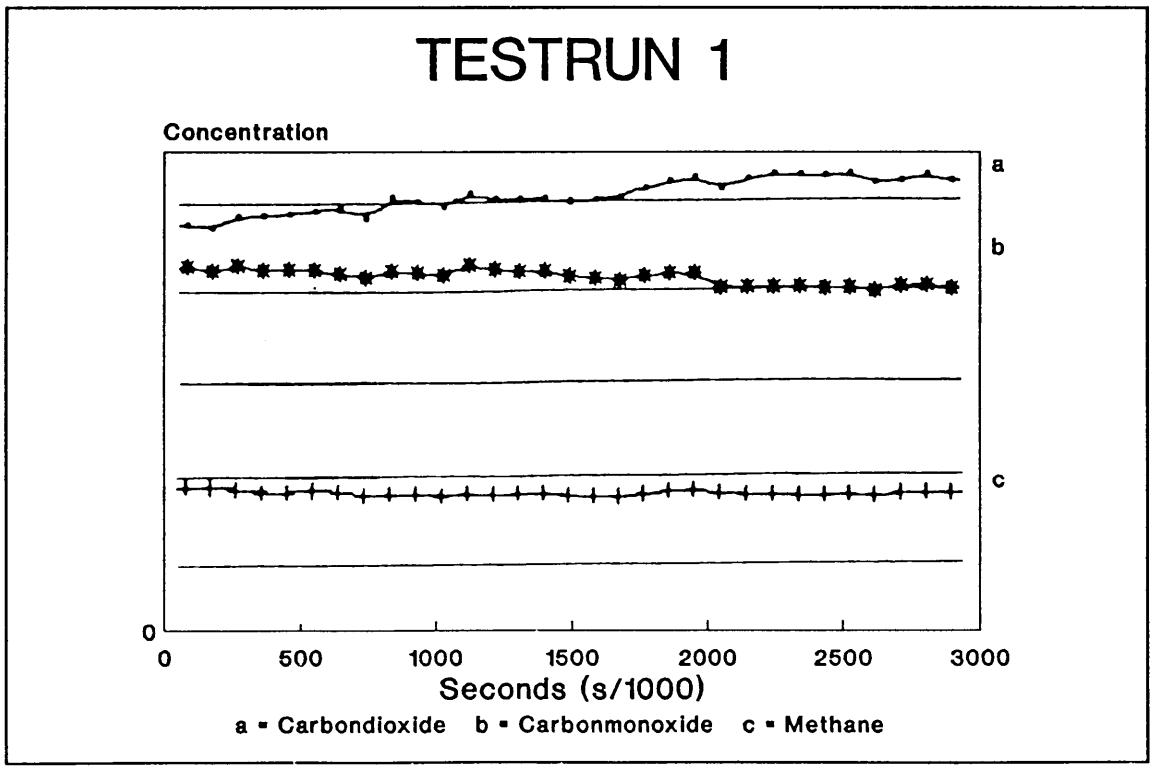

Fig. IV.2

The intensity of the CO_2 band centred as 2349 cm^{-1} is too high for analytical

measurements, therefore the combination bands centred at 3650 cm^{-1} were used as an alternative. The methane band centred at 3018 cm^{-1} was relatively free of spectral interferences but the band centred at 1306 cm^{-1} would also have been a good choice. The P-branch of the carbon monoxide band at 2143 cm^{-1} was used since the R-branch of carbon monoxide is too near to the P-branch of the CO_2 band at 2349 cm^{-1}.

The fact that FT-IR spectra of gases normally have a fairly even baseline led to the choice of the zero baseline for the intensity measurements of the absorption peaks. A direct proportionality between the concentration variation and the inaccuracy of the calculated concentration values existed. This is due to the small concentration variation of calibration standards taken from the gassification line.

The above spectra from which fig. IV.2 results were recorded with time intervals of 5 minutes. Making use of the BOMEM Michelson software it is also possible to record a FT-IR spectrum every 2 minutes on a continuous flow-through basis.

6. Conclusions

It can be concluded that a FT-IR spectrophotometer can be used with success as an online rapid monitor of the raw-gas originating from the Gasification plant. The K-matrix method resulted in good accuracy and the absolute error of the measurements was as follows: CO : 0,22%, CO_2 : 0,33% and CH_4 : 0,042%. The H_2 gas can not be measured with the FT-IR method but since the rest of the minor components add

up to less than one percent the H_2 concentration can easily be calculated with reasonable accuracy. The smallest time interval in which a spectrum could be recorded and analyzed is approximately 2 minutes.

The ambient temperature is also a very critical factor since the DTGS mid-infra-red detector seems to be very sensitive to temperature fluctuations. Temperature definitely influences the repeatability of the measurements. Temperature fluctuations can be minimized by placing the spectrophotometer inside a temperature controlled environment.

In doing so it might be rewarding to investigate the possible utilization of optical fibres as conveyers of the electromagnetic information from the pipe line to a temperature controlled control room. In this regard the vibrational overtones of fundamental modes occurring in the near infra-red may provide excellent possibilities.

Fig. IV.1 A typical FT-IR spectrum of the gas mixtures

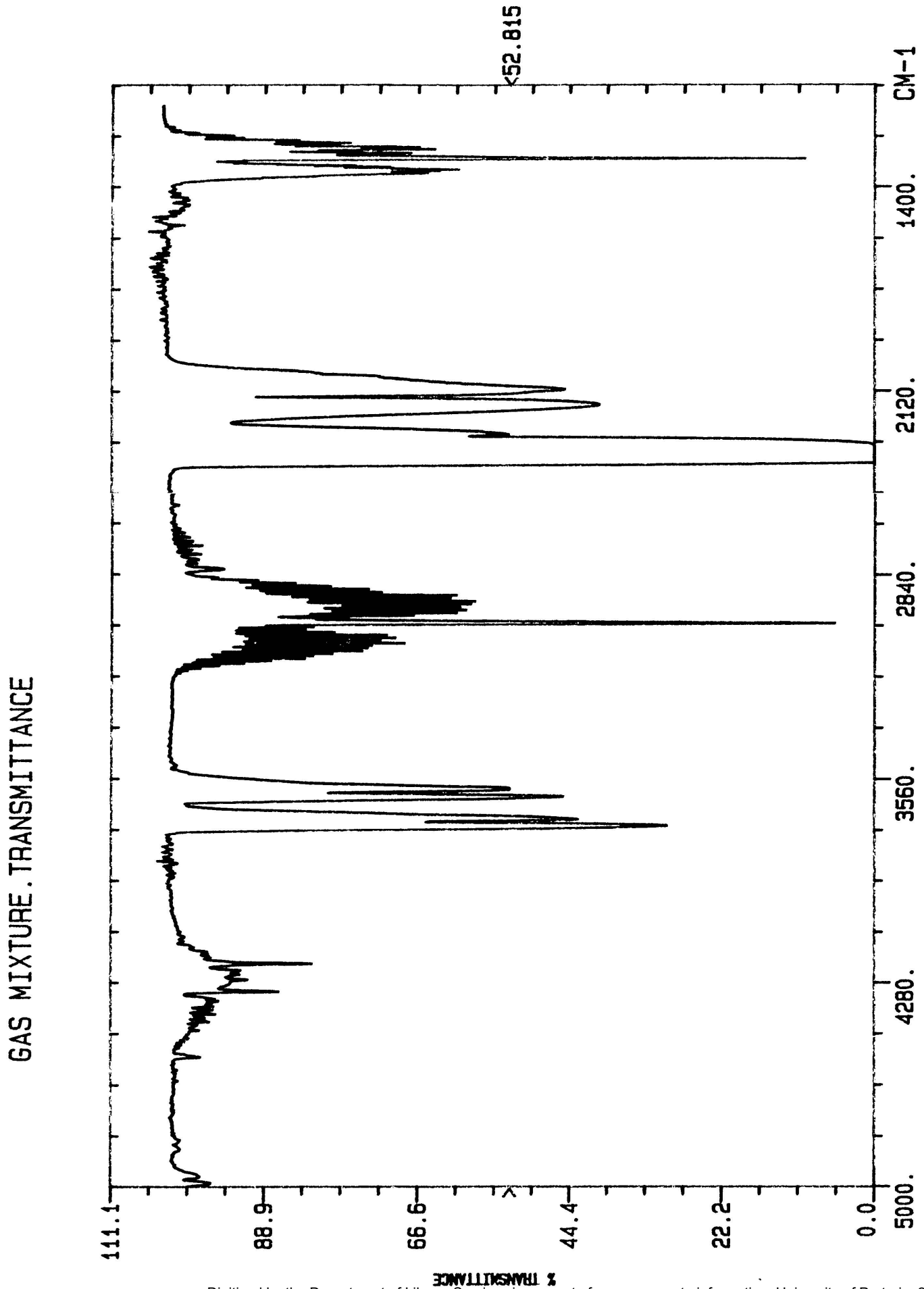

CHAPTER V

QUANTITATIVE ANALYSIS OF GASES, PRESENT IN LOW CONCENTRATIONS

1. Introduction

In the previous chapter the quantitative analyses of the main components of a gas mixture were discussed. Quantitative analyses of gases present in low concentrations are more difficult since the intensity of the infra-red peaks becomes comparible with that of the noise. If the characteristic peaks of the low concentration gases overlap with those of the main components, the situation becomes still more complex (Section 3, Chapter IV). A typical spectrum illustrating this point can be seen in fig. V.3 where the H_2S peaks, at 2056 cm^{-1} and 2072 cm^{-1} (marked by an asterisk), are obscured by the intense peak of CO at 2143 cm^{-1}. A standard technique to enhance a signal is to use a longpath gas cell. In this case the overlapping CO signal will also be enhanced. This illustrates the necessity for a technique to enhance a signal selectively. Two types of gas cells were originally designed, built and tested in our laboratories namely:

(i) Liebig type -

(ii) Liebig-Metal Light Pipe type gas cell.

2. Liebig type gas cell

(a) Apparatus and Procedure

A gas cell as is shown in fig. V.1 was used to condense the H_2S gas in order

to selectively enhance the H_2S signal. The working procedure of the gas cell can be summarized as follows:

(i) Cooling off

(ii) Condensation

(iii) Closing valves

(iv) Evaporation

(v) Recording

(vi) Purging

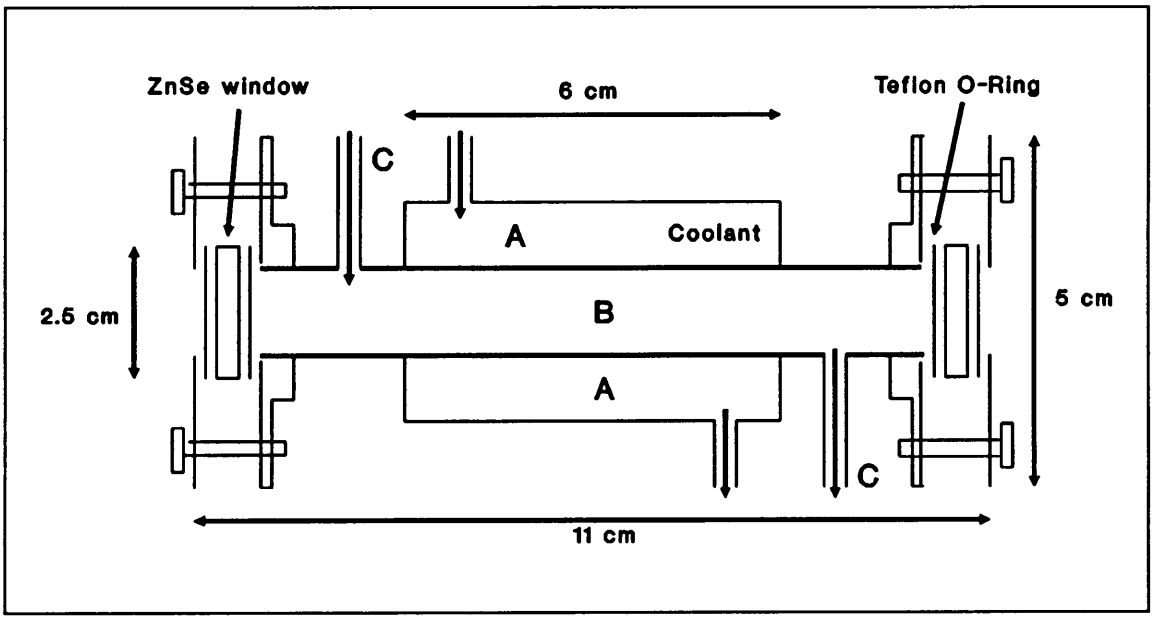

Fig. V.1 Liebig type gas cell

Cold nitrogen gas, generated by allowing N_2 gas to flow through a cooled copper spiral, is pumped through the compartment marked A. The copper tubing can be cooled by immersion in a liquid nitrogen bath. Various other cooling mixtures can also be used, depending on the desired cooling temperature. The gas mixture to be analized is allowed to flow through the cold tube, marked B. Depending on the vapour pressure of the components

as well as on their partial vapour pressure in the mixture, some of the components will be captured inside the gas cell by condensation against the sides of the tube. Those components without sufficient vapour pressure at the specific temperature will not condense, but flow through the gas cell.

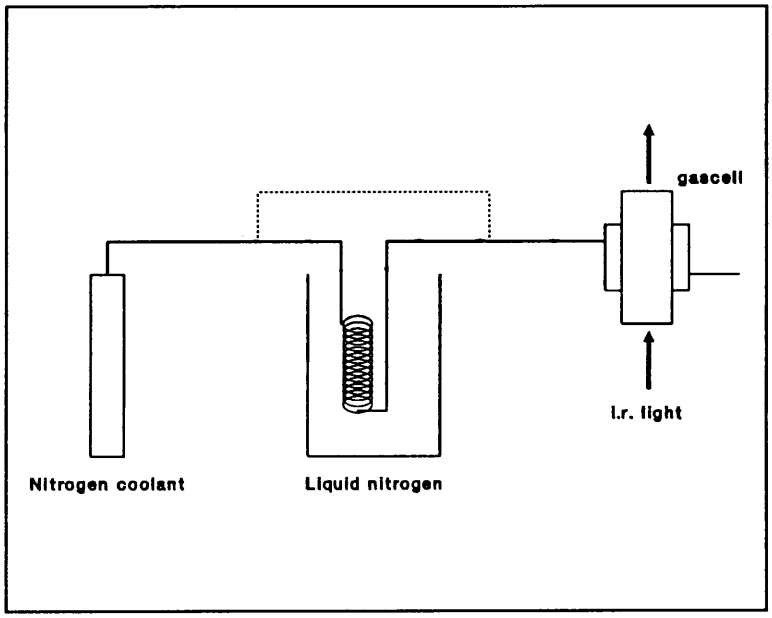

Fig. V.2a

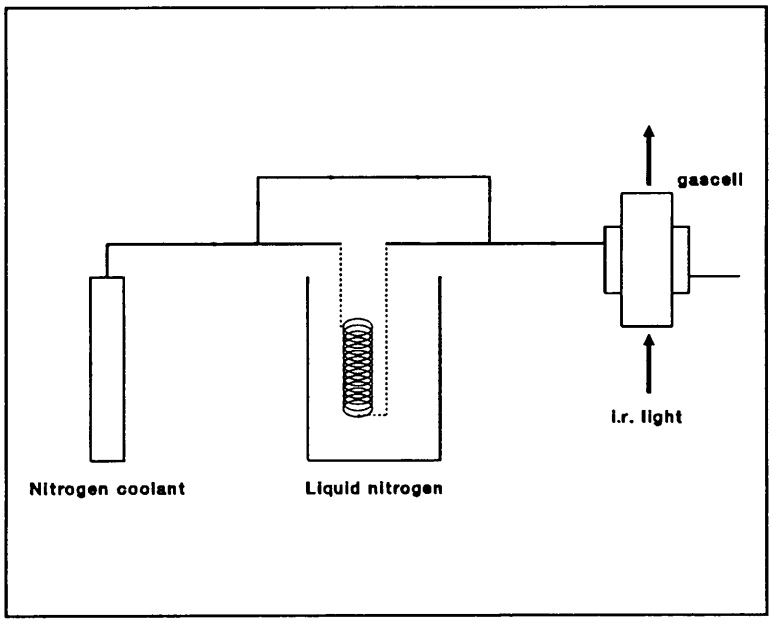

Fig. V.2b

The in- and outlet valves, marked C, are closed off after a certain time and the cooled copper spiral is bypassed as is shown in fig. V.2b. The condensed matter is heated by way of allowing nitrogen gas, at ambient temperature, to flow through compartment A, causing evaporation of the condensed matter into the i.r. light path.

(b) Results and discussion

After following the above procedure a spectrum was recorded. This spectrum is shown in fig. V.3(3). The spectrum marked 3(2) in the same figure is a spectrum of a gas mixture, containing both H_2S and CO, at room temperature. The concentrations of the various components are listed in table V-1. The flow-rate was 70 mℓ/min and the concentration time was 10 min at -150°C. As can be seen from fig. V.3 the H_2S:CO ratio increased, indicating that the H_2S was selectively captured inside the gas cell. The intensity of the CO_2 signal at 2349 cm^{-1} also increased but the CO and CH_4 did not condense.

Table V-1

	Percentage ($^v/_v$)	
CO_2	0,63	(6300 ppm)
N_2	0,79	
CO	28,59	
H_2	57,08	
CH_4	12,43	
Ar	0,47	
H_2S	0,1	(1000 ppm)

The mass of H_2S, necessary to give a signal comparable to that of CO, was

determined by allowing the standard gas mixture to flow through the cell for various periods of time at a constant flow-rate. As can be seen from the yellow spectrum this mass equals 0,195 mg.

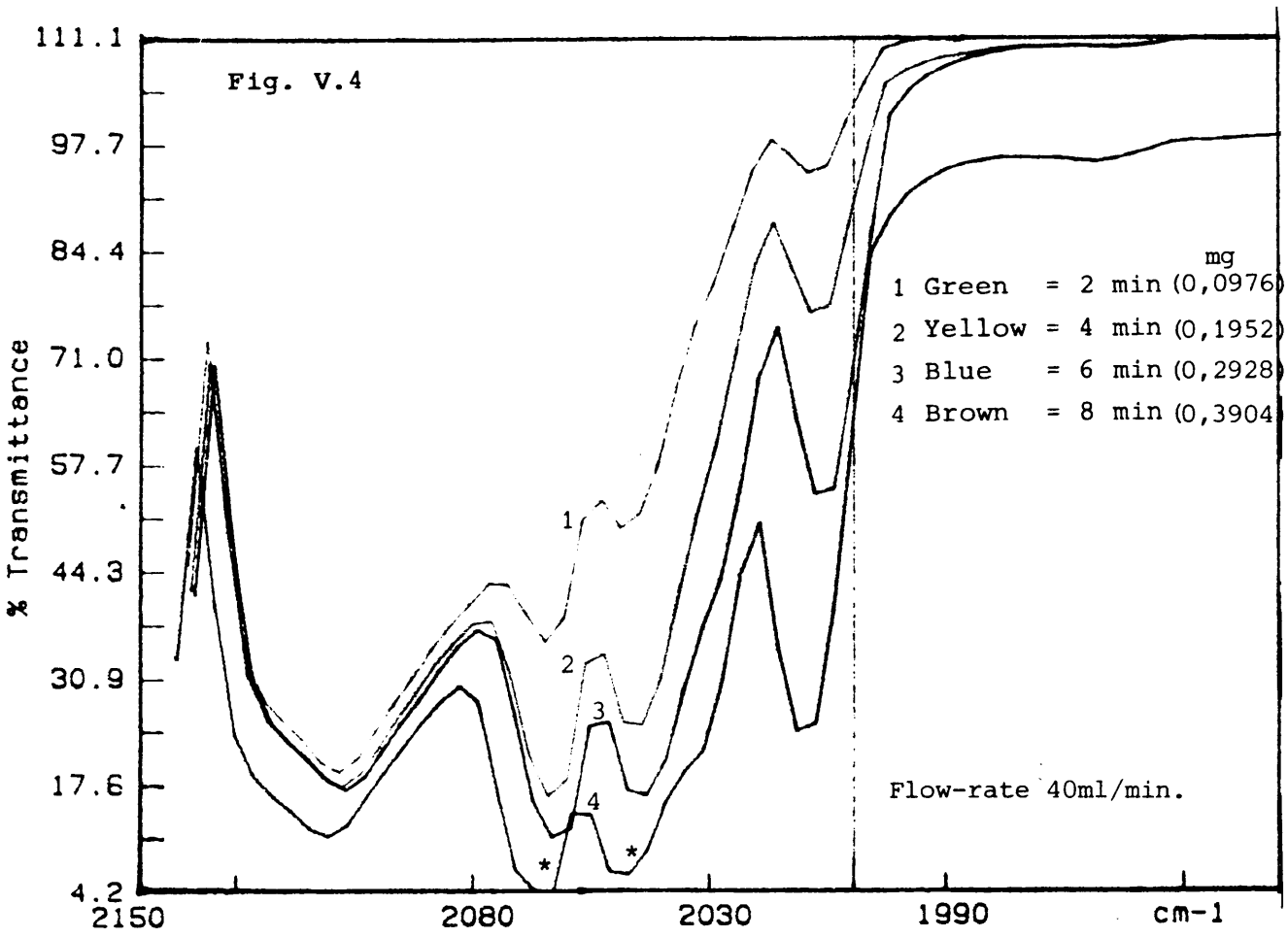

(i) Optimum flow-rate

A standard gas mixture (Table V-1) was used to condense a possible maximum of 0,22 mg H_2S inside the cell. The temperature was maintained at -155°C. The conditions are listed in table V-2. An

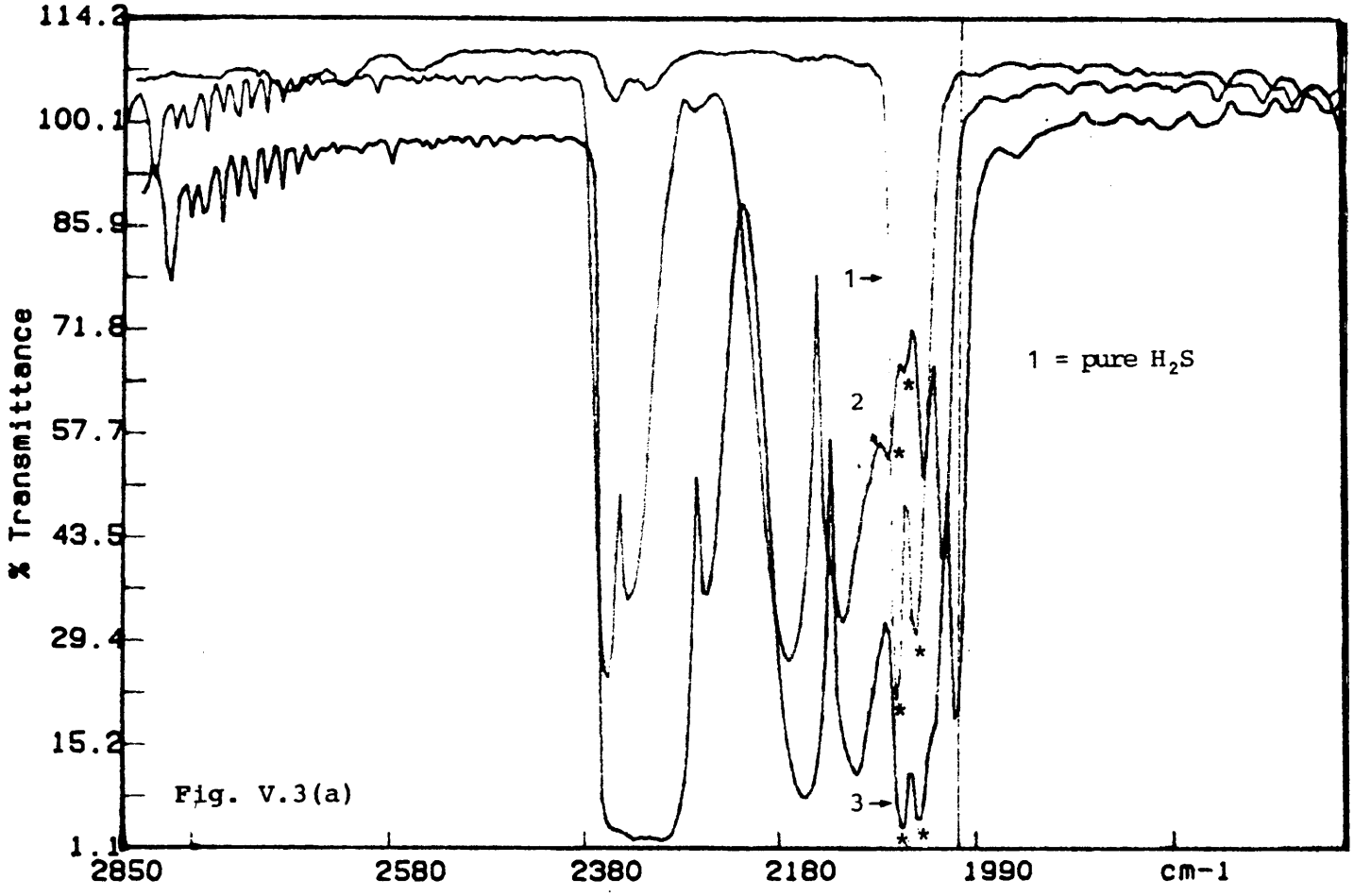

Fig. V.3(a)

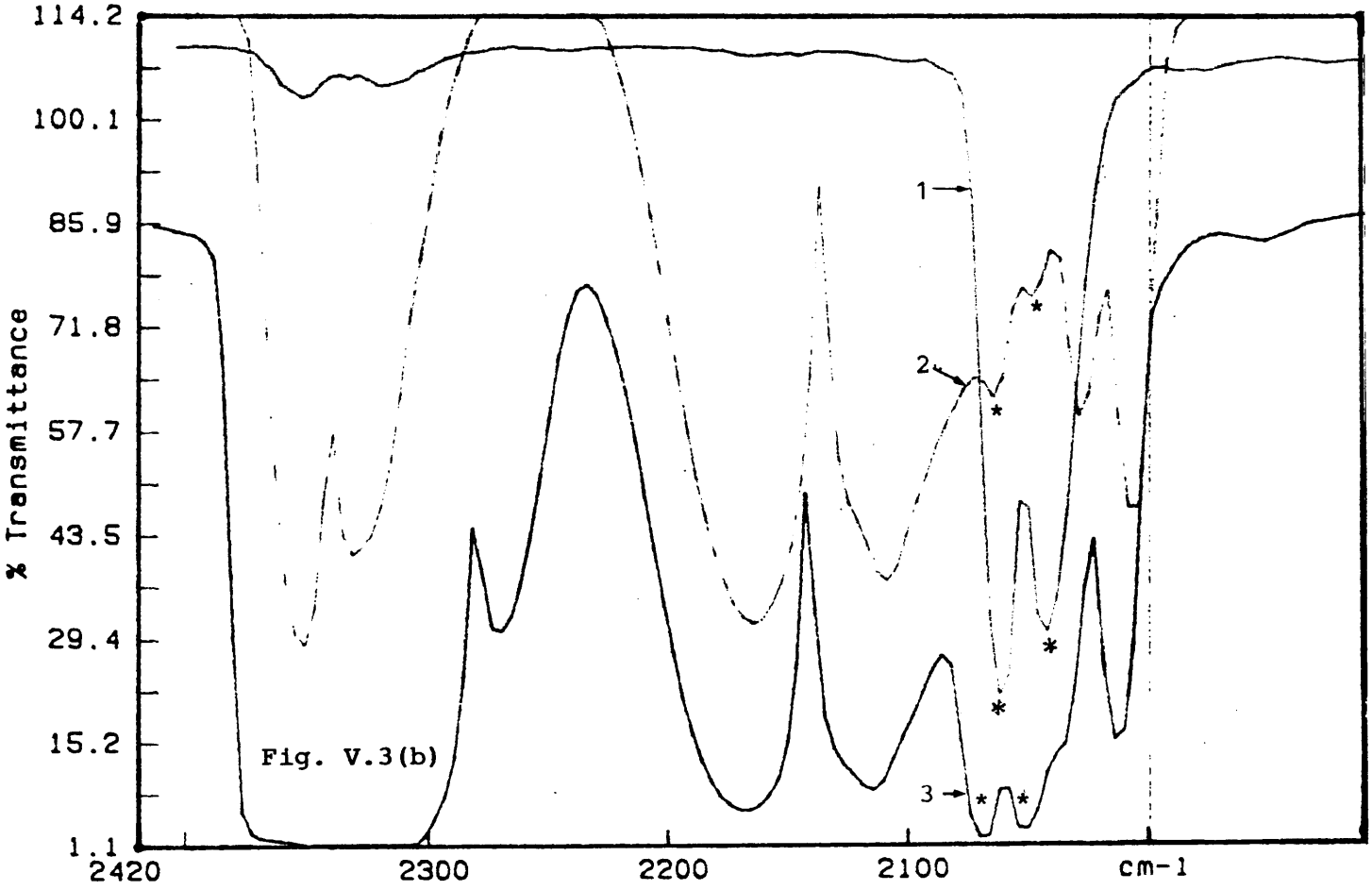

Fig. V.3(b)

attempt was made to keep the mass of H_2S passing through the cell constantly (columns 1 and 2).

Table V-2

FLOW ml/min	TIME min	TOT. VOL. ml	MASS H2S mg	SIGNAL (2054cm) Abs	SIG./MASS 2054
60	3	180	0.2213	0.9248	4.1789
95.8	1.3	172.44	0.212	0.9033	4.2608
134	1.3	174.2	0.2142	0.9605	4.4841
178.2	1	178.2	0.2191	0.8481	3.8708
219.7	0.82	180.15	0.2215	1.0241	4.6235
257.3	0.69	177.54	0.2183	0.9159	4.1956
281.5	0.6	168.9	0.2077	0.767	3.6928

The intensity of the H_2S peak at 2054 cm^{-1} is shown in the fifth column. Since the total volume that passed through the cell varied, the mass of the H_2S that could condense, also varied. Assuming a direct proportionality between signal strength and mass, the signal to mass ratio was calculated in an attempt to compensate for this variation. A plot of the signal to mass ratio can be seen in fig. V.5.. The gradient of this plot remains fairly constant up to 200 mℓ/min. The negative gradient, for flow-rates higher than

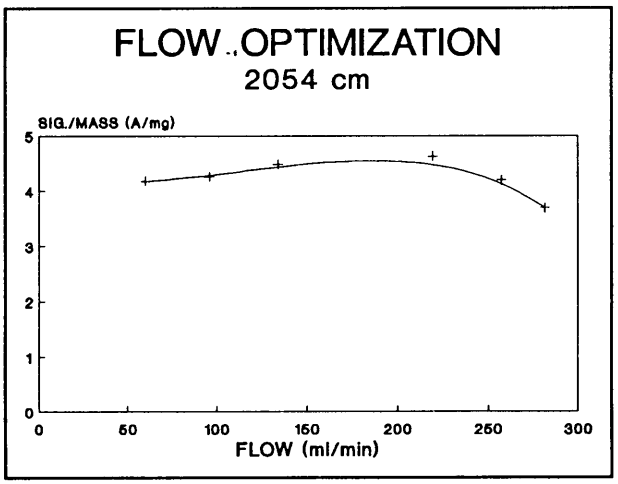

Fig. V.5

200 mℓ/min is an indication that the H_2S did not condense as effectively as was the case at flow-rates lower than 200 mℓ/min. This implies that the H_2S condensing time necessary to give a signal comparable to that of CO is 48 s and that the H_2S signal strength should be eight times that original signal after four minutes of condensation.

(ii) The effect of concentration

Dilutions were made from the standard gas mixture containing H_2S (1000 ppm) with pure nitrogen gas. The flow diagram in fig. V.6 gives an illustration of this procedure. The flow-rates and condensing times are shown in table V-3.

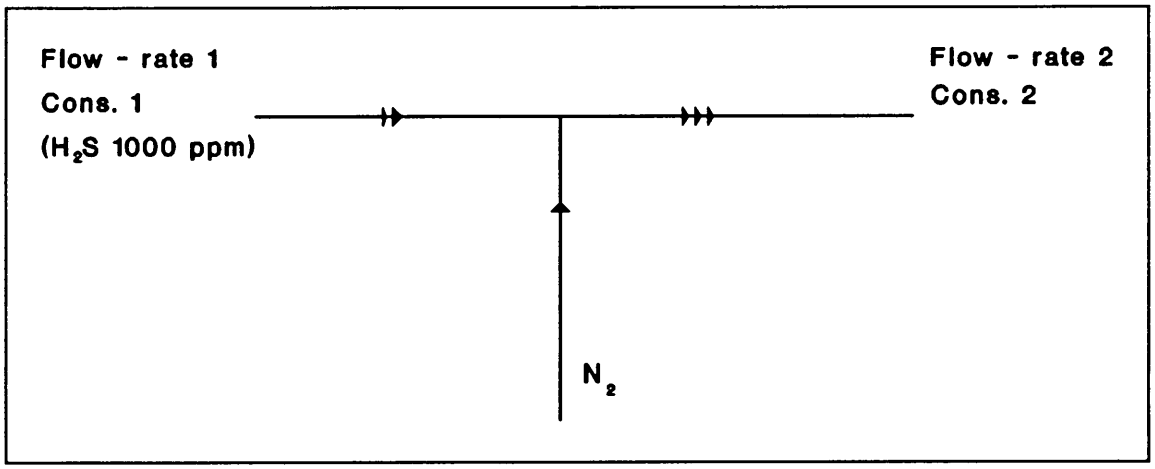

Fig. V.6

The total flow-rate was maintained well below 200 mℓ/min to ensure that all the H_2S was captured inside the cell. The temperature inside the cell was maintained at -160°C. The parameters were manipulated in such a way that an approximate maximum of 0,15 mg H_2S could be deposited inside the cell.

Table V-3

Flow-rate 1 (mℓ/min)	Flow-rate 2 (mℓ/min)	Cons 2 (ppm)	Cons 2 (mg/ℓ)	Condens-time (min)	CO peak	H_2S peak	H_2S/CO
20	19,6	1000	1,22	6,09	0,6875	0,6286	0,9143
15	30,9	500	0,6148	8,128	0,4389	0,4978	1,1342
14	55,1	250	0,3094	8,7	0,228	0,3208	1,4070
10	80,5	125	0,1537	12,19	0,1222	0,2096	1,7152

The spectra of the dilutions are shown in fig. V.7. It can be seen that

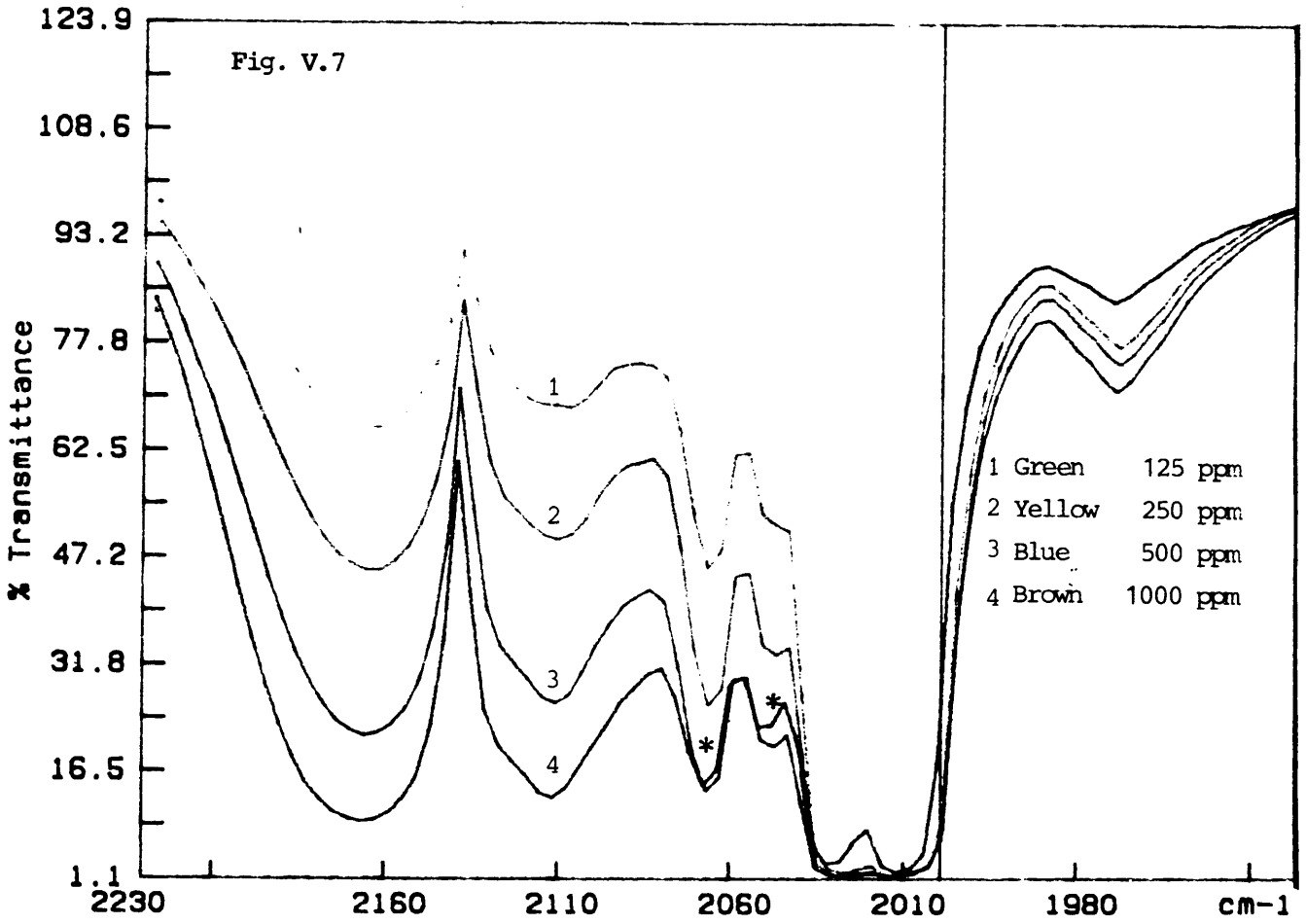

Fig. V.7

the H_2S:CO ratio (Table V-3) has increased but it did not double, for instance from the 250 ppm to 500 ppm spectra, as expected. The

answer to this phenomenon lies in the partial vapour pressure of the H_2S gas as will be described in the following section.

(iii) Vapour pressures and partial vapour pressures

A component (J) of a gas mixture can only condense if the partial vapour pressure (P_J) in the gas mixture exceeds the normal vapour pressure (P_{VJ}) of the component. P_{VJ} is the vapour pressure in the presence of condensed solid material of component J. The vapour pressure can be calculated according to the following equation

$$\log_{10} P_{VJ} = (-0{,}2185\ {}^{A}/_{K}) + B \qquad \text{V-1}$$

where P_{VJ} is expressed in Torr, K is the temperature in degrees Kelvin and A is the molar heat of vaporization in calories per gram mole [21]. The data required to calculate the vapour pressures of the various components of the gas mixture are tabulated in table V-4.

Table V-4

	A	B
CO_2	5539,0	8,9414
N_2	1489,8	7,0504
CO	1613,3	7,1006
H_2	250,6	5,5818
CH_4	2128,8	7,0277
Ar	1739,9	7,132
H_2S	4814,5	7,7351

The calculated vapour pressures of H_2S and CO_2 are tabulated in table V-5.

Table V-5

TEMP (°C)	CO_2 (Pa)	H_2S (Pa)
-160	2.268995	3.552035
-155	6.451529	8.809386
-150	16.84981	20.29286
-145	40.82768	43.79544
-140	92.55825	89.20622
-135	197.7504	172.5728
-130	400.6487	318.7935
-125	773.9104	564.9854
-120	1431.955	964.5425
-115	2548.324	1591.856
-110	4377.461	2547.639
-105	7281.214	3964.743
-100	11760.12	6014.361
-95	18489.39	8912.445
-90	28359.29	12926.18
-85	42519.33	18380.40
-80	62425.79	25663.63
-75	89891.47	35233.83
-70	127137.0	47623.49
-65	176842.9	63444.09
-60	242200.4	83389.77
-55	326961.5	108240.1
-50	435486.1	138862.3
-45	572786.1	176211.8
-40	744564.9	221332.7
-35	957252.4	275357.0
-30	1218034.	339502.8
-25	1534877.	415071.9
-20	1916545.	503446.7
-15	2372608.	606086.3
-10	2913453.	724521.9
-5	3550278.	860352.0
0	4295086.	1015236.
5	5160671.	1190892.
10	6160601.	1389084.
15	7309190.	1611622.

The partial vapour pressures of the gas mixture, used in the experiment, are tabulated in table V-6.

Table V-6.

	Percentage	P_J/Pa
CO_2	0,63	546,7896
N_2	0,79	685,6568
CO	28,59	24813,83
H_2	57,08	49540,87
CH_4	12,43	10788,25
Ar	0,47	407,9224
H_2S	0,1	86,792

The partial pressures of H_2S in the dilutions are listed in table V-7. The minimum temperatures required for condensation are listed in the fourth column.

Table V-7

H_2S conc. (ppm)	Percentage H_2S ($^v/_v$)	P_{VJ} (Pa)	Min. Temp. (°C)
1000	0,1	86,792	-140
500	0,05	43,496	-145
250	0,25	21,698	-150
125	0,0125	10,849	-155

The minimum vapour pressure required for condensation at -160°C is 3,552 Pa. As can be seen from table V-7 the partial vapour pressures of H_2S approaches this value as the concentration is lowered.

3. Metal Light Pipe-Liebig combination type cell

(a) Apparatus and Procedure

The Liebig-type gas cell described in section V-2a, was packed tightly with Nickel tubes with diameter 1.2 mm.

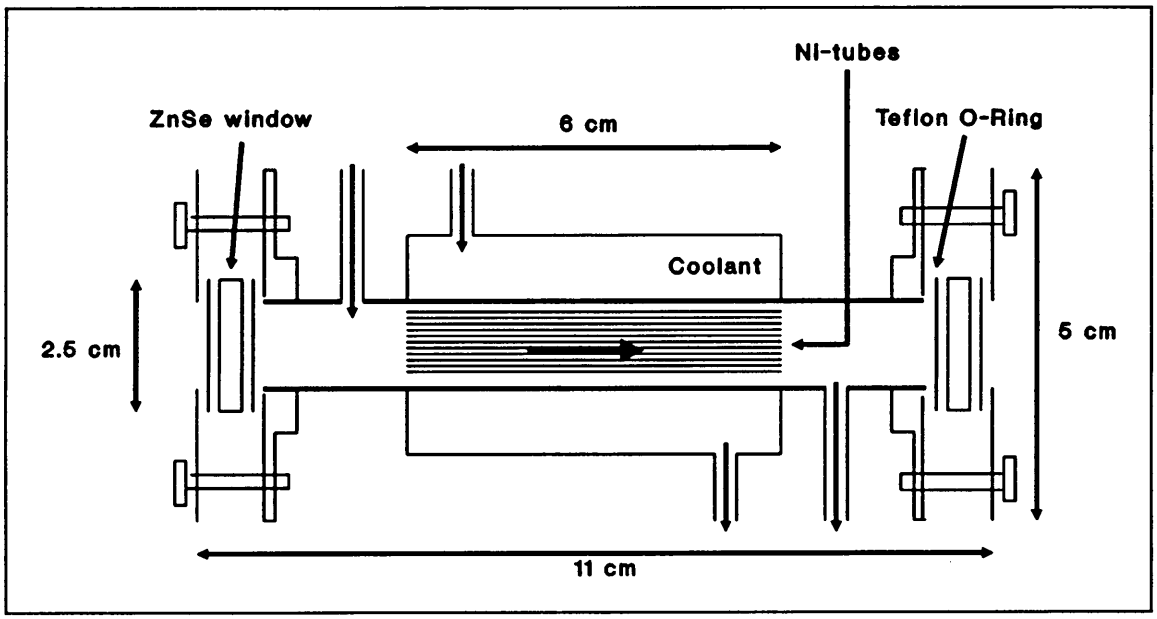

Fig. V.8 Liebig - Light Pipe type gas cell

The tubes are specular with excellent reflectivities [22]. The only difference from the first type of gas cell is that the cold gasses now condenses against the walls of the Nickel tubes, whilst the other gases flow through the cell. The nickel tubes should be packed tightly to ensure good thermal contact. The infra-red beam is focussed onto the tube entrances making numerous reflections as it passes through the tubes. The cylindrical symmetry of the light beam makes this instrument ideal for this application. The material layer may be a condensed monolayer or thicker. Spectra obtained in this way are

external reflection spectra which can be understood in terms of the optical constants or dielectric function of the material. (The theory of infra-red reflection in metal light pipes is presented by Hansen [23]).

(b) Spectral equations for the light pipe

For light propaganating down a curved light pipe

$$\frac{I}{I_o} = \exp[-(\alpha_{sm} + \alpha_m + \alpha_{sc})L] \qquad \text{V-2}$$

where the α's are effective extinction coefficients for sample absorption, metal absorption and losses by light scattering respectively. It is convenient to consider absorbance defined as

$$\log_{10} {}^{I_o}/I = A_L \qquad \text{V-3}$$

for a length (L) of light pipe. From eq. V-2

$$A_L \ln 10 = (\alpha_{sm} + \alpha_m + \alpha_{sc})L \qquad \text{V-4}$$

If the absorbance subtraction scheme, where the bare light pipe is taken as reference and therefore subtracted, only α_{sm} and α_{sc} are present. In many cases α_{sc} will be neglegible or unchanged by the samples presence. In such cases the resultant spectrum is given by

$$A_L = \alpha_{sm} L/_{\ln 10} \qquad \text{V-5}$$

To reduce eq. V-4 to actual numbers the sample and beam configuration need to be considered. First consider the sample to be a very thin film of complex index $\hat{n}_f = n_f + ik_f$, complex dielectric function ϵ_f, and thickness h/λ. For such a sample on the inside of a light pipe, the absorbance change per parallel

polarization reflection is given by

$$\frac{\Delta A\|}{N} = \frac{8\Pi}{\ln 10}\,\frac{h}{\lambda}\,\tan\theta_1\,\sin\theta_1\,I_m\frac{1}{\epsilon_p^*} \qquad \text{V-6}$$

where

$$I_m\left(\frac{1}{\epsilon_f^*}\right) = 2n_f k_f/(n_f^2 + k_f^2)^2 \qquad \text{V-7}$$

and θ_1 is the angle of incidence at the light pipe surface.

In a light pipe of length L and inside diameter d the number of reflections are

$$N = L/(d\tan\theta) \qquad \text{V-8}$$

By substitution of eq. V-7 and V-8 into eq. V-6 and by comparison of eq. V-5 it can be deduced that

$$\alpha_{sm} = 8\Pi\,\frac{h}{\lambda}\,\frac{\sin\theta_1}{d}\,\frac{2n_f k_f}{(n_f^2 + k_f^2)^2} \qquad \text{V-9}$$

A numerical calculation is instructive. For $\theta_1 > 80°$ $\sin\theta_1 \approx 1$ and the absorbtion sensitivity is indenpendent of the angle. Substituting this value for θ_1 into eq. V-8 amount up to 21 reflections for a pipe with $L/_d = 120$; thus the sensitivity is expected to be about 21 times that of a single reflection at 80°.

(c) Results and discussion

The standard gas mixture was purged through the gas cell at a flow rate of 38 mℓ/min. Spectra were recorded, with time intervals of 1 min, at various temperatures. See fig. 9a and 9b. The H_2S accumulated over a period of 20 minutes. The spectra in fig. 9a were recorded at a temperature of -40°C. It is impossible for the H_2S to condense at this temperature since the partial vapour pressure equals 86,792 Pa and is much lower than the required vapour pressure of 3,39502 x 10^5 Pa. This means that there must be another type of retardation mechanism. Polar molecules like H_2S adsorbes to metal oxide centres, in this case nickeloxide [24].

The spectra shown in fig. 9b were recorded at a temperature of -160°C. The partial vapour pressure, at this temperature, is well inside the limit for condensation. Fig. V.10 shows the accumulation curves of H_2S at various temperatures. It is interesting to note that the gradient of the -60°C curve is larger than those of the other temperatures. The reason for this phenomenon becomes clear if the spectra in figs. 11a - 11h are carefully studied. The spectra marked "1" were

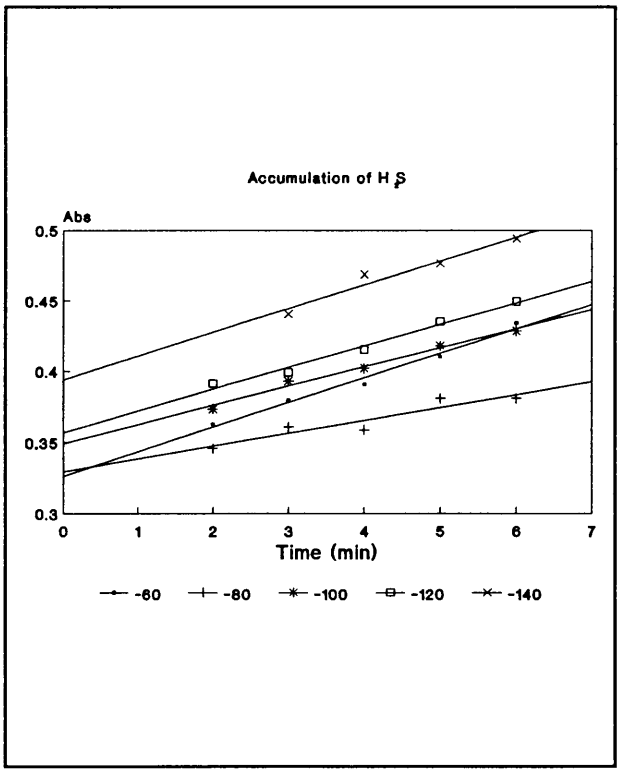

Fig. V-10

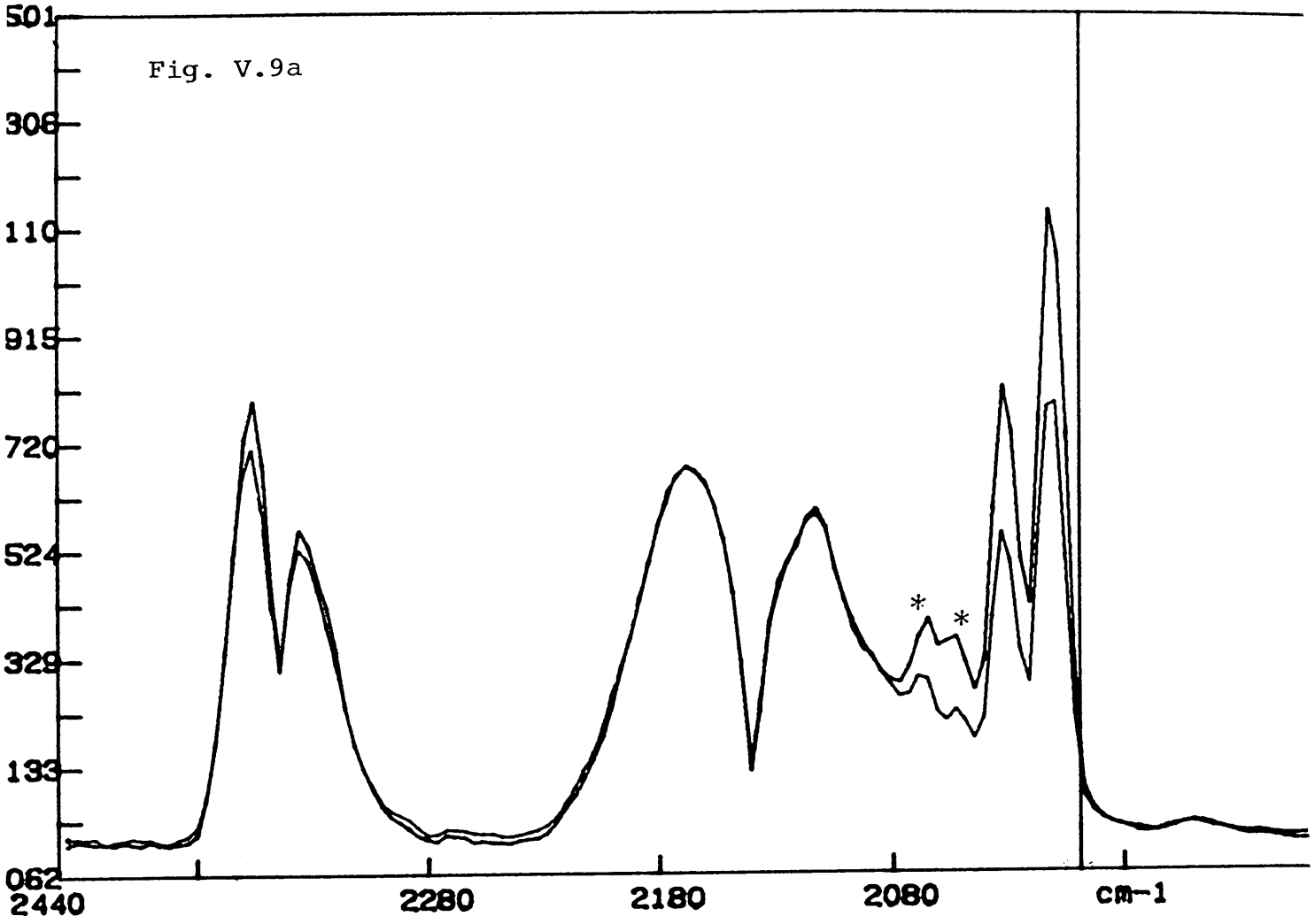

Fig. V.9a

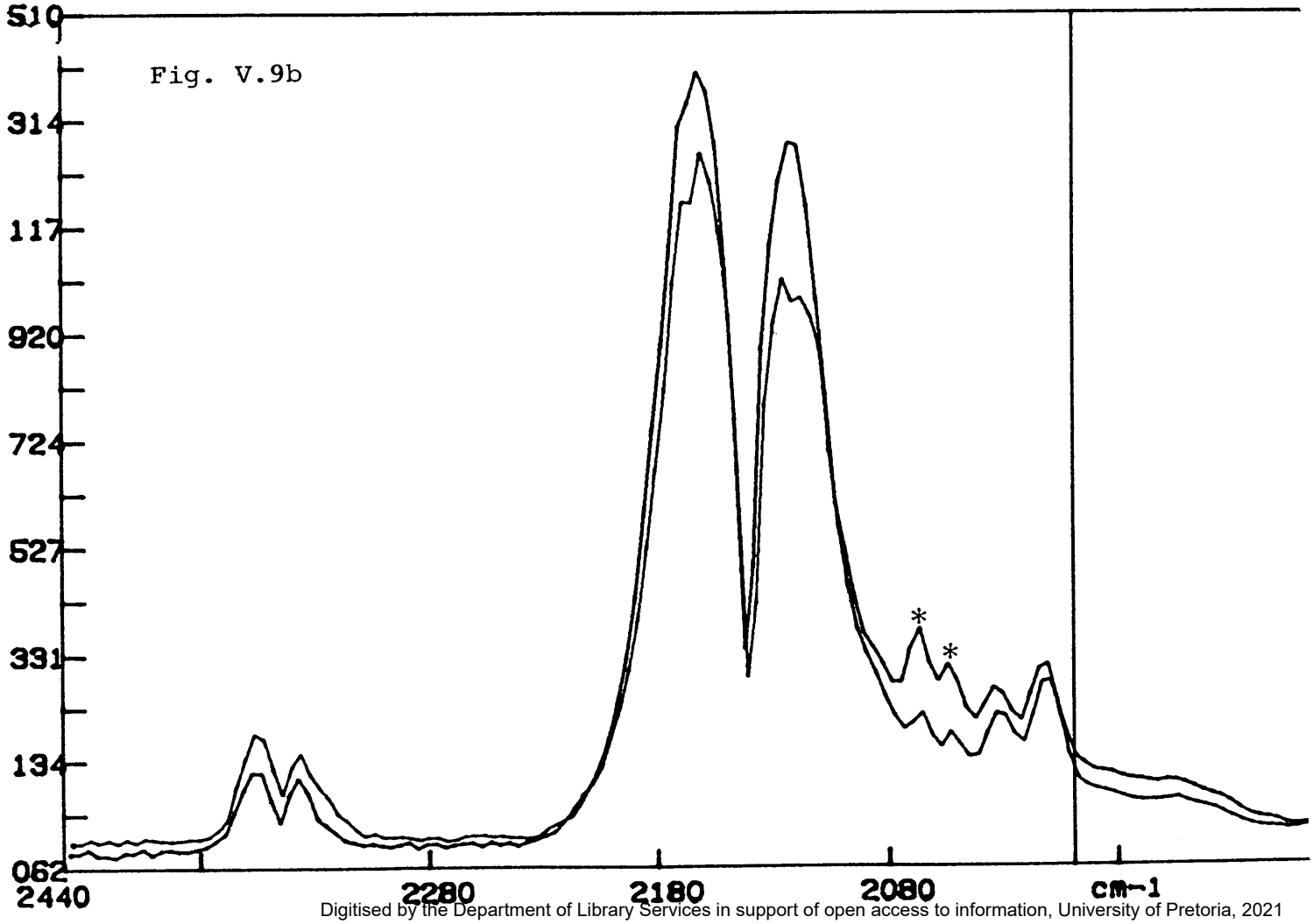

Fig. V.9b

recorded after an accumulation time of 10 minutes was allowed at various temperatures. The spectra marked "2" were recorded after closing the in- and outlet valves and allowing the condensed matter to evaporate.

Fig. 11g, recorded at -140°C shows that the carbon dioxide was captured inside the nickel tubes since there is an enormous difference between the "cold" and "evaporated" spectrum. By analogy it can be reasoned that the component with a peak at approximately 2010 cm^{-1} condenses at about -60°C. This implies that this component covers the nickel oxide layer and prevents the H_2S from being adsorbed rapidly at lower temperatures.

4. Conclusions

It was shown that the signal of the low concentration component H_2S could be enhanced selectively in the presence of an overlapping main component like CO. If the Liebig cell is to be used the freezing point of the low concentration component should be higher than that of the overlapping main component.

The vapour pressure is a critical factor which must be taken into account if the cells are used to capture the low concentration components by way of condensation. The partial vapour pressure of a specific component must exceed the vapour pressure at a specific temperature, for example, at -160°C the partial vapour pressure of the H_2S should exceed 3,55 Pa. This limits the minimum detection limit for H_2S down to 100 ppm ($^v/_v$) since it is difficult to reach temperatures lower than -160°C inside the cell using liquid nitrogen as coolant.

It was also shown that the H_2S (1000 ppm, $^v/_v$) condensation time necessary to give a signal comparable to that of CO under optimal condisions is 48s. The H_2S enrichment factor is 2,1 times the original signal strength in one minute.

The Liebig-Light Pipe cell can also be used to analyze H_2S at a temperature above its freezing point. The H_2S can be accumulated inside the nickel tubes by taking advantage of the polar adsorbtion of H_2S onto nickel oxide centres.

In general, the component to be analyzed must be polar in order to adsorb onto the metal oxide centres. A disadvantage is that the main components in the gas mixture with freezing points higher than that of the analyte will cover the metal oxide centres, thus preventing the polar molecules to adsorb as effective as it would have in the adsence of these components.

Although the enrichment factor is small (20% at -60°C) the cold spectra have better resolution than the evaporated spectra making the overlapping problem less severe. Advantages that the latter type of cell has above the Liebig cell are namely: The measurements do not depend on the vapour pressure of H_2S since accumulation occurs far above the freezing point of the H_2S. Secondly it is not necessary to close the in- and outlet valves after condensation. The vapour pressure of CO_2 is an enormous 7,3 x 10^6 Pa which can cause the glass cell to explode. Thirdly the higher temperatures (typically -60°C) requires a smaller effort in the cooling procedure thus saving time if the cell is to be used for online measurements.

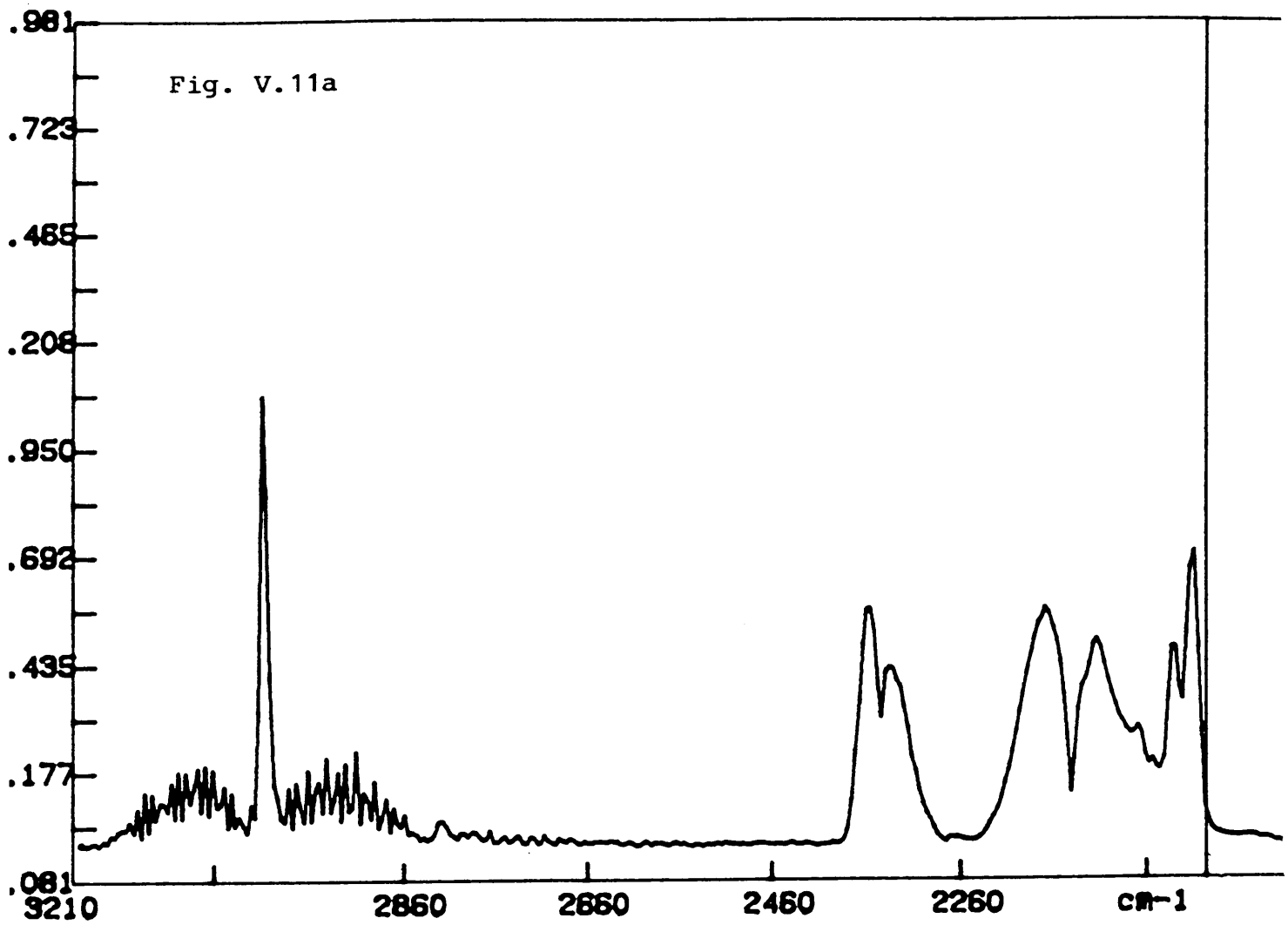

Fig. V.11a

Fig. V.11b

-40°C

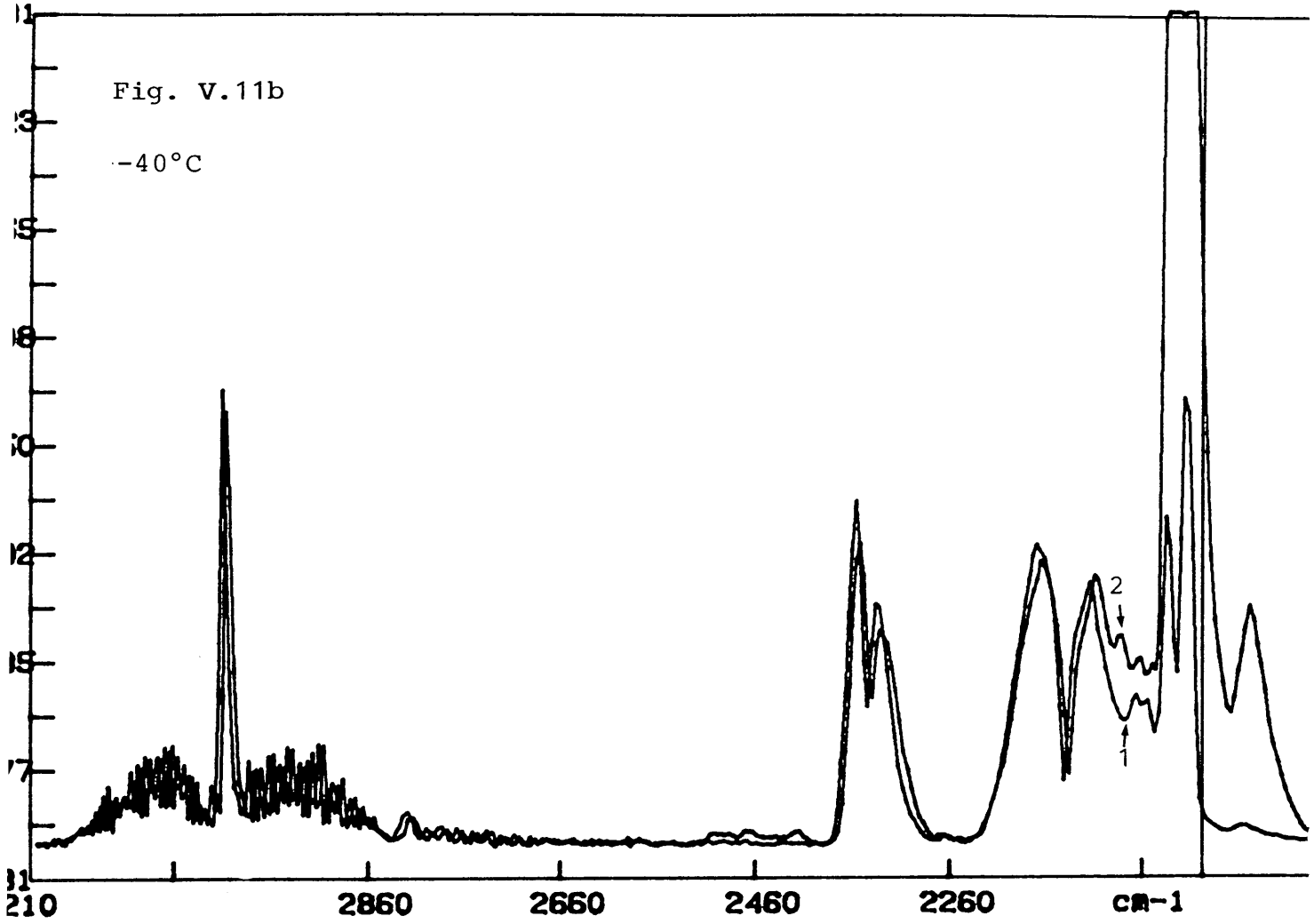

Fig. V.11c

-60°C

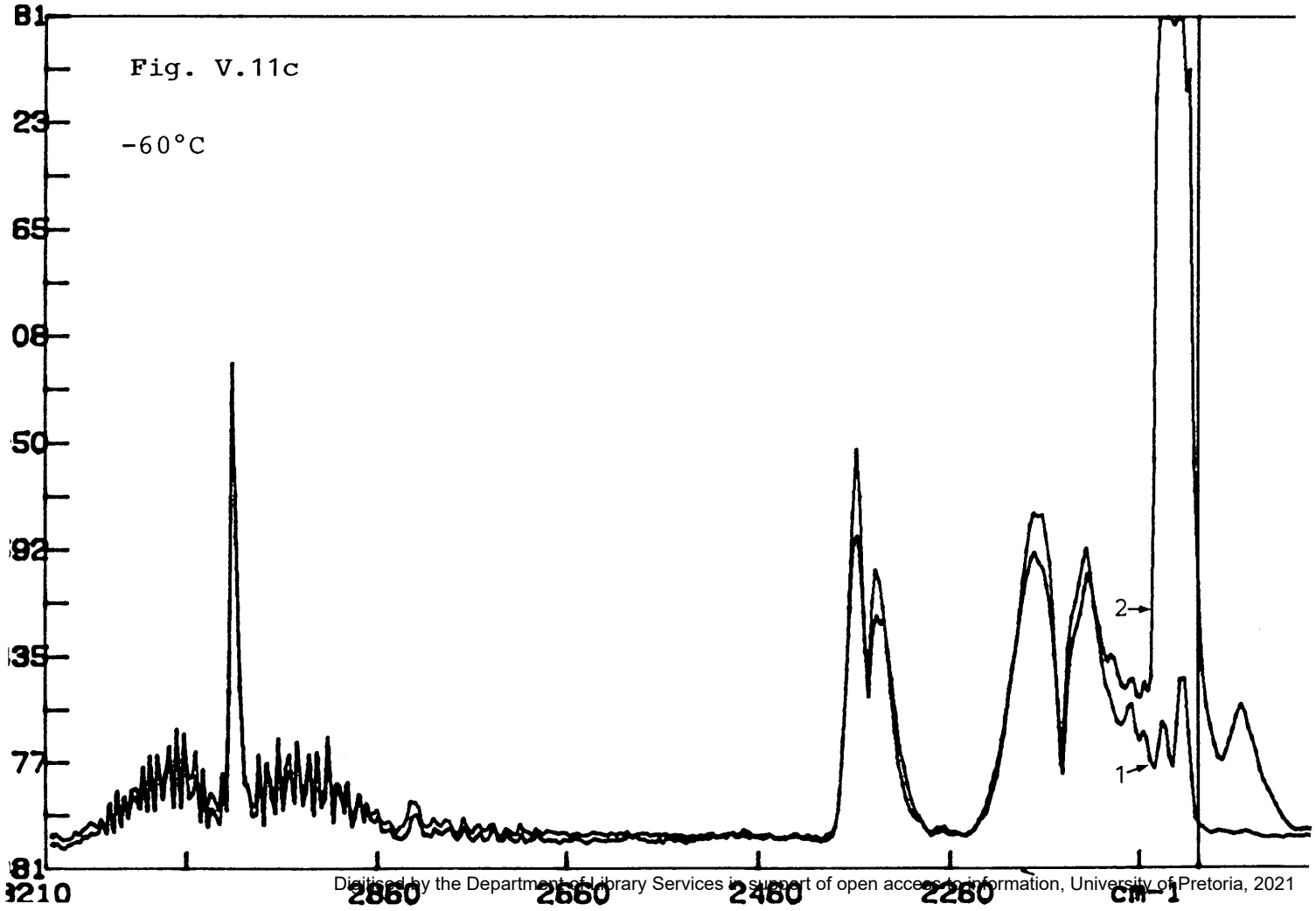

Fig. V.11d

-80°C

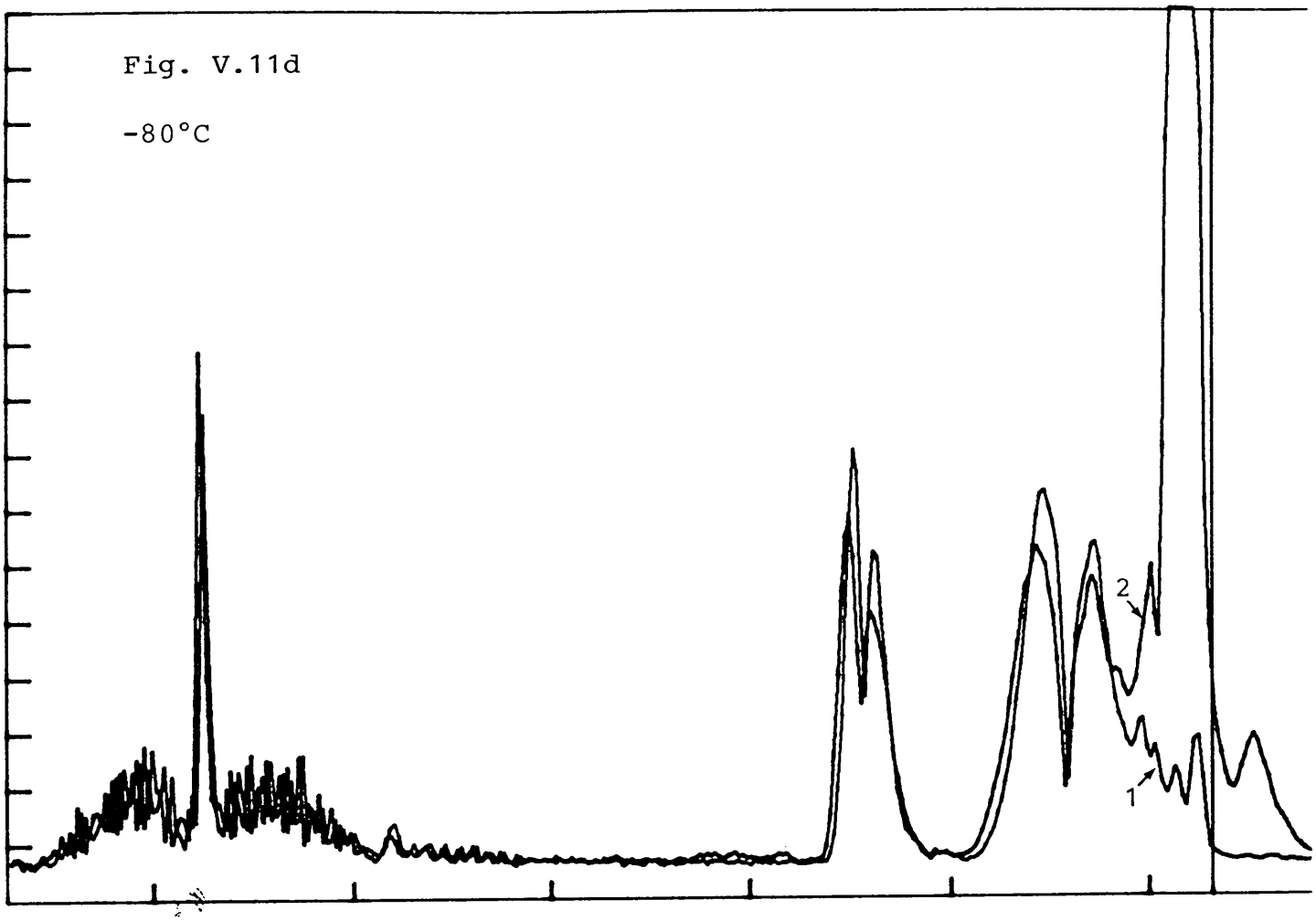

Fig. V.11e

-100°C

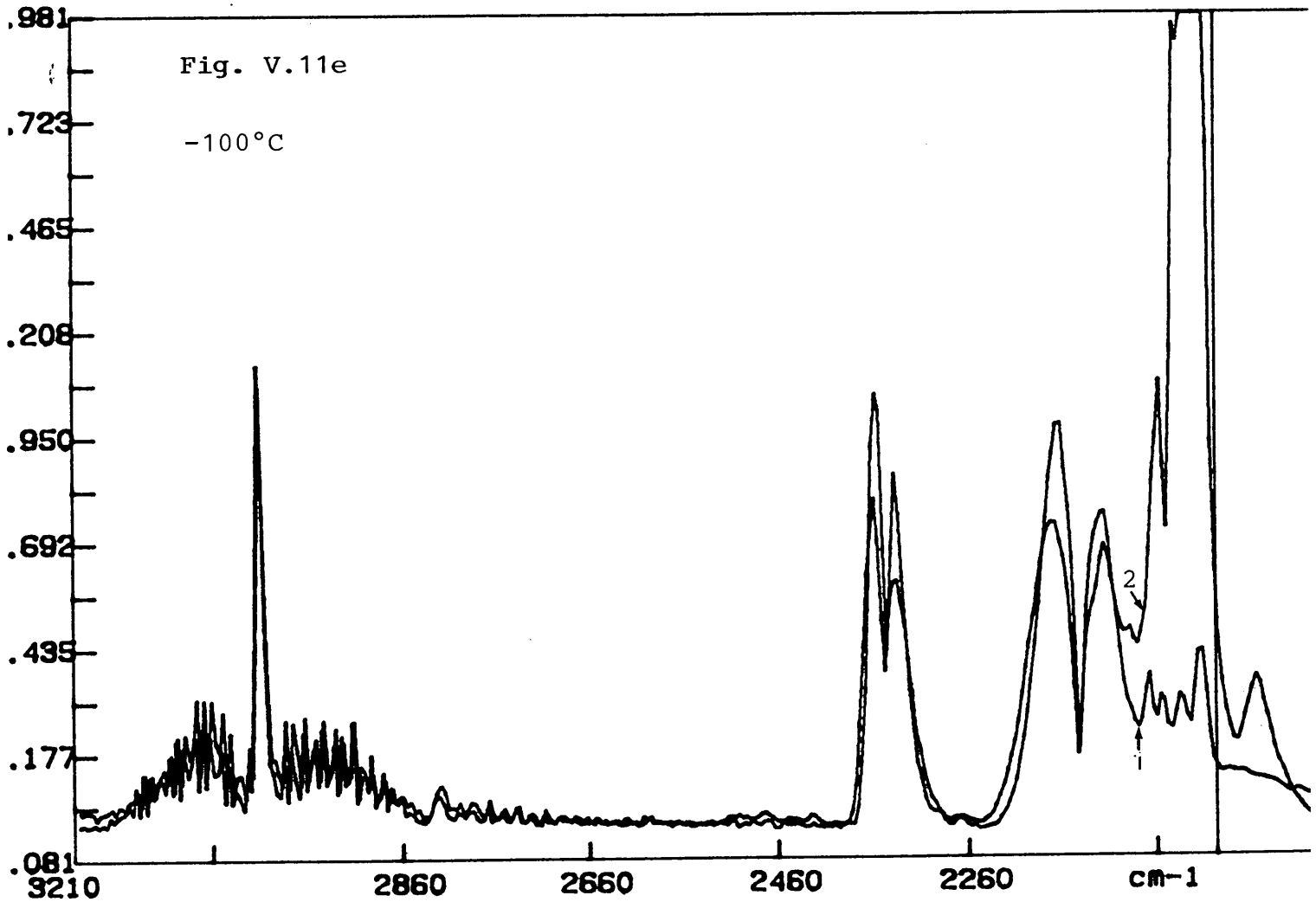

Fig. V.11f

-120°C

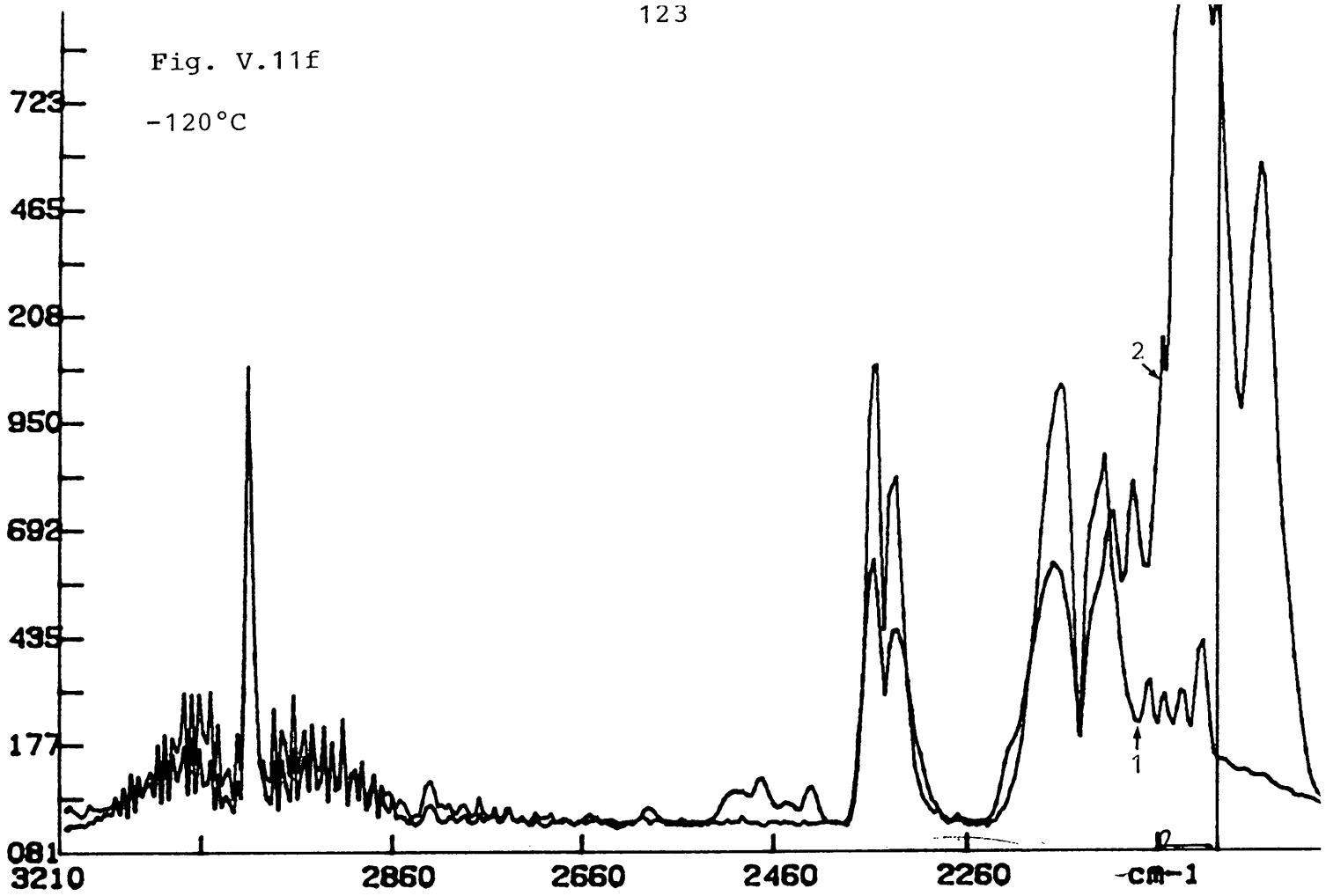

Fig. V.11g

-140°C

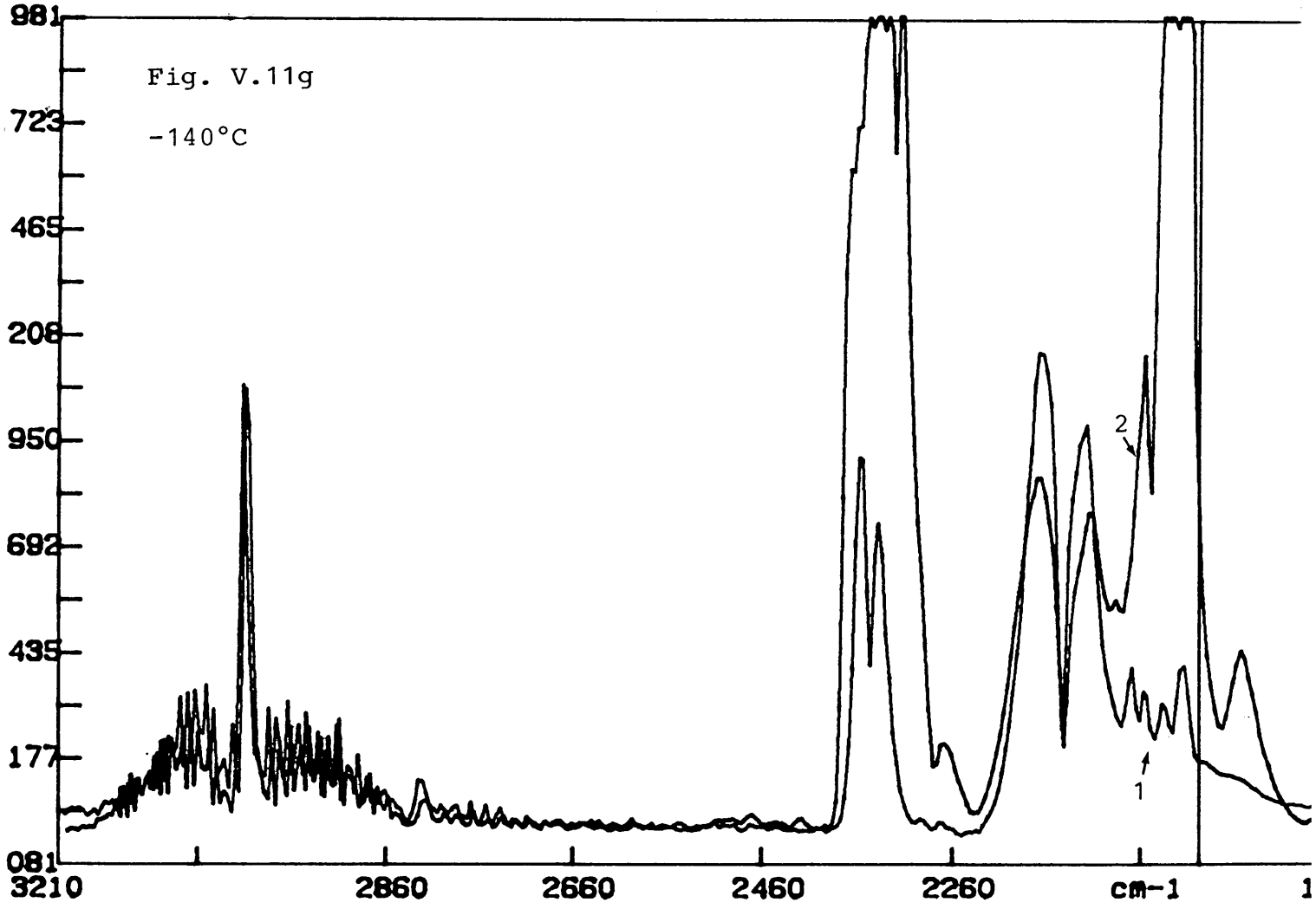

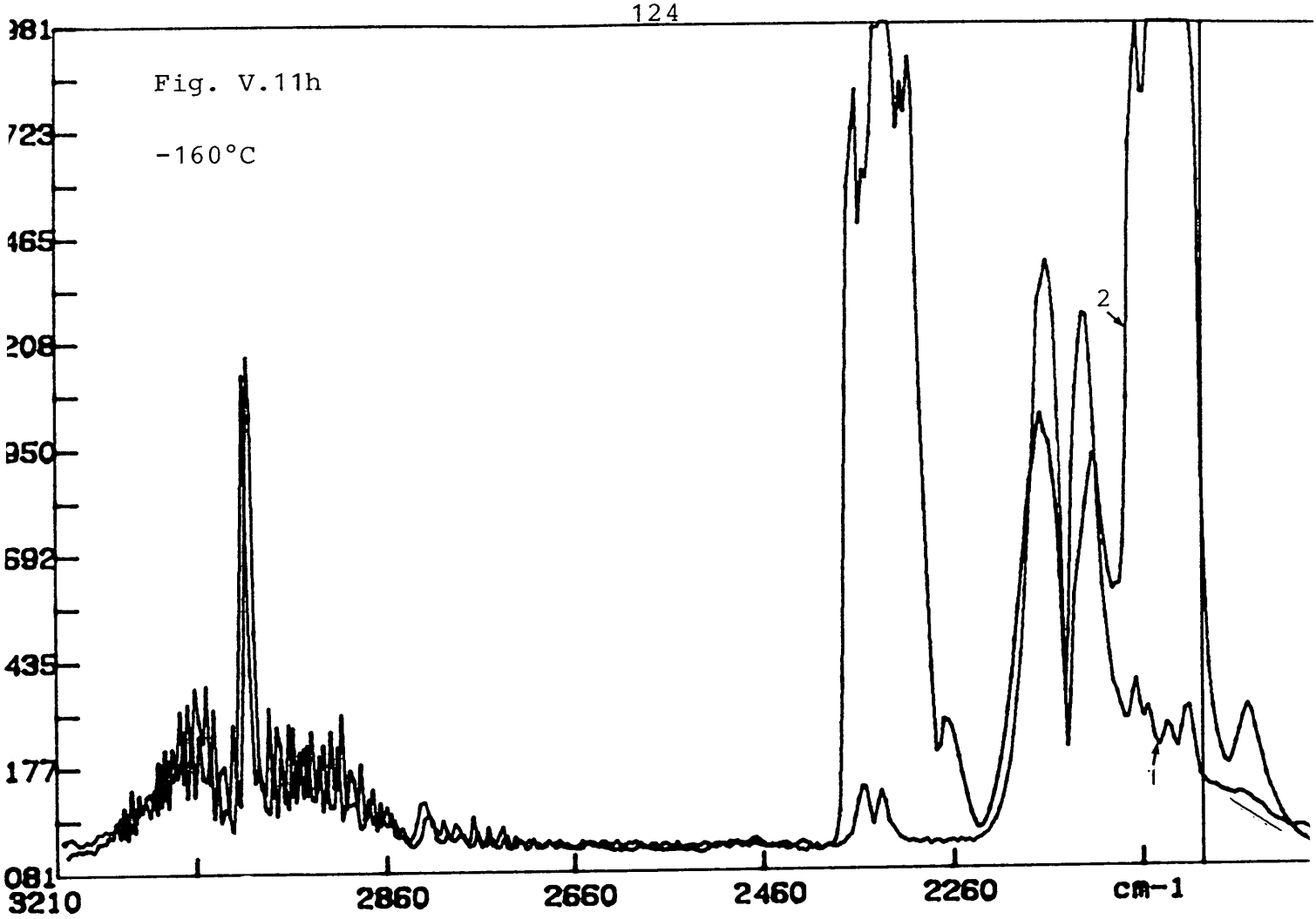

APPENDIX

Table II-3

(ν_2)

J	R(J)	P(J)
2	669.714196	665.796947
4	671.281096	664.230046
6	672.83293	662.678212
8	674.414896	661.126378
10	675.996863	659.589611
12	677.578829	658.052843
14	679.160796	656.50101
16	680.757828	654.964242
18	682.354861	653.442541
20	683.951894	651.905774
22	685.548327	650.384073
24	687.130893	648.862372
26	688.742992	647.34067
28	690.340025	645.834036
30	691.952124	644.327401
32	693.57929	642.820766
34	635.191389	641.314132
36	696.803488	639.822563
38	698.415587	638.315929
40	700.042753	636.82436
42	701.66918	635.347858
44	703.297084	633.85629
46	704.939315	632.379788
48	706.566481	630.903286
50	708.193646	629.426784
52	709.835878	627.950282
54	711.47811	626.488845
56	713.120342	625.389003
58	714.762574	623.565975
60	716.219872	622.119605
62	718.052104	620.673236

Table II-3

(ν_3)

J	R(J)	P(J)
2	2351.449994	2347.59301
4	2352.851165	2345.995977
6	2354.387932	2344.323612
8	2355.964832	2342.68138
10	2357.280671	2341.129547
12	2358.772239	2339.396917
14	2360.113144	2337.694419
16	2361.469115	2335.945723
18	2362.779887	2334.214093
20	2364.060527	2332.300667
22	2365.4164988	2330.59817
24	2366.591673	2328.760076
26	2367.812047	2326.891849
28	2369.032421	2325.053754
30	2370.207597	2323.04993
32	2371.367705	2321.196769
34	2372.452484	2319.177879
36	2373.567392	2317.189121
38	2374.682302	2315.21543
40	2375.72188	2313.106141
42	2376.776524	2311.072184
44	2377.770903	2308.993028
46	2378.765282	2306.88374
48	2379.714462	2304.744318
50	2380.648575	2302.589831
52	2381.552536	2300.435343
54	2382.44147	2298.235656
56	2383.285186	2296.005837
58	2384.128901	2293.760951
60	2384.927418	2291.485933
62	2385.710868	2289.195348
64	2386.464185	2286.845498
66	2387.18737	2284.540347
68	2387.895488	2282.159864
70	2388.573474	2279.779381
72	2389.221327	2277.368766
74	2389.854113	2274.928017
76	2390.456767	2272.472203

Table II-4

(ν_2)

J	R(J)	P(J)	R(J)-P(J) F′(J)	J+½	R(J-1)-P(J+1) F″(J)	J+½
2	669.714196	665.796947	3.917249	2.5		
3					5.48415	3.5
4	671.281096	664.230046	7.05105	4.5		
5					8.602884	5.5
6	672.83293	662.678212	10.154718	6.5		
7					11.706552	7.5
8	674.414896	661.126378	13.288518	8.5		
9					14.825285	9.5
10	675.996863	659.589611	16.407252	10.5		
11					17.94402	11.5
12	677.578829	658.052843	19.525986	12.5		
13					21.077819	13.5
14	679.160796	656.50101	22.659786	14.5		
15					24.196554	15.5
16	680.757828	654.964242	25.793586	16.5		
17					27.315287	17.5
18	682.354861	653.442541	28.91232	18.5		
19					30.449087	19.5
20	683.951894	651.905774	32.04612	20.5		
21					33.567821	21.5
22	685.548927	650.384073	35.164854	22.5		
23					36.686555	23.5
24	687.130893	648.862372	38.268521	24.5		
25					39.790223	25.5
26	688.742992	647.34067	41.402322	26.5		
27					42.908956	27.5
28	690.340025	645.834036	44.505989	28.5		
29					46.012624	29.5
30	691.952124	644.327401	47.624723	30.5		
31					49.131358	31.5
32	693.57929	642.820766	50.758524	32.5		

Table II-4 (Continued)

(ν_2)

J	R(J)	P(J)	R(J)-P(J) F′(J)	J+½	R(J-1)-P(J+1) F″(J)	J+½
33					52.265158	33.5
34	695.191389	641.314132	53.877257	34.5		
35					55.368826	35.5
36	696.803488	639.822563	56.980925	36.5		
37					58.487559	37.5
38	698.415587	638.315929	60.099658	38.5		
39					61.591227	39.5
40	700.042753	636.82436	63.218393	40.5		
41					64.694895	41.5
42	701.66918	635.347858	66.321322	42.5		
43					67.81289	43.5
44	703.297084	633.85629	69.440794	44.5		
45					70.917296	45.5
46	704.939315	632.379788	72.559527	46.5		
47					74.036029	47.5
48	706.566481	630.903286	75.663195	48.5		
49					77.139697	49.5
50	708.193646	629.426784	78.766862	50.5		
51					80.243364	51.5
52	709.835878	627.950282	81.885596	52.5		
53					83.347032	53.5
54	711.47811	626.488846	84.989264	54.5		
55					86.089107	55.5
56	713.120342	625.389003	87.731339	56.5		
57					89.564367	57.5
58	714.762574	623.565975	91.196599	58.5		
59					92.642969	59.5
60	716.419872	622.119605	94.300267	60.5		
61					95.746636	61.5
62	718.062104	620.673236	97.388868	62.5		

Table II-5

(ν_3)

J	R(J)	P(J)	R(J)-P(J) F′(J)	J+½	R(J-1)-P(J+1) F″(J)	J+½
2	2351.449994	2347.59301	3.856984	2.5		
3					5.258155	3.5
4	2352.851165	2345.995977	6.855188	4.5		
5					8.391955	5.5
6	2354.387932	2344.323612	10.06432	6.5		
7					11.63122	7.5
8	2355.954832	2342.68138	13.273452	8.5		
9					14.599291	9.5
10	2357.280671	2341.129547	16.151124	10.5		
11					17.642692	11.5
12	2358.772239	2339.396917	19.375322	12.5		
13					20.716227	13.5
14	2360.113144	2337.694419	22.418725	14.5		
15					23.774696	15.5
16	2361.469115	2335.946723	25.522392	16.5		
17					26.833164	17.5
18	2362.779887	2334.214093	28.565794	18.5		
19					29.846434	19.5
20	2364.060527	2332.300667	31.75986	20.5		
21					33.1158318	21.5
22	2365.4164988	2330.59817	34.8183288	22.5		
23					35.993503	23.5
24	2366.591673	2328.760076	37.831597	24.5		
25					39.051971	25.5
26	2367.812047	2326.891849	40.920198	26.5		
27					42.140572	27.5
28	2369.032421	2325.053754	43.978667	28.5		
29					45.153843	29.5
30	2370.207597	2323.04993	47.157667	30.5		

Table II-5 (Continued)

(ν_3)

J	R(J)	P(J)	R(J)-P(J) F′(J)	J+½	R(J-1)-P(J+1) F″(J)	J+½
31					48.317775	31.5
32	2371.367705	2321.196769	50.170936	32.5		
33					51.255715	33.5
34	2372.452484	2319.177879	53.274605	34.5		
35					54.389513	35.5
36	2373.567392	2317.189121	56.378271	36.5		
37					57.493181	37.5
38	2374.682302	2315.21543	59.466872	38.5		
39					60.50645	39.5
40	2375.72188	2313.106141	62.615739	40.5		
41					63.670383	41.4
42	2376.776524	2311.072184	65.70434	42.5		
43					66.698719	43.5
44	2377.770903	2308.993028	68.777875	44.5		
45					69.772254	45.5
46	2378.765282	2306.88374	71.881542	46.5		
47					72.830722	47.5
48	2379.714462	2304.744318	74.970144	48.5		
49					75.904257	49.5
50	2380.648575	2302.589831	78.058744	50.5		
51					78.962725	51.5
52	2381.562556	2300.435343	81.117213	52.5		
53					82.006127	53.5
54	2382.44147	2298.235656	84.205814	54.5		
55					85.04953	55.5
56	2383.285186	2296.005837	87.279349	56.5		
57					88.123064	57.5
58	2384.128901	2293.760951	90.36795	58.5		
59					91.166467	59.5

Table II-5 (Continued)

(ν_3)

J	R(J)	P(J)	R(J)-P(J) F′(J)	J+½	R(J-1)-P(J+1) F″(J)	J+½
60	2384.927418	2291.485933	93.441485	60.5		
61					94.224935	61.5
62	2385.710868	2289.195848	96.51502	62.5		
63					97.268337	63.5
64	2386.464185	2286.845498	99.618687	64.5		
65					100.341872	65.5
66	2387.18737	2284.540347	102.647023	66.5		
67					103.355141	67.5
68	2387.895488	2282.159664	105.735624	68.5		
69					106.41361	69.5
70	2388.573474	2279.779381	108.794093	70.5		
71					109.441946	71.5
72	2389.221327	2277.368766	111.852561	72.5		
73					112.485347	73.5
74	2389.854113	2274.928017	114.926096	74.5		
75					115.52875	76.5
76	2390.456767	2272.472203	117.984564	76.5		

Table II-6

$(\nu_1 - \nu_3)$

J	R(J)	P(J)	R(J)-P(J) F′(J)	J+½	R(J-1)-P(J+1) F″(J)	J+½
2	722.340946	718.438763	3.902183	2.5		
3					5.469079	3.5
4	723.922913	716.871867	7.051046	4.5		
5					8.617951	5.5
6	725.45968	715.304962	10.154718	6.5		
7					11.736684	7.5
8	727.011514	713.722996	13.288518	8.5		
9					14.855418	9.6
10	728.548281	712.156096	16.392185	10.5		
11					17.989218	11.5
12	730.100115	710.559063	19.541052	12.5		
13					21.107952	13.5
14	731.621816	708.992163	22.629653	14.5		
15					24.226686	15.5
16	733.17365	707.39513	25.77852	16.5		
17					27.360486	17.5
18	734.710417	705.813164	28.897253	18.5		
19					30.509352	19.5
20	736.232118	704.201065	32.031053	20.5		
21					33.61302	21.5
22	737.768886	702.619098	35.149788	22.5		
23					36.761887	23.5
24	739.275521	701.006999	38.268522	24.5		
25					39.880621	25.5
26	740.797222	699.3949	41.402322	26.5		
27					42.999355	27.5
28	742.303856	697.797867	44.505969	28.5		
29					46.118088	29.5

Table II-6 (Continued)

$(\nu_1 - \nu_3)$

J	R(J)	P(J)	R(J)-P(J) F′(J)	J+½	R(J-1)-P(J+1) F″(J)	J+½
30	743.810491	696.185768	47.624723	30.5		
31					49.221756	31.5
32	745.317126	694.588735	50.728391	32.5		
33					52.34049	33.5
34	746.823761	692.976636	53.847125	34.5		
35					55.474291	35.5
36	748.315329	691.34947	56.965859	36.5		
37					58.593024	37.5
38	749.821964	689.722305	60.099659	38.5		
39					61.711758	39.5
40	751.313532	688.110206	63.203326	40.5		
41					64.815425	41.5
42	752.8051	686.498107	66.306993	42.5		
43					67.934159	43.5
44	754.296669	684.870941	69.425728	44.5		
45					71.052893	45.5
46	755.788237	683.243776	72.544461	46.5		
47					74.156561	47,5
48	757.279805	681.631676	75.648129	48.5		
49					77.260228	49.5
50	758.771374	680.019577	78.751797	50.5		
51					80.363896	51.5
52	760.247876	678.407478	81.840398	52.5		
53					83.437431	53.5
54	761.73944	676.810445	84.928995	54.5		

Table II-8

(ν_2)

J	$(J+½)^2$	$F'(J)/(J+½)$	$F''(J)/(J+½)$
2	6.25	1.5668996	
3	12.25		1.5669
4	20.25	1.5669	
5	30.25		1.5641607273
6	42.25	1.5622643077	
7	56.25		1.5608736
8	72.25	1.5633550588	
9	90.25		1.5605563158
10	110.25	1.5625954286	
11	132.25		1.5603495652
12	156.25	1.56207888	
13	182.25		1.5613199259
14	210.25	1.5627438621	
15	240.25		1.561068
16	272.25	1.5632476364	
17	306.25		1.5608735429
18	342.25	1.5628281081	
19	380.25		1.561491641
20	420.25	1.5632253659	
21	462.25		1.561294
22	506.25	1.5628824	
23	552.25		1.56113
24	600.25	1.561980449	
25	650.25		1.560400902
26	702.25	1.5623517736	
27	756.25		1.5603256727
28	812.25	1.5616136491	
29	870.25		1.5597499661
30	930.25	1.5614663279	
31	992.25		1.5597256508
32	1056.25	1.5618007385	
33	1122.25		1.5601539701
34	1190.25	1.5616596232	
35	1260.25		1.5596852394
36	1332.25	1.5611212329	
37	1406.25		1.55966824
38	1482.25	1.5610300779	

Table II-8 (Continued)

(ν_2)

J	$(J+½)^2$	$F'(J)/(J+½)$	$F''(J)/(J+½)$
39	1560.25		1.5592715696
40	1640.25	1.5609479753	
41	1722.25		1.5589131325
42	1806.25	1.5605016941	
43	1892.25		1.5589170115
44	1980.25	1.5604672809	
45	2070.25		1.5586218901
46	2162.25	1.5604199355	
47	2256.25		1.5586532421
48	2352.25	1.5600658763	
49	2450.25		1.5583777172
50	2550.25	1.5597398416	
51	2652.25		1.5581235728
52	2756.25	1.5597256381	
53	2862.25		1.5578884486
54	2970.25	1.5594360367	
55	3080.25		1.5511550811
56	3192.25	1.5527670619	
57	3306.25		1.5574672522
58	3422.25	1.5589162222	
59	3540.25		1.5570246891
60	3660.25	1.5586820992	
61	3782.25		1.5568558699
62	3906.25	1.558221888	

Table II-9

(ν_3)

J	$(J+½)^2$	$F'(J)/(J+½)$	$F''(J)/(J+½)$
2	6.25	1.5427936	
3	12.25		1.50233
4	20.25	1.5233751111	
5	30.25		1.52581
6	42.25	1.5483569231	
7	56.25		1.5508293333
8	72.25	1.5615825882	
9	90.25		1.5367674737
10	110.25	1.5382022857	
11	132.25		1.5341471304
12	156.25	1.55002576	
13	182.25		1.5345353333
14	210.25	1.5461189655	
15	240.25		1.5338513548
16	272.25	1.5468116364	
17	306.25		1.5333236571
18	342.25	1.544096973	
19	380.25		1.530586359
20	420.25	1.5492614634	
21	462.25		1.5402712465
22	506.25	1.54748128	
23	552.25		1.5316384255
24	600.25	1.5441468163	
25	650.25		1.5314498431
26	702.25	1.5441584151	
27	756.25		1.5323844364
28	812.25	1.5431111228	
29	870.25		1.5306387458
30	930.25	1.5461530164	
31	992.25		1.533897619
32	1056.25	1.5437211077	
33	1122.25		1.5300213433
34	1190.15	1.5441914493	
35	1260.25		1.5320989577
36	1332.25	1.5446101644	
37	1406.25		1.5331514933
38	1482.25	1.5445940779	
39	1560.25		1.5318088608
40	1640.25	1.5460676296	
41	1722.25		1.5342260964
42	1806.25	1.5459844706	
43	1892.25		1.5333038851
44	1980.25	1.5455702247	
45	2070.25		1.5334561319
46	2162.25	1.5458396129	
47	2256.25		1.5332783579
48	2352.25	1.5457761649	

Table II-9 (Continued)

(ν_3)

J	$(J+½)^2$	$F'(J)/(J+½)$	$F''(J)/(J+½)$
49	2450.25		1.5334193333
50	2550.25	1.545717703	
51	2652.25		1.5332567961
52	2756.25	1.5450897714	
53	2862.25		1.5328248037
54	2970.25	1.5450608073	
55	3080.25		1.532423964
56	3192.25	1.5447672389	
57	3306.25		1.5325750261
58	3422.25	1.5447512821	
59	3540.25		1.5322095294
60	3660.25	1.5444873554	
61	3782.25		1.5321127642
62	3906.25	1.54424032	
63	4032.25		1.5317848346
64	4160.25	1.5444757674	
65	4290.25		1.5319369771
66	4422.25	1.5435642556	
67	4556.25		1.5311872741
68	4692.25	1.5435857518	
69	4830.25		1.5311310791
70	4970.25	1.5431786241	
71	5112.25		1.530656588874
72	5256.25	1.5427939448	
73	5402.25		1.5304128844
74	5550.25	1.5426321611	
75	5700.25		1.5301821192
76	5852.25	1.5422818824	

Table II-10

$(\nu_1 - \nu_3)$

J	$(J+½)^2$	$F'(J)/(J+½)$	$F''(J)/(J+½)$
2	6.25	1.5608732	
3	12.25		1.562594
4	20.25	1.5668991111	
5	30.25		1.5669001818
6	42.25	1.5622643077	
7	56.25		1.5648912
8	72.25	1.5633550588	
9	90.25		1.5637282105
10	110.25	1.5611604762	
11	132.25		1.5642798261
12	156.25	1.56328416	
13	182.25		1.563552
14	210.25	1.5606657241	
15	240.25		1.563012
16	272.25	1.5623345455	
17	306.25		1.5634563429
18	342.25	1.5620136757	
19	380.25		1.5645821538
20	420.25	1.5624903902	
21	462.25		1.5633962791
22	506.25	1.5622128	
23	552.25		1.564335617
24	600.25	1.5619804898	
25	650.25		1.5639459216
26	702.25	1.5623517736	
27	756.25		1.5636129091
28	812.25	1.5616136491	
29	870.25		1.5633250169
30	930.25	1.5614663279	
31	992.25		1.5625954286
32	1056.25	1.5608735692	
33	1122.25		1.5624026866
34	1190.25	1.5607862319	
35	1260.25		1.5626560845
36	1332.25	1.5607084658	
37	1406.25		1.56248064
38	1482.25	1.5610301039	

Table II-10 (Continued)

$(\nu_1 - \nu_3)$

J	$(J+½)^2$	$F'(J)/(J+½)$	$F''(J)/(J+½)$
39	1560.25		1.5623229873
40	1640.25	1.5605759506	
41	1722.25		1.5618174699
42	1806.25	1.5601645412	
43	1892.25		1.5617048046
44	1980.25	1.5601287191	
45	2070.25		1.561602044
46	2162.25	1.5600959355	
47	2256.25		1.5611907579
48	2352.25	1.5597552371	
49	2450.25		1.5608126869
50	2550.25	1.5594415248	
51	2652.25		1.560464
52	2756.25	1.5588647238	
53	2862.25		1.5595781495
54	2970.25	1.5583301835	

REFERENCES

1. G. Herzberg, Molecular Spectra and Molecular Structure II, New York, (1945).

2. G.M. Barrow, Molecular Spectroscopy, Mc Graw-Hill, (1962).

3. J.M. Hollas, High Resolution Spectroscopy, Butterworths, (1982).

4. D.M. Dennison, *Rev. Mod. Phys.* **3**, 280 (1931).

5. H.A. Jahn, *Proc. Roy. Soc. London*, **168**, 469 (1938).

6. H.A. Jahn, *Proc. Roy. Soc. London*, **168**, 495 (1938).

7. W.H.J. Childs, H.A. Jahn, *Proc. Roy. Soc. London,* **169**, 451 (1939).

8. H.A. Jahn, *Proc. Roy. Soc. London,* **168**, 469, 495 (1938).

9. E.B. Wilson, *J. Chem. Phys.*, **3**, 276 (1935).

10. Weitkamp, H. and Barth R., Einfuerung in die quantitative Infrarot Spectrophotometrie, Georg Thieme Verlag, Stuttgard (1976).

11. A. Beer, *Annalen der Physik und Chemie,* 86, **78**, (1852).

12. A.L. Smith, Applied Infrared Spectroscopy, Wiley, New York (1979).

13. H.A. Willis *et. al.*, Laboratory Methods in Vibrational Spectroscopy (1987), 3rd Ed., John Wiley & Sons.

14. C.W. Brown and F. Lynch, *Anal. Chem.*, **54**, 1472, (1982).

15. J.C. Sternberg, H.S. Stillo, R.H, Schwendeman, *Anal. Chem.*, **32**, 84, (1960).

16. C.W. Brown and R.J. Obrenski, *Appl. Spectr. Rev.*, **20** (3+4), 373, (1984).

17. C.W. Brown, *Journal of Testing and Evaluation (JTEVA)*, **12**, 86, (1984).

18. A. Junker and G. Bergman, *Frezenius Z. Anal. Chem.*, **272**, 267, (1974).

19. A. Junker and G. Bergman, *Frezenius Z. Anal. Chem.*, **278**, 191-198, (1976).

20. H.J. Kisner, C.W. Brown and G.J. Kavanos, *Anal. Chem.*, **55**, 1703, (1983).

21. CRC Handbook of Chemistry and Physics, 53rd Edition, CRC Press.

22. V. Pretorius and E.R. Rohwer, *Journal of Chromatography*, **289**, 17, (1984).

23. Wilford N. Hansen, *Appl. Spectrosc.*, **41**, 46, (1987).

24. J.C. Lavalley *et. al.*, *J.C.S. Chem. Comm.*, **146**, (1979).